TRANSPORT AND MOBILIZATION OF PATHOGENIC MICROBES AND MICROSPHERES IN UNSATURATED FRACTURED MEDIA: EFFECT OF MICROBE SIZE, SOIL PHYSICAL HETEROGENEITY, AND INTERMITTENT FLOW

AND

EFFECT OF REDOX CONDITIONS ON THE RELEASE OF TRACE ELEMENTS FROM SUBMERGED COAL ASH NEAR THE KINGSTON FOSSIL PLANT

by

MARK CHARLES DAVID BULICEK

B.S., Bradley University, 2010

A thesis submitted to the
Faculty of the Graduate School of the
University of Colorado in partial fulfillment
of the requirement for the degree of
Master of Science
Department of Civil, Environmental, and Architectural Engineering
2013

This thesis entitled:

Transport and Mobilization of Pathogenic Microbes and Microspheres in Unsaturated Fractured Media: Effect of Microbe Size, Soil Physical Heterogeneity, and Intermittent Flow

And

Effect of Redox Conditions on the Release of Trace Elements from Submerged Coal Ash near the Kingston Fossil Plant

written by Mark Charles David Bulicek
has been approved for the Department of Civil, Environmental, and Architectural Engineering

Dr. Joseph Ryan

Dr. Diane McKnight

Dr. Ronald Harvey

Dr. George Aiken

Date: 10/28/2013

The final copy of this thesis has been examined by the signatories, and we
Find that both the content and the form meet acceptable presentation standards
Of scholarly work in the above mentioned discipline.

ABSTRACT

Bulicek, Mark Charles David (M.S., Civil, Environmental, and Architectural Engineering)

Transport and Mobilization of Pathogenic Microbes and Microspheres in Unsaturated Fractured Media: Effect of Microbe Size, Soil Physical Heterogeneity, and Intermittent Flow

and

Effect of Redox Conditions on the Release of Trace Elements from Submerged Coal Ash near the Kingston Fossil Plant

Thesis directed by Professor Joseph N. Ryan

The potential of intermittent rainfall to mobilize microbes of diverse size, shape, and taxa in heterogeneous soil systems is important in assessing groundwater contamination risks. We investigated the transport, retention, and mobilization of microbes through an intact soil core. Microbes (MS-2 bacteriophage, *Pseudomonas stutzeri* bacteria, and *Cryptosporidium parvum* oocysts), microspheres, and a bromide tracer were applied to the core and breakthrough was measured to resolve the effect of soil physical heterogeneity. After breakthrough, the core was subjected to intermittent rainfalls to mobilize the attached microbes and microspheres. This study demonstrated that intermittent flows mobilize attached microbes and microspheres in a physically heterogeneous soil regardless of size or taxa; however, the degree of mobilization was dependent on microbe size and shape. Mobilization of larger, spherical *C. parvum* oocysts was greater than that of smaller, spherical MS-2 bacteriophage and rod-shaped *P. stutzeri* bacteria. Cumulatively, the order of recovery was *C. parvum* oocysts > microspheres > MS-2 bacteriophage > *P. stutzeri* cells.

The release of coal ash because of a storage pond dike failure at the Tennessee Valley Authority's Kingston Fossil Plant in December 2008 is a concern because of the potential ecological and human health risks posed by the release of toxic elements from the coal ash into surrounding waters. The effects of redox conditions were examined in this study, which focused on how the differences between elements affect their release as a function of varied redox conditions. Using Emory River sediments and water, and Kingston coal ash, a batch reactor system was created. This experiment was conducted in three stages – oxidizing, transition, and reducing – in order to simulate redox changes that might occur during weathering of the released coal ash on riverbed sediments. The results suggest that the release of several trace elements, from the coal ash may present water quality issues based on their increasing concentrations during the reducing stage. The differences in release can be attributed to changes in chemical properties (e.g., pH, redox potential), presence and aromaticity of DOC, dissolution of mineral phases, competition or interaction with other species, precipitation of immobile phases, or release of mobile phases.

DEDICATION

To Nicki, for being supportive throughout my time in the Master's program. To my family, for showing me that hard work will pay off in the end and pushing me to my full potential. Finally, to Midge, my lab partner and Dog of Science, for keeping me company in in the lab for long hours, all-nighters, and frustrating moments.

ACKNOWLEDGEMENTS

When I first started graduate school I knew I wanted to be part of a research team and write a thesis, but the issues involved with finding funding or writing a grant were daunting. I went into my now advisor's office, Dr. Joseph Ryan, and asked him if there was any way I could get involved with research down in his lab. That meeting transformed my graduate school career, as soon after I began volunteering with Dr. Sanjay Mohanty and working with him on a side-project before he left for Stanford University. I want to first thank Joe for giving me an opportunity to gain valuable research experience, without which I would not have received a research assistantship, nor would I have been able to conduct two experiments that really made my experience in graduate school worthwhile.

That being said, I also want to deeply thank Dr. Sanjay Mohanty for allowing me to work with him in the lab, teaching me all of the lab techniques that you don't learn in class, and especially for including me in his microsphere work, which we will soon be publishing. I found volunteering with Sanjay to be a great learning experience, and running a duplicate experiment for him when he first moved to Stanford really helped me to receive the funding that brought me to write this thesis. Without Sanjay's great recommendation to Joe, and the amount he trusted me to get involved with, I don't think I would have gotten the opportunities I did. I want to also acknowledge all of the help Sanjay gave me during my microbe study; without his deep knowledge of the core set-up and calming demeanor, I wouldn't have known what to do.

I would also like to thank the people who collaborated and helped on the microbe transport study from the USGS office in Boulder: Dr. Ronald Harvey, Jennifer Underwood, and most importantly David Metge. First, thank you to Ron for letting me volunteer in his lab and use countless materials, and for being part of my thesis committee. Also, thank you to Jen for giving me some pointers on my microbiology lab skills and helping me with the virus while Dave was sampling. Thank you most of all to Dave Metge, who brought me through the virology “school of hard knocks”, and without whom the microbe study would not have been possible. Dave was a constant source of knowledge and encouragement, and I want to especially thank him for helping me in the lab during the microbe injection, which at the time was the most stressful point in my life. I would also like to acknowledge Emmy Metge, who helped me for months at USGS to culture the virus.

I would like to thank everyone that was involved with the coal ash work. The Tennessee Valley Authority and the Oak Ridge Associated Universities provided funding for the coal ash research. I also want to thank Dr. Alison Craven, who guided me through the coal ash project and helped me to design the long-term weathering experiment. Additionally, thanks go to Dr. George Aiken for being a member on my committee, and to Neil Carriker, Adam Johnson, Jesse Morris, and Edward Arnold of the TVA for all of their help sampling in the Emory River and the information and support they provided.

I am also very thankful to Kenna Butler and everyone working at the Aiken lab at the USGS for help with sample analysis, and providing a lot of help and advice. I would also like to thank Dr. Alex Blum for his help with XRD and the fine clay analysis.

I want to also acknowledge the current and past members of the Ryan research group – Dr. Tim Dittrich, Catherine Carella, Jessica Dehart – for their help in the lab, and especially thank Brett Poulin and Jack Webster for all of their help and advice with my research and teaching me to use nearly every instrument at the USGS.

Also, thank you to Dr. Diane McKnight for being a member on my committee.

Finally, I want to thank my family for their support and encouragement.

TABLE OF CONTENTS

LIST OF TABLES

LIST OF FIGURES

CHAPTER 1

INTRODUCTION

General Information

Chapter one serves as an introduction to the second and third chapters of this thesis. This dissertation involved work on two separate projects. As the two projects are unrelated, a general introductory chapter is not necessary. Therefore, an abstract and introduction specific to each project will be presented at the beginning of the corresponding chapter. This introduction is meant to provide information on the organization of this thesis, and also to give a brief overview of the two projects of which it is comprised. Chapter two and Chapter three will contain individual introductions in order to provide specific information related to each corresponding project.

Overview: Chapter 2

Chapter two is titled, "Transport and Mobilization of Pathogenic Microbes and Microspheres in Unsaturated Fractured Media: Effect of Microbe Size, Soil Physical Heterogeneity, and Intermittent Flow". The main objective of this project was to study the transport and mobilization of three microbes of varying size and taxa in an intact fractured shale saprolite soil core subjected to intermittent rainfall events. Intermittent flow was simulated in the laboratory using a rainfall simulator and a series of rainfall events separated by antecedent drying periods. Soil physical heterogeneity was maintained using intact soil cores, and microbe size was investigated using three microbes of varying size and 0.5 µm microspheres. The three microbes used in this study were (1) MS-2 bacteriophage, about 26 nm, smallest size class (i.e., virus); (2) *Pseudomonas stutzeri* bacteria, about 1 µm diameter, medium size class; (3) *Cryptosporidium parvum* oocysts, 3 to 4 µm diameter, largest size class. Using three microbes and microspheres allowed for the transport, attachment, and subsequent mobilization during intermittent flow events to be evaluated in a physically heterogeneous soil system as a function of microbe size.

Overview: Chapter 3

Chapter three is titled, “Effect Redox Condition on the Release of Trace Elements from Submerged Coal Ash near the Kingston Fossil Plant”. The main objective of this project was to evaluate the effect of weathering processes (i.e., redox potential) on the release of trace elements from submerged coal ash in the Emory River near Kingston, TN. A series of batch reactors were used to simulate the river environment, in which three coal ash batch reactors contained Emory River sediment and water, and Kingston Fossil Plant coal ash, and one control batch reactor contained only Emory River sediment and water. The control reactor served as a reference, simulating the baseline chemical conditions of the Emory River unaffected by coal ash. The triplicate coal ash reactors allowed for the determination of changes in chemical conditions, concentration of elements released or attenuated, as well as the nature of organic matter in the Emory River water affected by coal ash. Weathering was simulated by changing the redox conditions in the batch reactors from oxidizing to reducing. By comparing the results of the oxidizing and reducing portions of this project, the elements released from the coal ash as it weathers can be determined. The results of this study indicate which elements or metals may be water quality issues in the Emory River.

CHAPTER 2

TRANSPORT AND MOBILIZATION OF PATHOGENIC MICROBES AND MICROSPHERES IN UNSATURATED FRACTURED MEDIA: EFFECT OF MICROBE SIZE, SOIL PHYSICAL HETEROGENEITY, AND INTERMITTENT FLOW

To be submitted as a manuscript with the same title to *Environmental Science & Technology* with co-authors David W. Metge[2], Sanjay K. Mohanty[3], Ronald W. Harvey[2], and Joseph N. Ryan[1]

[1]Department of Civil, Environmental and Architectural Engineering, University of Colorado, Boulder, CO
[2]United State Geological Survey, Boulder, CO
[3]Department of Civil and Environmental Engineering, Stanford University, Stanford, CA

Abstract

Intermittent flows of rainwater may mobilize pathogenic microbes attached to subsurface soils, thereby causing groundwater contamination. The potential of intermittent rainfall to mobilize microbes of diverse size, shape, and taxa in heterogeneous soil systems is important in assessing groundwater contamination risks. To address this lack of knowledge on microbe transport, we investigated the combined effects of microbe size and shape, intermittent flow, and soil physical heterogeneity on the transport, retention, and mobilization of microbes through an intact core of fractured shale saprolite. Microbes (MS-2 bacteriophage, *Pseudomonas stutzeri* bacteria, and *Cryptosporidium parvum* oocysts), fluorescent microspheres, and a bromide tracer were applied to the core and breakthrough was measured in 19 outlet ports at the core base to resolve the effect of soil physical heterogeneity. After breakthrough, the core was subjected to intermittent rainfalls to mobilize the attached microbes and fluorescent microspheres.

This study demonstrated that intermittent flows mobilize attached microbes and microspheres in a physically heterogeneous porous medium regardless of size or taxa; however, the degree of mobilization was dependent on microbe size and shape. Macropore and matrix flow was indicated by water infiltration through only eight of the 19 sampling ports, and by spatially heterogeneous flux and bromide recovery. Bromide recovery was 23%, which indicated diffusion of bromide into the soil matrix. Macropore- and matrix-dominated flow were categorized based on the cumulative bromide recovery within individual sampling ports, where lower bromide recovery was attributed to increased matrix diffusion and higher recovery indicated the presence of macropores. Intermittent flow altered flow paths in the soil and promoted pore-water exchange between macropores and soil matrices. Greater mobilization occurred through macropores compared to soil matrices. Mobilization varied with the size of

microbes and microspheres. Mobilization of larger, spherical *C. parvum* oocysts was greater than that of smaller, spherical MS-2 bacteriophage and rod-shaped *P. stutzeri* bacteria. This suggested shear forces mobilize larger particles. Cumulatively, the order of recovery was *C. parvum* oocysts > microspheres > MS-2 bacteriophage > *P. stutzeri* cells.

Introduction

From both public health and water resource protection perspectives, improving the understanding of geochemical and physical controls upon fate, transport, and persistence of pathogenic microbes within physically heterogeneous geologic media remains a key concern. This is particularly true within areas vulnerable to heavy rainfall. Infiltrating rainwater often mobilizes microbes originating from agricultural runoff, leaky sewer pipes, sanitary and septic systems, and wastewater discharge (Gerba et al., 2005). As water permeates through subsurface soil layers, microbes are removed from infiltrating water by adsorption or diffusion into soil matrices and some are transported all the way to the capillary fringe, where they enter the aquifer. Roughly 70% of waterborne diseases in the United States have been associated with groundwater (Han et al., 2006). To understand the processes that lead to contamination of groundwater, numerous studies have investigated the transport of various pathogenic microbes through ideal, homogeneous porous media under varying physical and geochemical conditions (Abudalo et al., 2005; Kenst et al., 2008; Cheng et al., 2010). However, few studies investigated the transport, retention, and mobilization of several pathogenic microbes concurrently within intact, heterogeneous porous media under unsaturated conditions. An improved understanding of the processes that govern microbe transport within subsurface soils is essential for accurate assessment of contamination risk of groundwater aquifers.

Five main processes control subsurface microbe transport in subsurface media: advection, dispersion, attachment, release, and inactivation. Similar to soil colloids, microbes exhibit subsurface transport behavior by advection and diffusion processes as well as immobilization by attachment to soil surfaces and the air-water interface (Wan et al., 1994; Majdalani et al., 2008). Many studies have focused on microbe transport (Brennan et al., 2011; Sen, 2011; Chen et al., 2012; Li et al., 2012), but far less investigation has focused on mobilization of attached microbes. Colloid mobilization, a two-step process, involves colloid detachment from soil grains (detachment step) and colloidal transport from detachment sites to the mobile porewater (transport step). Within the detachment step, colloid release from soil grains depends primarily upon geochemical and physical changes (Ryan et al., 1994b, a; Kretzschmar et al., 1999). Physical changes include fluctuating flow rates and transient moisture content; while geochemical processes comprise changes in ionic strength and pH, and displacement from more strongly sorbing colloids (DeNovio et al., 2004). The changes in geochemical and physical conditions are prevalent during intermittent flows and affect the mobilization of colloids. Subsequently, during transport processes, detached colloids migrate through soil pores and may be translocated from stagnant water into more mobile water. A number of studies (El-Farhan et al., 2000; Schelde et al., 2002; Zhuang et al., 2007) found that intermittent flow, categorized by periods of rainfall separated by antecedent drying periods, causes the release of considerably more colloids than steady flow does. Mobilization of colloids during intermittent flow events can be credited to diffusion (Schelde et al., 2002), shear forces (El-Farhan et al., 2000), hydrodynamic drag during flow increases (Li et al., 2005), scouring during movement of the air-water interface (Saiers et al., 2003), and reduced surface tension and capillary forces during rewetting (Wan et al., 1997). Consequently, variations in flow rates, moisture content, and the location of the wetting front and the air-water interfaces effectively control the magnitude of colloidal release during these intermittent flow events.

Colloid detachment, stimulated by physical and geochemical changes, is also a function of soil physical heterogeneity. Physical heterogeneity describes the spatial and temporal variability in soil physical properties, including differences in grain size distributions, soil types, moisture content, hydraulic conductivity, as well as the system of interconnecting pores within the soil. For example, a difference in flow rates between macropores and the matrix could cause differential transport of dissolved solutes or ions in rainwater and creation of a gradient in ionic strength from the pore waters of macropores to the soil matrix. A difference in ionic strength could trigger different amounts of colloid release (Mohanty, 2011). Kjaergaard et al. (2004) proposed that the dispersion of colloids may occur where the ionic strength of the less-mobile matrix pore water gradually decreases due to infiltration and displacement of high ionic strength soil water with rainwater of low ionic strength. The diffusion of colloids upon interaction with low ionic strength rainwater may be an important factor controlling colloid mobilization during rainless periods or in the absence of water infiltration. Moisture content has been shown to dramatically affect the degree of colloid mobilization during intermittent flow (Schelde et al., 2002; Majdalani et al., 2008). A difference in pore sizes between the soil matrix and macropores causes a differential gravitational drainage of water during intermittent flow; therefore, moisture content could vary between macropores and the matrix. A difference in the hydraulic conductivities of macropores and the matrix causes increased flow in macropores.

Rainwater infiltrates rapidly through soil macropores or preferential flow paths, but slowly through the soil matrix. Colloidal transport and mobilization have been shown to occur through preferential flow paths in saturated sand (Saiers et al., 1994; Bradford et al., 2002), unsaturated sand (Kenst et al., 2008; Mishurov et al., 2008), laboratory soils (Jacobsen et al., 1997; Kjaergaard et al., 2004), and field soils (Mailloux et al., 2003; Cey et al., 2009; Passmore et al., 2010; Nielsen et al., 2011). While these studies demonstrate the role of macropores in promoting colloidal transport, more research is needed to examine the effect of macropore distribution and the importance of water exchange between macropores and the matrix on the release of colloids. Schelde et al. (2002) demonstrated that colloids may be mobilized by diffusion through water-filled pores in the soil matrix during rainfall pauses. This suggests that colloids can be mobilized in macropores during flow events and the soil matrix may contribute to colloid transport during pauses in rainfall. The soil matrix may act as a long-term source of pathogenic microbes, trapping and releasing them slowly, while macropores promote a more rapid transport of the microbes during flow events (Flury et al., 1994; Bundt et al., 2001). Previous studies focused on steady infiltration or steady flow, or used homogenous and model porous media. Experiments using physically heterogeneous soil and intermittent flows are lacking.

Whereas transport of microbes in porous media has been studied extensively (DeNovio et al., 2004; Sen, 2011), little research has focused on comparison of the transport of microbes of varying size and taxa through heterogeneous porous media subjected to intermittent flow. Virus transport has been studied extensively under saturated and unsaturated flow conditions (Han et al., 2006; Kenst et al., 2008), in varying types of porous media (Ryan et al., 2002; Harvey et al., 2004; Abudalo et al., 2005), and under varying geochemical conditions (Bales et al., 1993; Zhuang et al., 2003). However, these studies did not investigate effects of varying microbe size or intermittent flow on transport and mobilization of viruses. The transport of protozoa, specifically *C. parvum* oocysts, has been studied under varying geochemical conditions (Abudalo et al., 2005; Hijnen et al., 2005; Metge et al., 2010a; Metge et al., 2011), and through disturbed and undisturbed soil columns (Darnault et al., 2004; Harter et al., 2008). Darnault et al. (2004) investigated the importance of macropore flow on *C. parvum* oocyst transport in intact soil cores; however, the effects of microbe size and intermittent flow on transport and mobilization remained uncertain. Bacteria have been studied (Ginn et al., 2002; Brennan et al., 2011; Chen et al., 2012; Li et al., 2012) under conditions similar to those examined for virus and protozoa transport. A recent study examined the role of macropore flow on *Escherichia coli* transport through intact soil cores subjected to several injections of bacterial cells (Martins et al., 2012). Although the role of transient flow was investigated, mobilization of attached bacteria was not. A similar study showed that 13% of attached *Escherichia coli* were mobilized during intermittent flows; however, homogeneous media (i.e., sand) was used (Mohanty et al., 2013b). Therefore, further study is needed to investigate microbial mobilization from intermittent flows in heterogeneous porous media. Hijnen et al. (2005) investigated the transport of MS-2 bacteriophage, *Escherichia coli*, *Cryptosporidium parvum*, and *Giardia intestinalis* concurrently in a sandy and a gravel soil; however, this investigation used hand-packed soil columns and a constant flow rate. While that study highlights the effects of microbe size on transport potential, it remained unclear how microbe release relates to intermittent flows through physically heterogeneous soil. Consequently, the combined effects of microbe size, soil physical heterogeneity, and intermittent flow are not well understood.

This study assesses the effects of soil physical heterogeneity upon transport and mobilization of three microbes of varying sizes: MS-2 bacteriophage, *Pseudomonas stutzeri* bacteria, and *C. parvum* oocysts, as well as 0.5 µm fluorescent carboxylated polystyrene microspheres, through an intact core of a fractured soil during intermittent rainfall events. Fractured soil cores were used in this study because their soil structure exemplifies soil physical heterogeneity; where the bedding planes and fractures provide colloidal transport pathways or corridors for microbes to move through the soil, while the soil matrix prevents rapid colloid movement. It was hypothesized that intermittent flow mobilizes microbes and microspheres within the soil, but the degree of mobilization likely depends on microbe size and soil macroporosity. To test these hypotheses, water samples were collected by a multi-port sampling grid at the base of the soil core. Microbes of three distinct sizes and microspheres were used to examine the effect of microbe size on their transport and mobilization during intermittent rainfall events.

Experimental Materials and Methods

MS-2 bacteriophage**:** The MS-2 bacteriophage was used in this study because of its structural similarities to human enteric viruses and its common use as a human virus surrogate in several transport and tracer studies (Bales et al., 1993; Tufenkji et al., 2011). MS-2 is also a fecal indicator (Mesquita et al., 2012). MS-2 is an icosahedral, single-stranded RNA (ssRNA) virus with an average diameter of 26.0 to 26.6 nm (Van Duin et al., 1988) and an isoelectric point of 3.9 (Powelson et al., 1994). Due to its isoelectric point, MS-2 possesses a net negative surface charge at the near-neutral pH employed in this column study. MS-2 infects male-specific *Escherichia coli* (*E. coli*) bearing an F-pilus. Its specific host strain, *E. coli* HS(pFamp)R (*Escherichia coli* ATCC® 700891™), contains genes resistant to both ampicillin and streptomycin sulfate antibiotics, which prevents bacterial growth contamination and allows MS-2 to be enumerated specifically. The MS-2 virus was plated with its *E. coli* host on trypticase soy agar (TSA), and plaque-forming units (PFU) were estimated using the double agar layer (DAL) assay (Williams et al., 2001).

Due to large concentrations of MS-2 virus needed for this study, a modified production agar technique was developed to allow propagation of large viral titers. Freeze dried MS-2 was obtained from the American Type Culture Collection (MS-2 bacteriophage, ATCC®15597-B1™) and initially propagated using methods described previously (Adams, 1959). Once an initial volume of filtered MS-2 solution was obtained, the production agar technique was applied to rapidly propagate a titer of about 10^{11} PFU. The production agar technique uses a softer agar overlay of 0.35% TSA instead of the 0.7% TSA top agar layer used in the DAL method, but employs the same 1.5% TSA bottom agar layer. After 24 h of incubation, the softer production agar was flooded with an anti-coagulant, phosphate buffered saline (PBS, pH 7.5), in order to suspend viral plaques in the production agar and to prevent MS-2 plaques from aggregating once centrifuged. After several minutes of soaking in PBS, the production agar was scraped off the surface of the plates with a sterile loop. The production agar-PBS mixture was then centrifuged (4,750 rpm, 50 min, 10°C) to sediment the agar and cellular debris. The supernatant was collected, filtered through 0.45 µm Millipore filter, stored, and then used iteratively to propagate additional MS-2. This production agar technique was used repeatedly until the desired concentration of about 10^{11} PFU was met, suspended in 2 L of PBS. However, PBS may adversely affect microbe sorption and promote transport (Zhuang et al., 2003; Wang et al., 2011). Therefore, the MS-2 and PBS were separated by centrifugation in a super-speed centrifuge (Sorvall SS-34 Centrifuge, 10°C, 6 h, 50,228 g), pelleting the MS-2 bacteriophage and leaving a PBS supernatant. The PBS supernatant was discarded, and the MS-2 'pellet' was re-suspended in 5 mL of PBS, thereby significantly reducing the volume of the MS-2 suspension and preventing excess PBS from affecting sorption or transport of the microbes. The MS-2 bacteriophage concentration was $4.65 \pm 1.9 \times 10^{7}$ PFU mL^{-1} in a total 2 L injectate volume used in the column study.

***Pseudomonas stutzeri* bacteria**: A groundwater bacterium, *Pseudomonas stutzeri*, was used as the model bacterium in this study. *P. stutzeri* cells are about 1 µm in diameter and their surface charge is negative at the near-neutral pH of this study (Harvey et al., 2011). The *P. stutzeri* cells were modified by insertion of a gene coding for production of blue fluorescent protein (*bfp*), in order to enumerate the bacteria using epifluorescence microscopy and to avoid the negative effects of staining cells will DNA-specific fluorescent dyes (Metge et al., 2007; Haack et al., 2012). A nutrient broth containing 1% TSB, 90% filtered deionized water (DI; Millipore, Milli-Q, >18 Mohm resistivity), 9% soil-extract broth, 10 mg L^{-1} arabinose, and 50 mg L^{-1} ampicillin was used to grow *P. stutzeri* cells to the desired concentration. After growth, the *P. stutzeri* suspension was centrifuged, washed in filtered DI, and suspended in about 10 mL of PBS to prevent coagulation (Haack et al., 2012). The *P. stutzeri* cell concentration was $2.67\pm0.08\times10^{8}$ cells mL^{-1} in the 2 L injectate used in the column study. *P. stutzeri* enumeration was performed using epifluorescence microscopy; peak excitation and emission wavelengths for *P. stutzeri* are 359 and 461 nm, respectively.

***Cryptosporidium parvum oocysts*:** Formalin-inactivated *C. parvum* oocysts were obtained from the Sterling Parasitology Laboratory (SPL) at the University of Arizona, Tucson. The oocysts were shed from a calf infected by the Iowa isolate of *C. parvum* (Dr. Harvey Moon, National Disease Center, Ames, Iowa), purified, inactivated in formalin, and enumerated as described previously (Abudalo et al., 2005). Prior to use in this study, oocysts were centrifuged as described previously (Harvey et al., 2008), stained with the DNA-specific fluorescent dye 4’,6-diamidino-2-phenyl-indole (DAPI, 0.1 mg L^{-1}, final concentration, >90 min staining time), filtered through a 1.0 µm filter, washed with 10^{-3} M sodium chloride to remove excess stain, and re-suspended in 10^{-3} M sodium chloride. The formalin-inactivated *C. parvum* oocysts have an average diameter of 3.6 µm with an isoelectric point of about 3, which results in a net negative surface charge at the pH range in this study (Abudalo et al., 2005). The final oocyst concentration was $7.6\pm1.5\times10^{5}$ cells mL^{-1} in the 2 L injectate. Oocyst enumeration was performed using epifluorescence microscopy; peak excitation and emission wavelengths for DAPI-stained oocysts are 359 and 461 nm, respectively (Metge et al., 2010b).

***Microspheres*:** A well-dispersed mixture of 0.5 µm diameter fluorescent, carboxylated polystyrene microspheres (Polysciences, Warrington, Pennsylvania) was prepared in 2 L of DI water to achieve a final concentration of $6.59 \pm 0.44\times10^{7}$ particles mL^{-1}. Microsphere concentration in the injectate was determined by epifluorescence microscopy and replicate counts allowed for standard error to be determined.

Error calculations**:** Errors in enumerations were calculated for MS-2 bacteriophage, *P. stutzeri*, *C. parvum* oocysts, and microspheres. For MS-2, standard errors were calculated for samples that required serial dilutions, or samples with counts outside of optimal range that required additional viral assays. Only MS-2 samples that required replicate double agar layer assays were analyzed for error. Standard errors for *P. stutzeri* cells, *C. parvum* oocysts, and microspheres were calculated from replicate epifluorescence microscopy cell counts. Standard deviations from the mean were calculated for MS-2 bacteriophage, *P. stutzeri*, *C. parvum* oocysts, and microspheres and divided by the square root of the number of replicate samples to obtain standard error.

Intact soil core sampling**:** Intact soil cores were sampled from the base of a hill slope in the Melton Branch watershed on land in the Oak Ridge Reservation, Tennessee (Luxmoore et al., 1987). The soil is comprised of fractured shale saprolite weathered by an average of 130 cm y^{-1} of rainfall. Bedding planes and fractures conduct the predominant amount of infiltrating water. These bedding planes and fractures contain iron(III) and manganese oxyhydroxides and translocated clay mineral coatings (Jardine et al., 1993). The bedding planes and fractures in the soil core used in this experiment have a dip of 30° at a strike of roughly 90°.

A hand-sculpting method was used to collect intact soil cores (Jardine et al., 1993). Vegetation and the organic layer of the soil horizon were removed from sample sites. Soil in the A-horizon was excavated to expose a circular soil core which was trimmed to fit inside polyvinylchloride (PVC) pipe of 30.5 cm height and 25.4 cm width. To prevent the soil from moving within the PVC housing, the approximately 1.2 cm gap between the soil and PVC pipe was filled with expandable polyurethane foam (US Composites).

Soil cores used in this study were cut to a height of 15 cm. A hole was cut into the PVC housing at 7.5 cm from the top soil surface to allow insertion of a soil moisture probe (Delta-T Devices, Theta Probe MLX2), which allowed real-time moisture content monitoring (1 min intervals) by a data logger (DATAQ Instruments, DI 710). This moisture content monitoring provided experimental integrity by providing evidence that the soil core never reached fully saturated conditions.

***Experimental setup*:** Bromide tracer and microbe and microsphere transport and mobilization experiments were conducted using a rainfall simulator comprised of a rainfall reservoir, a peristaltic pump, the soil core, a 19-port sampling grid, and sample tubes (Figure 2.1). The peristaltic pump delivered rainfall solutions of varying composition (10^{-4} and 10^{-5} M sodium chloride, 10^{-3} M bromide, microbes and microspheres) to the rainfall reservoir. Rainfall was simulated by dripping solutions uniformly (2.0 cm h^{-1}) over the surface of the soil core through 85 needles (stainless steel, 25 gauge) located underneath the rainfall reservoir. The intact soil core was positioned underneath the rainfall reservoir, on top of the 19-port sampling grid that directed water to discrete sample tubes (glass, 2.5 cm diameter, 25 cm length). The rainfall simulator and the location and numbering of the 19 ports in the sampling grid are illustrated in Figure 2.1. The total collection area of the soil core was 340 cm^2, with each of the 19 ports collecting an area of 11.4 cm^2. This spatial distribution of sampling ports allowed for water flow through macropores (e.g., bedding planes, fractures, roots, worm burrows) and the soil matrices, as well as identification of the amount of water flowing along different paths. A waste channel (1.3 cm width) collected any water that flowed around the column or perimeter of the soil core. Water flowing to each sampling port from the base soil surface was under zero tension.

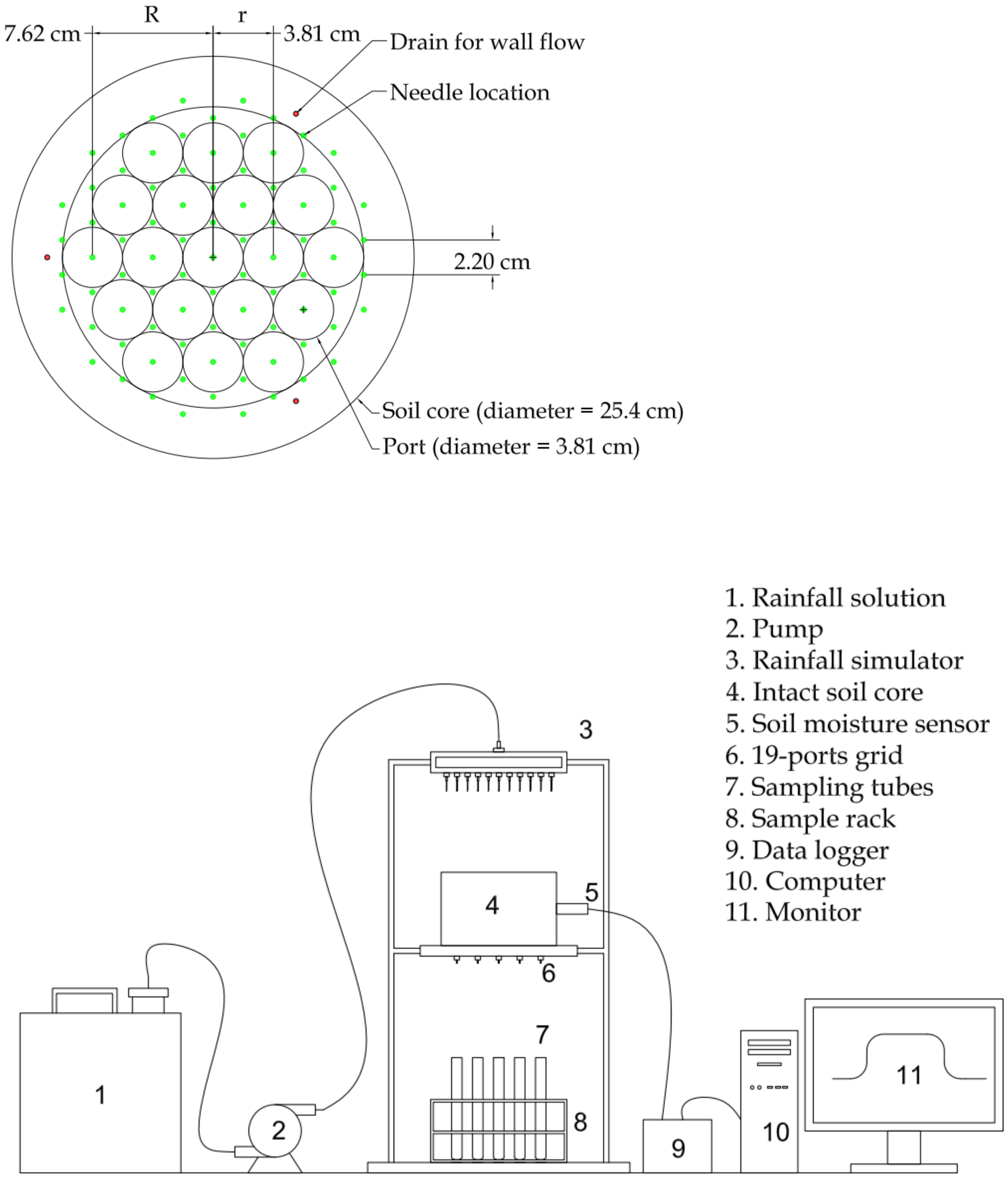

Figure 2.1. Column setup to examine the mobilization of microspheres and microbes from an intact fractured soil core. The 19 ports (3.81 cm diameter) were arranged in a hexagonal pattern. The center port is designated as “00”. The inner hexagon contains six ports at a center-to-center distance of a maximum of 3.81 cm from port 00 and is designated as “r” followed by an angle. The outer hexagon contains 12 ports at center-to-center distance of a maximum of 7.62 cm and is designated as “R” followed by an angle. The 85 needles of the rainfall reservoir, shown as green dots, were arranged in hexagonal pattern with a closest distance between two needles of 2.2 cm (Mohanty, 2011).

***Bromide tracer*:** A bromide tracer (9.1×10^{-4} M) was applied to the intact soil core after the flow rates in active ports were equilibrated, a process in which 10^{-5} M sodium chloride is applied onto the soil core for three days until flow rates reach a quasi-steady state. Because of limited sample volumes in some ports, the bromide tracer test was performed in the soil core three days prior to the microbe injection. Bromide in the core effluent was measured with a bromide ion-specific electrode (Orion, model 9435BN) and meter (Orion, 3-Star Plus pH Benchtop Meter), after daily calibrations with serially diluted bromide standards (10^{-1}-10^{-6} M).

***Identification of physical heterogeneity*:** To examine the effect of soil physical heterogeneity on the mobilization of microbes and microspheres, infiltrating water samples were collected at the 19-spatially arranged ports and monitored for bromide. Previous experiments by Jardine et al. (1993) showed rapid infiltration through bedding planes and fractures, and slow percolation through shale saprolite and clay layers; thus, similar results were expected in this study. Flow was quantified at the ports where flow paths culminate, not within specific flow paths. Ports with higher flow rates (or flux) are assumed to contain more macropores than ports with low flow rates. Bromide breakthrough curves were calculated for each actively-flowing port by applying the bromide tracer solution described previously. The rainfall application rate (2.0 cm h^{-1}) is typical of a heavy rainfall event in Oak Ridge, Tennessee (Wilson et al., 1990). Bromide recoveries at the sampling ports were used to indicate whether macropores were present or absent and to estimate the matrix diffusion. A decreased recovery of bromide was associated with increased residence time and increased diffusion into the soil matrix (Mohanty et al., 2013a).

***Microbe injectate*:** The microbe injectate consisted of the MS-2 solution, *P. stutzeri* cell solution, *C. parvum* oocyst solution, and the microsphere solution in DI water, resulting in a 2 L injectate volume total (Table 2.1). First, 1 L of DI water was placed into the rainfall reservoir along with a stir bar and the microspheres. Next, the MS-2 solution in PBS, the *P. stutzeri* solution in PBS, and the *C. parvum* oocyst solution in 10^{-3} M sodium chloride were added to the rainfall reservoir. After allowing solution to mix for 10 min, DI water was added to the reservoir until the desired 2 L volume was reached, determined gravimetrically.

Table 2.1. Concentration of microbes and microspheres in microbe injectate.

Solution Constituent	Final Injectate Concentration	Units
MS-2	$4.65\pm1.9\times10^{7}$	PFU mL^{-1}
P. stutzeri	$2.67\pm0.08\times10^{8}$	cells mL^{-1}
C. parvum	$7.6\pm1.5\times10^{5}$	cells mL
Microspheres	$6.59 \pm 0.44\times10^{7}$	particles mL

***Transport and mobilization experiments*:** To investigate the transport and mobilization of microbes and microspheres, the injections were carried out in four phases: application and recovery phases of bromide, followed by attachment and release phases of microbes and microspheres. The bromide tracer injection was carried out separately from the microbe and microsphere injection because of sample volume limitations. During the bromide tracer application phase, a 10^{-3} M sodium bromide solution was applied at a rate of 2.0 cm h^{-1} for 2.5 h, followed by an application of bromide-free solution (10^{-4} M sodium chloride) for 4 h. Next, the bromide recovery phase ensued with two intermittent flow events (10^{-4} M sodium chloride, 2.0 cm h^{-1}, 4 h) to transport bromide diffused in soil matrices. Intermittent flow events were simulated by 4 h rainfall periods separated by 20 h pauses in rainfall during which pore water drained from the soil core under gravity.

During the microbe and microsphere attachment phase, the injectate (Table 2.1) was applied at a rate of 2.0 cm h^{-1} for 3.8 h followed by an application of microbe/microsphere-free solution (10^{-3} M sodium chloride) for 17.3 h (Figure 2.2). The microbe and microsphere release phase followed the bromide injection with three intermittent rainfall events (4-6 h duration, 10^{-3} M sodium chloride solution, 2.0 cm h^{-1} rainfall rate) separated by pauses in rainfall of 24 h (Figure 2.2). In the microbe and microsphere release phase of the experiment, 24 h pauses were used instead of 20 h pauses used for the bromide injection because of the 24 h-steady applications of the microbe and microsphere injectate and 10^{-3} M sodium chloride rinse. In order to prevent the soil core from approaching saturated condition, additional drying time was required between intermittent rainfall events during the microbe and microsphere injection.

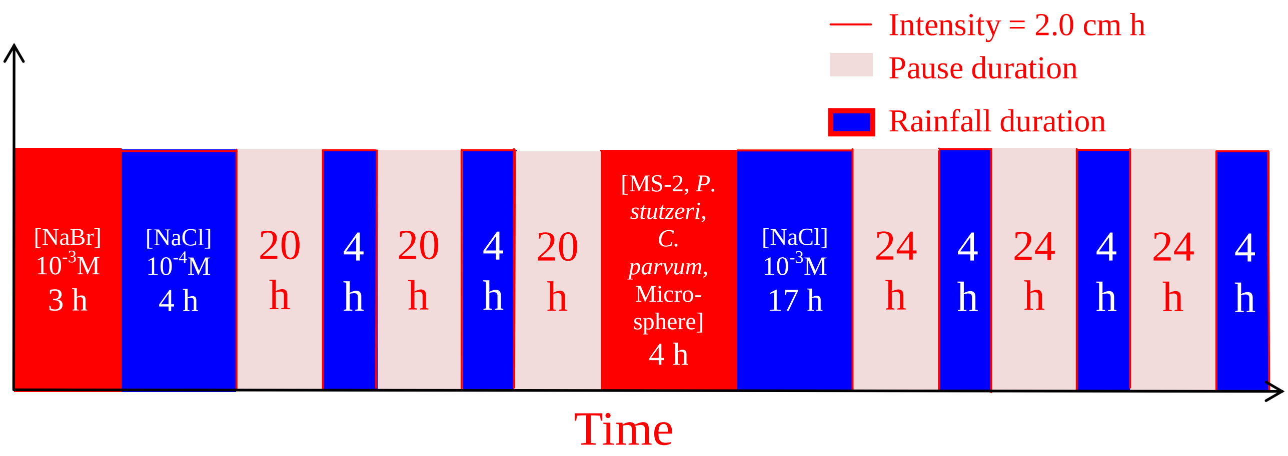

Figure 2.2. Experimental timeline of bromide tracer and microbe and microsphere injections.

***Analysis of water samples*:** Samples from the 19 ports were analyzed to measure sample volume, pH, specific conductivity, turbidity, and the concentration of bromide, microbes, and microspheres. The sample volumes were measured gravimetrically. The pH was measured using a pH meter (Orion 3-Star Plus pH Benchtop Meter) and combination electrode (Orion, model 9157BNMD). The specific conductivity was measured using a conductivity meter (Oakton pH/CON 300) and electrode (Accumet Conductivity Probe). Turbidity was measured using a turbidity meter (Hach, model 2100N). Turbidity was converted from nephelometric turbidity units (NTU) into colloid concentration (mg L^{-1}) using methods described previously (Mohanty, 2011). Bromide concentration was measured using a meter (Orion 3-Star Plus pH Benchtop Meter) and bromide ion-selective electrode (Orion, model 9435BN).

Concentrations of *P. stutzeri* cells, *C. parvum* oocysts, and fluorescent microspheres were measured by epifluorescence microscopy (Nikon Eclipse 2000i, 63-100× magnification). If needed, samples were diluted and filtered through black polycarbonate membranes (0.2 µm, 25 mm diameter, GE Osmonics). The membrane filters were applied to a glass slide, followed by a drop of immersion oil (Type FF, Cargille Laboratories, NJ) and a cover slip. The slides were placed under the microscope and the microbes and microspheres were counted manually. The DAPI-stained oocysts and *P. stutzeri* were counted at excitation and emission wavelengths of 359 nm and 461 nm, respectively. The fluorescent microspheres were counted at excitation and emission wavelengths of 535 nm and 590 nm, respectively. Microbes and microspheres were distinguished by a difference in fluorescent color, size, and shape. They were enumerated in at least 10 random fields on each membrane with approximate values recorded as the average and standard error.

Concentrations of MS-2 bacteriophage were measured by double agar layer assay (Williams et al., 2001). Samples were serially diluted and plated individually. After 16-24 h of incubation, petri dishes containing the MS-2 plaques were counted on a magnified colony counter (Quebec Dark field counter, Reichert Jung Ltd.). The desired number of MS-2 plaque counts per plate ranges from zero to 300 PFU (Telliard, 2001). Therefore, all MS-2 samples with PFU counts higher than 300 were serially diluted and re-plated.

Results

Distribution of water in soil core during rainfalls**:** The average flux varied widely within the multiple sampling ports during the bromide injection (Table 2.2). Of the 19 sampling ports, only eight were active, which suggests that over half of the soil core did not conduct infiltrating rainwater during the simulated rainfall periods. Rainwater was conducted through only 42% of the bottom surface, which suggests that preferential flow occurred. Flux during each sampling time was calculated and used to determine the average flux in each active port overall. Spatial variations in flux were apparent from the averaged flux values observed in the eight active ports (0.57 to 10.5 cm h^{-1}). The flux in active ports also had temporal variations during steady rainfall application, and smaller temporal variations during intermittent flow, which was marked by increasing flux in some ports and decreasing flux in others throughout the experiment (Figure 2.3). While flux in individual ports varied temporally throughout the experiment, the total flux through the core remained relatively unchanged during the bromide tracer (2.24 to 2.40 cm h^{-1}), which indicated that exchange of infiltrating water between flow paths (matrix versus macropore flow) and different active ports occurred. This change in flow path was also observed directly during the bromide tracer injection, when flux in Port r300 ceased and the flux in adjacent Port r0 started at a nearly identical rate (Figure 2.4). This change in flow path occurred within the first hour of the first intermittent rainfall event during the bromide injection. For comparison with breakthrough curves of the microbes, the flux, bromide breakthroughs, and recoveries for Ports r300 and r0 were combined and reported as Port r0.

Table 2.2. Average flux and percent bromide recovery in active ports during bromide tracer. Standard error in the average flux was determined by the flux calculated in each port during each sampling time and the standard deviation. Bromide recoveries (%) are expressed as the bromide mass recovered out of the total bromide mass transported through each port individually.

Port ID	Flux (cm h^{-1})	Bromide Recovery in Individual Ports (%)		
		Total[a]	BTC[b]	Transient[c]
R90	0.6 ± 0.1	2.94	2.90	0.04
r240	2.2 ± 0.4	18.0	17.9	0.15
R120	3.1 ± 0.4	11.1	10.4	0.66
R60	4.9 ± 0.6	10.8	10.0	0.89
r180	8.7 ± 1.1	44.9	44.8	0.02
R240	8.7 ± 1.4	15.8	15.6	0.17
r0	9.7 ± 2.2	28.4	28.2	0.19
R150	10.5 ± 1.7	15.3	15.1	0.19

[a] Total mass percent of bromide recovered in each port overall
[b] Mass percent of bromide recovered during the initial breakthrough application of bromide
[c] Mass percent of bromide recovered in each port during intermittent flow events

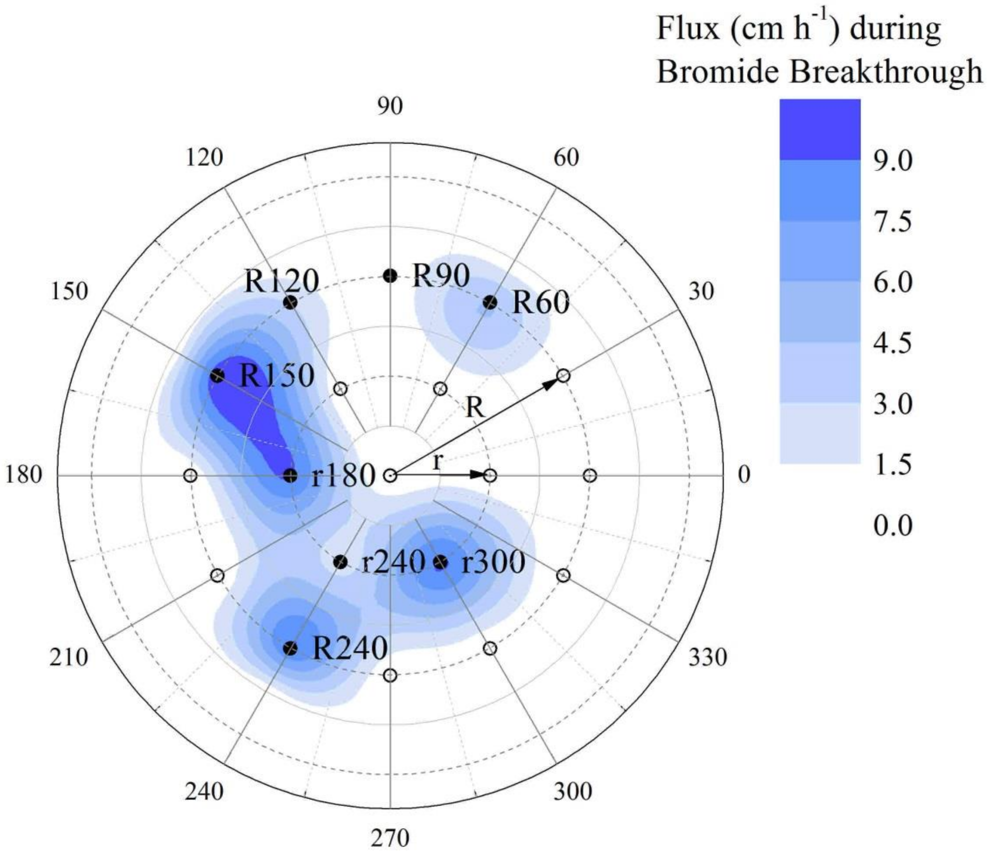

Figure 2.3. Distribution of average flux in 19 ports at the base of the core during injection and breakthrough of bromide tracer. The eight active ports are designated by solid circles and the remaining eleven ports are marked with open circles. The bedding planes in the soil dipped at 30° with a strike of 90° on this coordinate system.

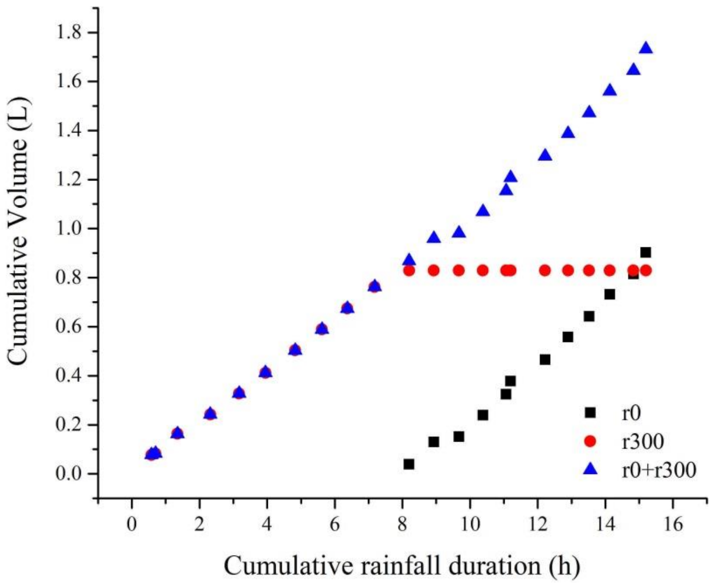

Figure 2.4. Cumulative volume as a function of rainfall duration for Ports r0 and r300. Cumulative volume is the total amount of water that passed through the corresponding port at a given time.

Bromide recovery and the shape of bromide breakthrough curves exhibited different behavior among the various active ports (Table 2.2). About 23% of the total bromide tracer injected was recovered from the core, but the recovery varied among active ports (Figure 2.5). Bromide recovery at each port was weakly correlated to flux at corresponding ports (Pearson's r = 0.62, $R^2 = 0.27$) (Figure 2.6). In general, the bromide recovery was greater in sampling ports with higher fluxes. For example, the greatest flux occurred through Port R150, but the greatest bromide recovery occurred in Port r180. The bromide breakthrough curve characteristics also varied amongst active ports. In general, active ports with high flux exhibited a high maximum in the bromide breakthrough curves; while ports with lower fluxes showed more tailing (Figure 2.5.a). Breakthrough and breakthrough curves (BTC) are expressed in terms of M/M_0, the ratio of the mass measured in the effluent sample (M) to the input mass (M_0). Cumulative recovery is expressed as the cumulative mass breakthrough in each port, or the summation of M/M_0 over time [$\Sigma(M/M_0)$].

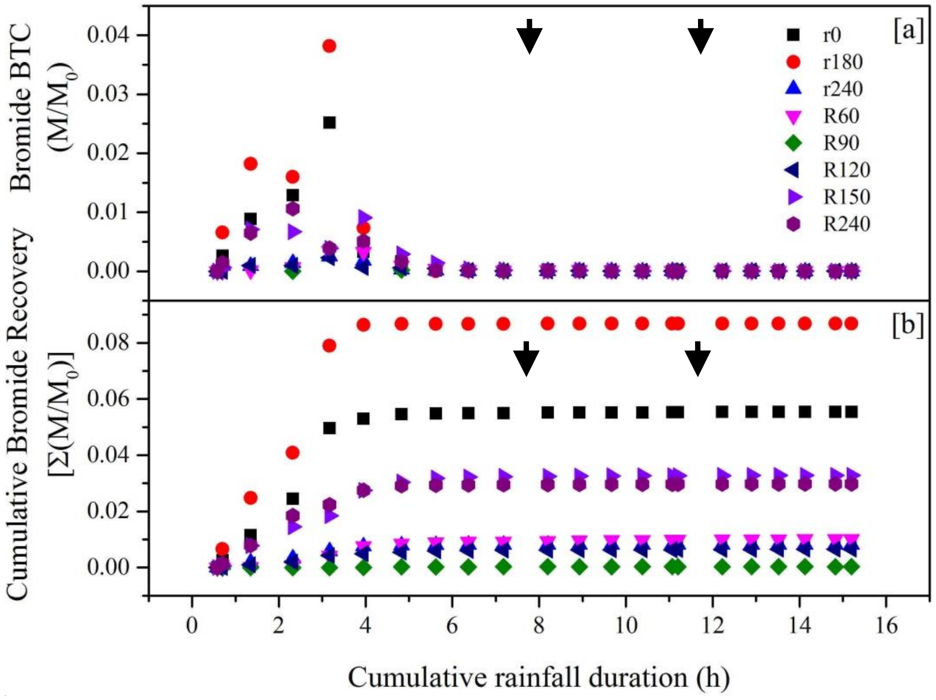

Figure 2.5. (a) Bromide breakthrough (M/M_0) as a function of rainfall duration and (b) cumulative bromide recovery [$\Sigma(M/M_0)$] as a function of rainfall duration. Arrow marks indicate pause in rainfall for 24 h.

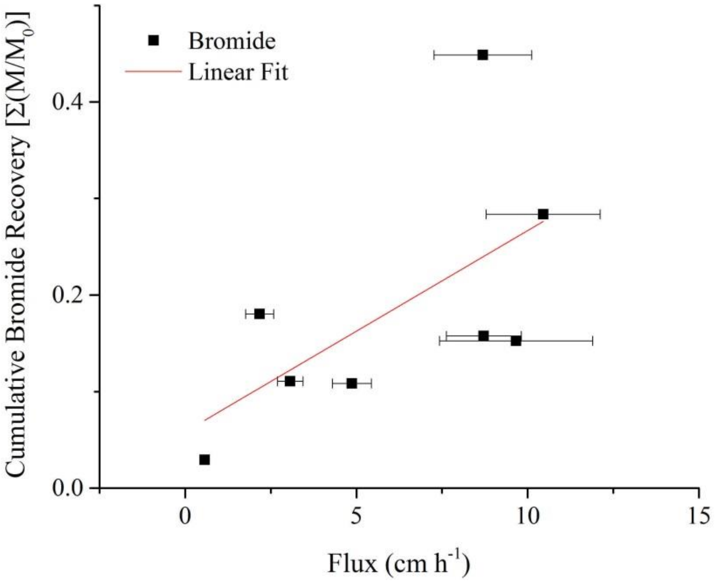

Figure 2.6. The recovery of bromide in eight active ports as a function of flux at the corresponding sampling ports.

The average flux during the microbe injection varied dramatically within the multiple active sampling ports (Table 2.3). Spatial variations in flux were observed in the active ports (0.17 to 5.77 cm h^{-1}). The flux in active ports also varied temporally during intermittent flow periods, with some ports experiencing increases and others experiencing decreases in flux (Figure 2.7). However, the total flux exhibited by the core remained relatively unchanged during the microbe injection (1.11 to 1.24 cm h^{-1}).

Table 2.3. Average flux in active ports during the microbe injection.

Port ID	Flux cm h^{-1}
R90	0.2 ± 0.1
r240	1 ± 0.6
R120	2.4 ± 0.5
R60	3.5 ± 0.9
r180	4.3 ± 2.3
R240	4.4 ± 0.9
R150	5.4 ± 1.6
r0	5.8 ± 1.4

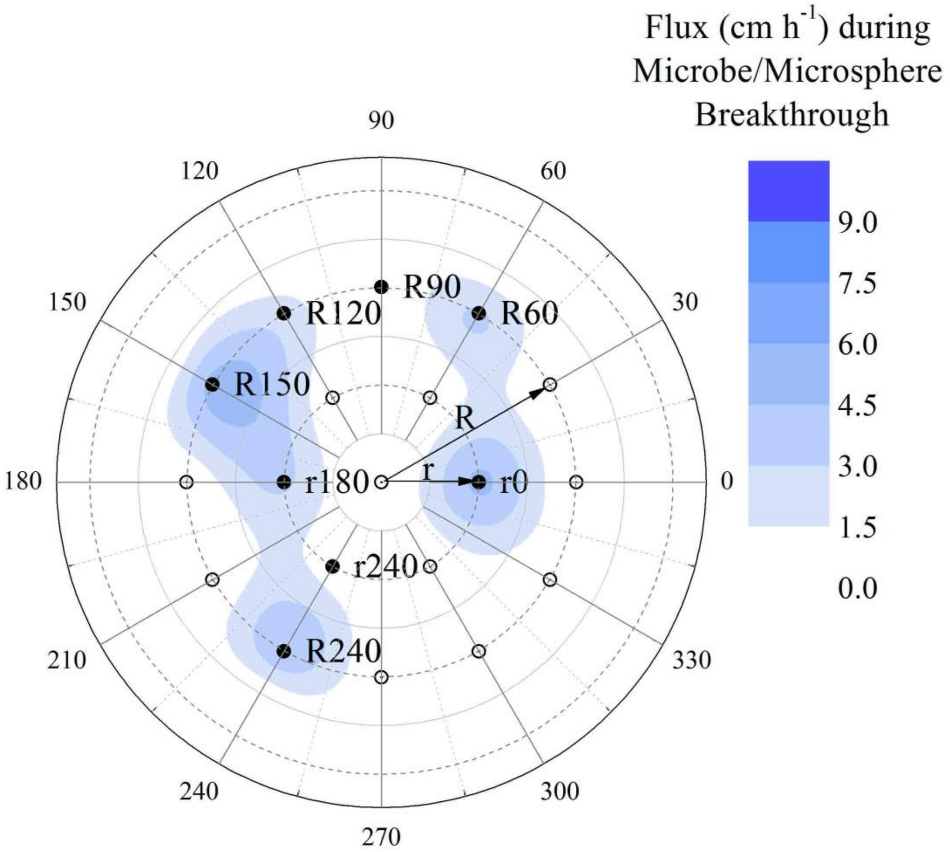

Figure 2.7. Distribution of average flux in 19 ports at core base during injection of microbes and microspheres. The eight active ports are designated by solid circles and the remaining eleven ports are marked with open circles. The bedding planes in the soil dipped at 30° with a strike of 90° on this coordinate system.

***Transport and mobilization of colloids, microspheres and microbes*:** The effluent turbidity, a measure of colloid concentration (mg L^{-1}), increased during the microbe injection and decreased during flushing with microbe-free solution. The effluent colloid concentration also peaked during the start of successive intermittent rainfall events, and the height of the colloid peak increased with successive intermittent flow events (Figure 2.8.a). Breakthrough of MS-2, *P. stutzeri* cells, *C. parvum* oocysts, and microspheres occurred at all active ports; however, the breakthrough curve characteristics varied among ports. The peaks of the microbes' breakthrough were independent of flux (Figure 2.8.b). In general, the spherical *C. parvum* oocysts, MS-2 bacteriophages, and microspheres were recovered more than the rod-shaped *P. stutzeri* bacteria (Table 2.4). However, the order of recovery varies among ports. The cumulative recoveries of microbes and microspheres among ports varied (Figure 2.9). There was a constant flux of microspheres in the effluent over 38.6 h, while 80% of *C. parvum* oocysts, 70% of MS-2, and 86% of *P. stutzeri* were recovered in 5 h. The remaining *C. parvum*, MS-2, and *P. stutzeri* were recovered slowly over the next 33 h. Overall, the microbes and microspheres were transported and recovered according to the following order (Table 2.4):

C. parvum oocysts > microspheres > MS-2 bacteriophage > *P. stutzeri* cells

Table 2.4. Cumulative recoveries for MS-2 bacteriophage, *P. stutzeri* cells, *C. parvum* oocysts, and microspheres in all ports total during the microbe experiment (breakthrough and intermittent flows).

Microbe	Cumulative Recovery (%)
MS-2 bacteriophage	5.2%
P. stutzeri cells	4.3%
C. parvum oocysts	8.4%
Microspheres	7.9%

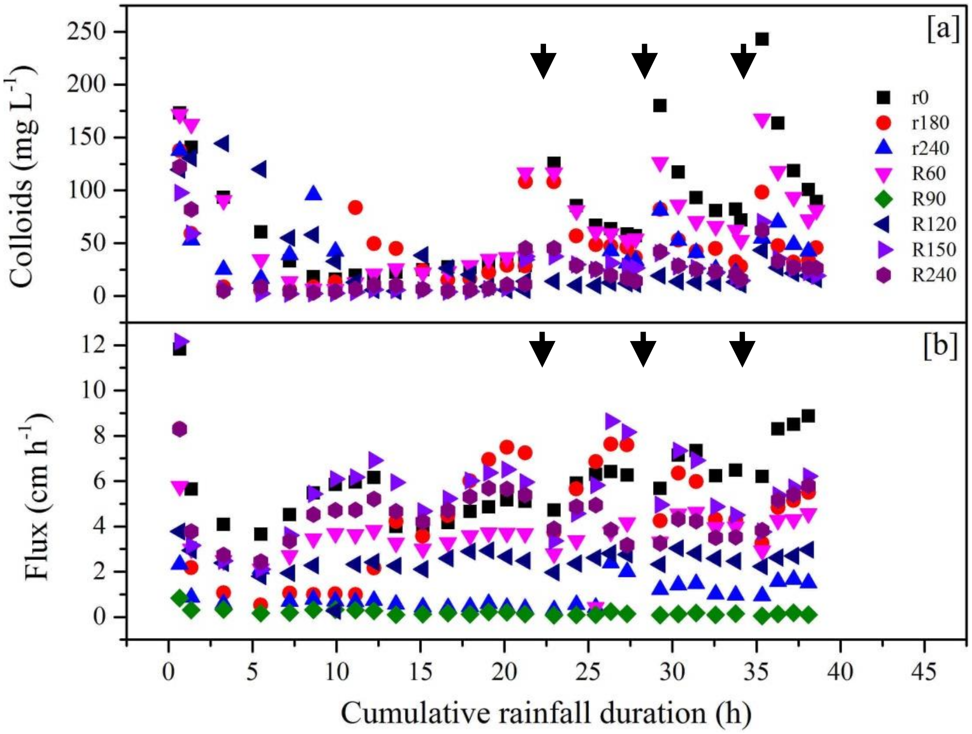

Figure 2.8. (a) Flux and (b) colloid concentration at eight active ports out of total 19 ports during microbe injection. Arrow marks indicate pause in rainfall and start of gravity drainage of pore water for 24 h.

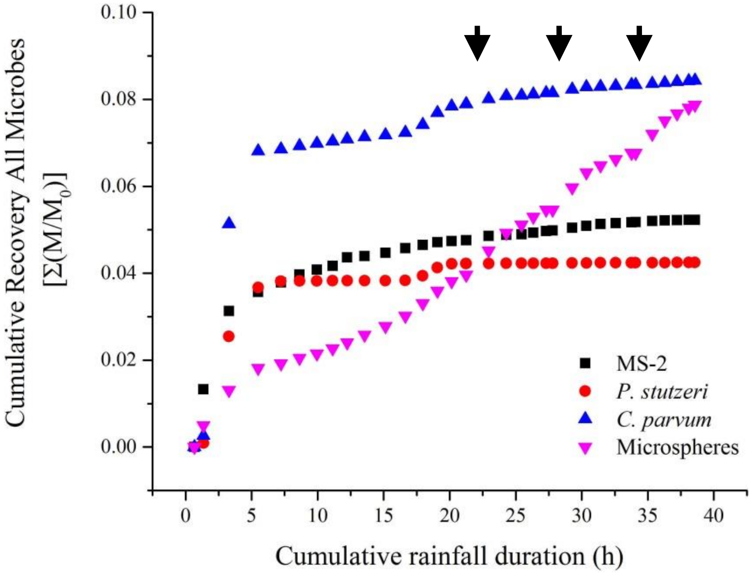

Figure 2.9. Cumulative recoveries for MS-2, *P. stutzeri* cells, *C. parvum* oocysts, and microspheres in all ports during the microbe experiment. Arrow marks indicate pause in rainfall for 24 h.

Recovery varied between active ports. The eight active ports have been separated and grouped into three categories: matrix ports, intermediate macropore ports, and preferential flow path ports. Each of the three port categories are grouped together due to similar microbe breakthroughs, behavior of individual microbes, and order of recoveries. The matrix ports were R60, R90, and R240; the intermediate ports were r180, r240, and R150; and the macropore ports were r0 and R120. One port from each category (R90, r180, R120; Figure 2.10) will be explained and analyzed in depth in the Discussion.

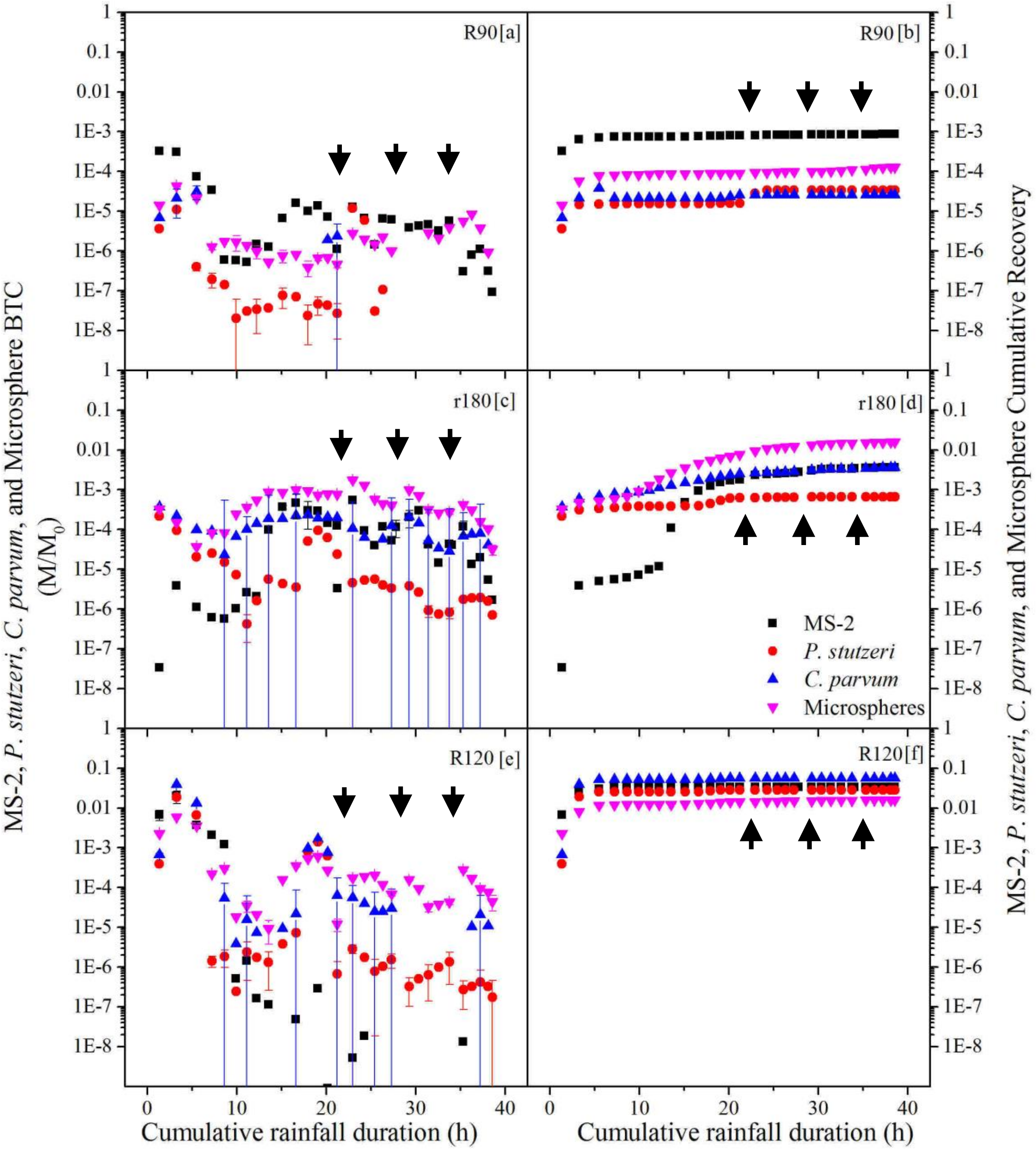

Figure 2.10. Breakthrough curves and cumulative breakthroughs for representative matrix port (a and b), intermediate macropore port (c and d), and preferential flow path port (e and f). Microbes were applied for 3.8 h followed by an application of 10^{-3} M sodium chloride for another 17.3 h. Arrow marks indicate pause in rainfall and start of gravity drainage of pore water for 24 h. Error bars indicate standard error.

Intermittent flow caused the mobilization of microbes and microspheres that were previously attached during their injection (Figure 2.10.a-f). A peak in microbe and microsphere concentration occurred at the commencement of rainfall, and the concentration of microbes and microspheres decreased as rainfall continued. In general, the heights of the peaks decreased with successive intermittent flow events; however, the height of the peak increased with consecutive intermittent flows in several instances (e.g., *P. stutzeri* cell mobilization in port R120 at 29.3 to 34.1 h; Figure 1.10.e). Intermittent flows mobilized 0 to 1.85% of the MS-2, 0 to 0.13% of the *P. stutzeri*, 0 to 1.80% of the *C. parvum*, and 0.28 to 14.5% of the microspheres retained in individual ports during injection (Table 2.5).

Table 2.5. Quantity of microbes and microspheres transported and retained during breakthrough and the quantity mobilized through eight ports during intermittent flows.

Port	MS-2 bacteriophage			*P. stutzeri* Cells			*C. parvum* Oocyst			0.5 µm microsphere		
	Transported[a]	Retained[b]	Mobilized[c]	Transported[a]	Retained[b]	Mobilized[c]	Transported[a]	Retained[b]	Mobilized[c]	Transported[a]	Retained[b]	Mobilized[c]
R90	3.86%	96.1%	0.29%	0.25%	99.7%	0.13%	0.47%	99.5%	0.00%	0.67%	99.3%	0.28%
r240	0.06%	99.9%	0.48%	0.06%	99.9%	0.02%	0.42%	99.6%	0.72%	0.46%	99.5%	3.63%
R120	19.2%	80.8%	0.00%	25.3%	74.7%	0.02%	49.7%	50.3%	0.38%	12.6%	87.4%	1.80%
R60	3.87%	96.1%	0.97%	0.07%	99.9%	0.03%	0.95%	99.1%	0.70%	1.74%	98.3%	4.13%
r180	1.87%	98.1%	1.85%	1.06%	98.9%	0.06%	4.04%	96.0%	1.80%	12.3%	87.7%	14.5%
R240	0.05%	100.0%	0.00%	0.14%	99.9%	0.02%	0.71%	99.3%	0.23%	1.37%	98.6%	2.58%
R150	0.00%	100.0%	0.01%	0.10%	99.9%	0.01%	0.79%	99.2%	0.56%	1.31%	98.7%	3.94%
r0	5.13%	94.9%	0.67%	2.32%	97.7%	0.03%	1.10%	98.9%	0.54%	2.16%	97.8%	3.72%

[a] Ratio of total amount transported to the port to the total amount injected during breakthrough.
[b] Ratio of total amount removed to the port to the total amount injected during breakthrough.
[c] Ratio of total amount mobilized to the port during intermittent flow to total amount removed during breakthrough.

In each of the port categories and their representative ports (r180, R90, R120), a "secondary peak" in microbe and microsphere concentration was observed at about 10 h of cumulative rainfall duration. This secondary peak in microbe and microsphere concentration crested and decreased up to the start of the first intermittent rainfall event and antecedent drying period (Figure 2.10.a, c, e). Initial peak breakthrough occurred within the first few hours of microbe injection, and microbe and microsphere concentration decreased until about 7 to 10 h, at which point the secondary peaks began to take shape in all port categories. In intermediate macropore ports, the secondary peaks in breakthrough occurred for all microbes regardless of size. In matrix ports, the secondary peaks in breakthrough occurred for only MS-2, microspheres, and *P. stutzeri*, owing to the nearly complete retention of *C. parvum* during breakthrough in Port R90. In preferential flow path ports, the arrival of the secondary peak was slightly retarded compared to intermediate macropore and matrix ports.

The mobilization varied with size of the microbes and microspheres as well as the port. Each port varied in terms of physical heterogeneity: flux and degree of macroporosity. In matrix ports (R90, Figure 2.10.a-b), the mobilization of MS-2 was greatest, followed by microspheres, *C. parvum* oocysts, and *P. stutzeri*, respectively. In intermediate macropore ports (r180, Figure 1.10.c-d), the microspheres were mobilized to the greatest extent, followed by *C. parvum* oocysts, MS-2, and *P. stutzeri*, respectively. In preferential flow path ports (R120, Figure 2.10.e-f), the mobilization of *C. parvum* oocysts was highest, followed by MS-2, *P. stutzeri*, and microspheres, respectively.

The fractions of microbes and microspheres retained, transported, and mobilized were analyzed as a function of flux to determine if any correlations existed (Figure 2.11.a-c). The fraction of microbes and microspheres transported through the soil core has no direct relationship with flux (Figure 2.11.b). Port R120 transported the largest fraction of microbes and microspheres, while Port r180 and R90 transported far less. Similarly, the fraction of microbes retained in the soil core cannot be correlated to flux (Figure 2.11.a). The fraction of microbes and microspheres mobilized during the experiment, on the other hand, appear to correlate to flux in some cases (Figure 2.11.c). *C. parvum*, and microspheres have strong correlations, and MS-2 has a weak correlation with flux (*C. parvum*: Pearson's r=0.79, R^2=0.56; microspheres: Pearson's r=0.86, R^2=0.68; MS-2: Pearson's r=0.49, R^2=0.083). However, the fraction of *P. stutzeri* mobilized does not correlate to flux (*P. stutzeri*: Pearson's r=0.41, R^2=0.0035) (Figure 2.12).

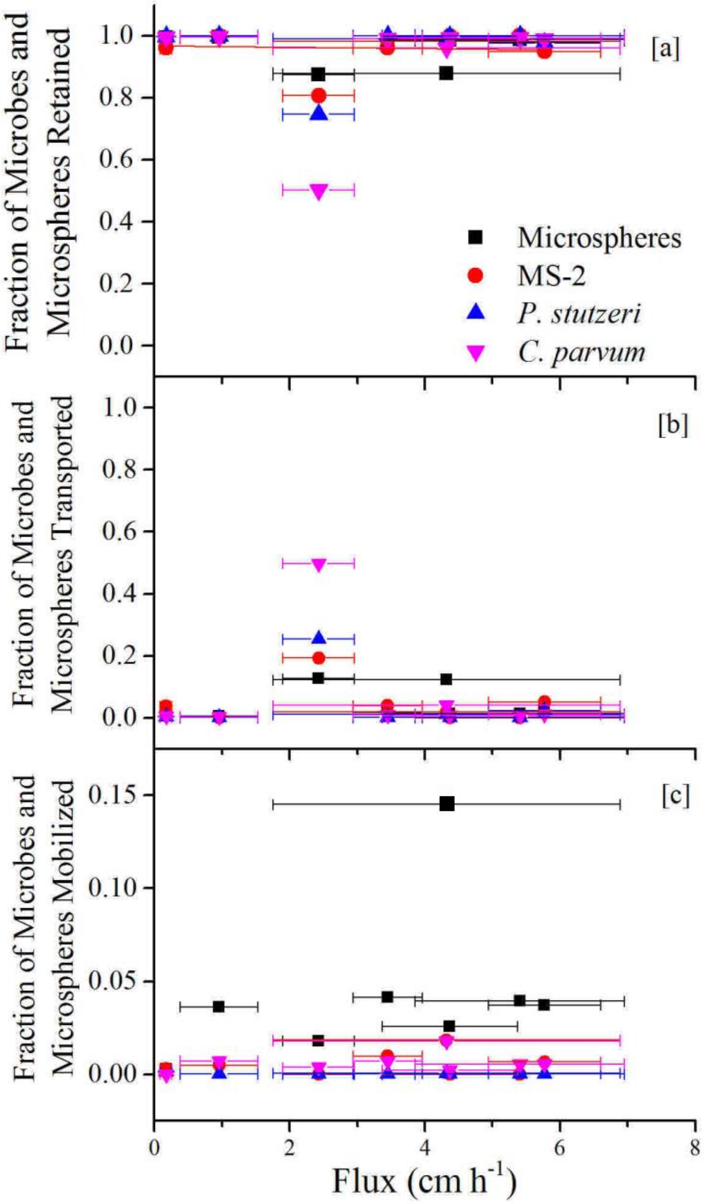

Figure 2.11. (a) The fraction of microbes and microspheres retained, and (b) the fraction of microbes and microspheres transported during breakthrough, and (d) the fraction of attached microbes and microspheres mobilized during intermittent flow varied with flux.

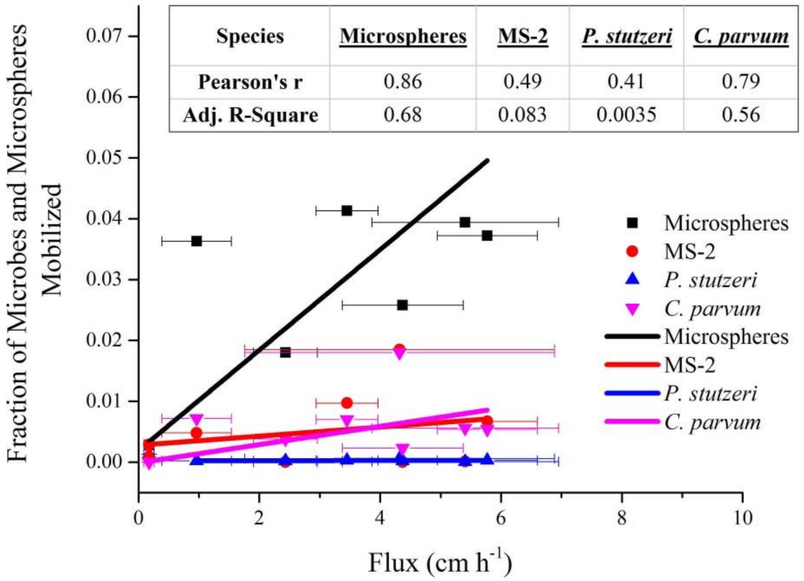

Species	Microspheres	MS-2	*P. stutzeri*	*C. parvum*
Pearson's r	0.86	0.49	0.41	0.79
Adj. R-Square	0.68	0.083	0.0035	0.56

Figure 2.12. Fraction of attached microbes and microspheres mobilized during intermittent flow varied with flux. Lines indicate the best fit linear regression. The table at the top of the figure shows the species and corresponding fit statistics (Pearson's r, R^2) used to determine correlation to flux for all microbes and microspheres. Error bars indicate standard error of average flux values.

Discussion

Effect of soil core physical heterogeneity on water flow**:** Soil physical heterogeneity caused spatial and temporal variations in effluent flux through individual sampling ports. Rainwater infiltrated through only 42% of the soil base area, which suggested that preferential flow paths conduct water through the soil core. The exclusion of 58% of the soil column base area from water flow may be due to low-permeability of matrix layers within the soil that block infiltrating water. Effluent flux of active ports was greater than influent flux (i.e., rainfall rate) on the surface of the soil core (2.0 cm h^{-1}) in both bromide and microbe injections because all applied rainwater passed through specific flow paths (matrix, intermediate macropore, or preferential flow path) leading to eight outlet ports. The infiltrating rain water flowed through only 42% of the sampling port area; therefore, the average effluent flux rate was greater the rainfall rate. Higher hydraulic conductivity was expected through soil macropores, whereas lower hydraulic conductivity was expected through the soil matrix. Intermediate macropore ports were expected to have intermediate hydraulic conductivity.

Soil physical heterogeneity, specifically the spatial distribution of macropores and impermeable layers, may account for the significant spatial variation in effluent flux. First, the distribution of macropores and the soil matrix could vary spatially. These differences may lead to variations in hydraulic conductivity of the soil on the flow path to each port. Second, relatively impermeable matrix layers may block water access to a larger soil fraction in the core. In a previous study by Mohanty et al. (2011), rhodamine dye was applied to another Oak Ridge soil core with the intent of examining flow paths. The rhodamine dye test showed that the applied dye followed a circuitous path, infiltrating through fractures or openings between bedding planes, but did not penetrate into regions with high clay content. These results indicated that individual sampling ports in this study could collect water from overlying soil with varying degrees of macroporosity.

Transport of a dissolved solute (e.g., bromide tracer) through the intact soil core was affected by soil physical heterogeneity. For each sampling port, bromide recovery was assumed to relate, at least qualitatively, to the proportion of soil macropores to matrix porosity contributing flow to each port. A lack of bromide recovery after the tracer application was attributed to diffusion of bromide into the matrix because bromide was considered to be a conservative tracer (Pace et al., 2003). Bromide recoveries at individual ports ranged from 2.9% to 44.9% (Table 2.1), which was indicative of matrix diffusion of bromide that was not recovered over the time scale of this experiment, as well as different amounts of bromide diffusion into the matrix along different flow paths. The port with the lowest bromide recovery also had the lowest flux (Table 2.1), which suggested the presence of fewer macropores along the flow path to the port. Bromide recovery at each port was weakly correlated to flux (Pearson's $r = 0.62$, $R^2 = 0.27$) at corresponding ports (Figure 2.6), which supported this idea.

Flux also varied temporally during intermittent flows. The temporal variation in flux was more pronounced during the three intermittent flow events, and also during the secondary peaks of Ports r180, R90, and R120. One possibility for deviations in flow paths could be blockage of active ports by colloids mobilized during intermittent flow. High colloid concentration in ports that may have been blocked supported this idea (Figure 2.8). The temporal change in flux became more pronounced during intermittent flow compared to steady injection and the secondary peak, possibly due to wedging in grain to grain contacts in soil pores, leading to further pore-blockage (Johnson et al., 2010). Another study attributed the temporal change in flow pattern to wetting front instability driven by gravity (Glass et al., 1988). The wetting front can become unstable when a denser phase (i.e., water) displaces a less dense phase (i.e., air) at a rapid rate, resulting in fingered flow. This implied that intermittent flow events may potentially alter flow paths by promoting porewater exchange between macropores and the soil matrix. Decreases or increases in flux could also indicate a change in flow paths or exchange of water between adjacent macropores and the matrix leading to outlet ports. This exchange of water could cause introduction of soil and associated pathogenic microbes that otherwise may otherwise be sequestered in soil matrices.

Transport of microbes and microspheres**:** The results from this experiment suggested that an increase in size of spherical-shaped microbes (MS-2, *C. parvum* oocysts) and microspheres increased transport in this soil (Table 2.5). The increased transport of *C. parvum* oocysts relative to MS-2 and microspheres may be attributed to effects related to size, including pore-exclusion, diffusion and Brownian motion. The smaller MS-2 and microspheres could access finer pores from which *C. parvum* can be excluded. This exclusion may limit the interaction of *C. parvum* oocysts with soil grains, thus decreasing the likelihood of their attachment or facilitating their transport. Additionally, due to their small size it is likely that greater numbers of MS-2 and 0.5 µm microspheres could diffuse into the soil matrix or toward grain surfaces compared to the larger *C. parvum* oocysts. Mohanty et al. (2013) suggested that 0.5 µm microspheres were retained by diffusion into the soil matrix to a greater degree than 1.8 µm microspheres because limited diffusion of larger microspheres into the matrix may have reduced their removal by wedging or settling. This suggested that diffusion of *C. parvum* in this study may also have been limited by its large size relative to the MS-2 and 0.5 µm microspheres. Smaller microspheres are also more likely to diffuse into the matrix by Brownian motion and become trapped in stagnant porosity than larger microspheres (Cumbie et al., 1999). The higher diffusivity of MS-2 and the subsequently higher Brownian motion and interaction with grain surfaces (Weisbrod et al., 2013) may also explain the decrease in MS-2 transport relative to *C. parvum* found in this study.

Similarly, the increased transport of microspheres compared to MS-2 may have been caused by the small size of MS-2 relative to the microspheres. Decreased transport of MS-2 relative to larger colloidal particles in fractured soils has been attributed to greater matrix diffusion of the phage previously, where enhanced diffusivity and Brownian motion of the smaller particles resulted in increased interaction with fracture walls (McKay et al., 1993; Zvikelsky et al., 2006; Weisbrod et al., 2013).

The transport of the rod-shaped microbe, the *P. stutzeri* bacteria, was less than that of the spherical-shaped MS-2, *C. parvum* oocysts, and microspheres, which suggested that colloid shape affects transport and removal. A recent study using *P. stutzeri* also found that rod-shaped microbes have decreased transport and increased removal, which they attributed to numerous points of surface-to-surface contact with adsorption sites on soil grains (Harvey et al., 2011).

Transport of microbes and microspheres varied at active ports, which indicated that soil physical heterogeneity may affect removal. Unfavorable attachment may have occurred between microbes and grain surfaces via wedging in grain-to-grain contacts (Johnson et al., 2010), deposition on the air-water interface (Wan et al., 1994), and attachment on surface roughness (Shen et al., 2011). In general, the water flux was greatest in preferential flow path ports, and decreased in intermediate macropore and matrix ports, respectively. Similarly, the recovery of microbes and microspheres was greatest in preferential flow path ports, intermediate macropore ports, and matrix ports, respectively. There are three possible explanations for this relationship. Primarily, increased flux in preferential flow path ports or intermediate macropore ports decreased the overall residence time of microbes and microspheres, which could have limited interaction with attachment sites on soil grains. Additionally, increased shear forces resulting from fast-moving water in preferential flow path or intermediate macropore ports may overcome the attractive drag force keeping colloids near grain surfaces (Johnson et al., 2010). Lastly, preferential flow path and intermediate macropore ports are expected to receive water from regions with greater macroporosity, which may have decreased the removal by wedging (Bradford et al., 2004). These processes could limit attachment of microbes and microspheres on soil grains. A challenge in comparing the effect of microbe size upon transport is that different microbes may have different surface chemistries and charges, which can affect their attachment to surfaces; however, for this study the focus was mainly on the effects of size.

***Effect of intermittent rainfall on microbe and microsphere mobilization*:** Intermittent flow caused mobilization of attached microbes and microspheres, regardless of size or taxa. However, the results indicated that size, shape, and the degree of soil physical heterogeneity affect the quantity of mobilized microbes and microspheres during intermittent flow (i.e., the degree of mobilization).

Results from the recovery of microbes (MS-2, *P. stutzeri* cells, and *C. parvum* oocysts) indicated greater mobilization of larger microbes compared to smaller microbes, and greater mobilization of spherical-shaped microbes compared to rod-shaped microbes during intermittent flows (Table 2.5). One possible explanation is that the larger *C. parvum* experience shear forces adequate enough to detach the oocysts from grain surfaces. Similar results were found for oocyst-sized microspheres, where the larger particles were subjected to shear forces adequate to detach the microspheres from grain surfaces (Johnson et al., 2010). A positive correlation between the fraction of mobilized oocysts and flux (Pearson's r=0.79, R^2=0.56) suggested that shear forces from intermittent flows caused mobilization of *C. parvum* oocysts in this study (Figure 2.12). A previous study also found that significant amounts of *C. parvum* oocysts were mobilized by increased flux after being initially removed (Harter et al., 2000).

Greater mobilization of the microspheres compared to *C. parvum* oocysts was not indicative of smaller colloids being more likely to mobilize during intermittent flows than large colloids (Table 2.4). Several studies have shown that the applicability of microspheres as microbial surrogates is questionable and that differences in physical and chemical properties affect their transport and attachment (Mohanram et al., 2010; Harvey et al., 2011; Metge et al., 2011). Specifically, Harvey et al. (2011) suggested that microspheres may be subject to more frequent attachment onto grain surfaces and that their spherical morphology would limit their contact area on grain surfaces. Therefore, there was increased vulnerability of microspheres for mobilization during intermittent flow events. Additionally, the strong positive correlation between the fraction of mobilized microspheres and flux (Pearson's r=0.86, R^2=0.68) suggests that shear forces, or movement of the air-water interface and wetting fronts from intermittent flows, contributed to the mobilization of microspheres in this study (Figure 2.12). Thus, the increased propensity for attachment on soil grains and vulnerability for mobilization during flow events may have caused the microspheres to be mobilized to a greater extent than *C. parvum* oocysts.

The indication that microbe size is a distinct factor in mobilization of previously attached particles implied that the small size of MS-2 decreased its mobilization potential compared to *C. parvum* oocysts and microspheres. At about 26 nm in diameter, MS-2 mobilization would not likely be triggered by shear forces (McKay et al., 2002). Additionally, MS-2 mobilization was poorly correlated to flux (Pearson's r=0.48, R^2=0.08), which supports the supposition that MS-2 mobilization was not affected by shear forces generated from water flux (Figure 2.12). One likely cause of MS-2 mobilization may be colloid-facilitated transport, where the movement of mobile colloids may facilitate the transport of contaminants (DeNovio et al., 2004). Colloid mobilization was apparent from increased sample turbidity during intermittent flows (Figure 2.10), and these mobilized colloids could potentially carry the MS-2 bacteriophage into mobile groundwater (McCarthy et al., 1989; McKay et al., 1993; DeNovio et al., 2004).

The limited mobilization of *P. stutzeri* cells compared to the spherical-shaped microbes and microspheres may be due, in part, to its rod-shaped structure (Harvey et al., 2011). Lack of correlation between the mobilized fraction of *P. stutzeri* with flux (Pearson's r=0.41, R^2=0.00) suggests that shear forces generated by intermittent flows were not sufficient enough to detach *P. stutzeri* bacteria from grain surfaces (Figure 2.12). This indicated that *P. stutzeri* mobilization was independent of flux, and may depend on its shape, physical heterogeneity in soil overlying the port, or movement of the air-water interface and wetting fronts during intermittent, unsaturated flow events.

Porewater exchange between the soil matrix and macropores during intermittent flow may be responsible for the observed increased mobilization of MS-2 compared to *P. stutzeri* (Flury et al., 1994; Bundt et al., 2001). Infiltrating rainwater in this experiment was shown to exchange between flow paths (matrix vs. macropore flow); and therefore, the MS-2 may have diffused from flow paths into the soil matrix during pauses in rainfall and contributed to increased release when flow ensued. A similar study concluded that the soil matrix may contribute to colloid transport during pauses in rainfall, due to diffusion of colloids through water-filled pores in the soil matrix into macropores (Schelde et al., 2002).

Variations in microbe and microsphere mobilization between active ports indicate that soil physical heterogeneity may have affected their mobilization during intermittent flow. The mobilized fractions of attached microbes and microspheres were not related to flux, but they were related to port category: matrix ports, intermediate macropore ports, and preferential flow path ports. Mobilization of previously attached microbes and microspheres was most pronounced in intermediate macropore ports, followed by matrix ports and preferential flow path ports, respectively. The limited mobilization of attached microbes and microspheres from preferential flow path ports may be attributed to limited residence time of the infiltrating water, and initial removal by wedging (Mohanty et al., 2013a). Mobilization in matrix ports was greater overall than in preferential flow path ports. Mohanty et al. (2013) noted that the mobilization potential of microspheres that are diffused into the soil matrix was limited due to inadequate shear forces required to detach particles from soil grains. Mobilization of microbes and microspheres was greatest in intermediate macropore ports (Table 2.5). The increased flux in intermediate macropore ports compared to matrix ports during intermittent flow may have overcome the attractive drag forces holding particles near grain surfaces (Johnson et al., 2010). The effect of increased flux during intermittent flow may explain the increased mobilization of retained microbes and microspheres in intermediate macropore ports. Comparing the effect of microbe size on mobilization can be challenging because microbes of varying taxa can have different surface chemistries and charges, which may affect their detachment from surfaces; however, for this study the focus was predominantly on the effects of microbe size.

***Effect of rainfall duration on secondary peak in breakthrough*:** The secondary peak in microbe and microsphere breakthrough observed in each port category may be attributed to soil physical heterogeneity (Figure 2.10.a, c, e). The initial peak may have been caused by the earlier breakthrough of microbes from macroporous structures within the flow path leading to the port. Later arrival of the secondary peaks in breakthrough could correspond to microbes and microspheres that had moved through the matrix or smaller pores in the flow paths, as it takes longer to travel through the matrix. Secondary peaks in tracer breakthrough have been observed and attributed to dual-porosity of heterogeneous soils, where the tracer was partially introduced into the matrix and partially bypassed the matrix through vertical fractures (Jardine et al., 1990; Van den Daele et al., 2007). The results indicated that small pores retained water and solutes longer, and water flux caused transport of solutes from small to large pores. Vertical fractures intersecting horizontal fractures forced the tracer to move slower through the matrix, causing secondary peaks in breakthrough. Another possible explanation for secondary peaks in breakthrough could be decreased water content during drainage, which could cause movement of air-water interfaces or fluid shear during changes in flux, and may be responsible for observed pulses in colloid mobilization (Zhuang et al., 2007). However, decreased water content from draining was unlikely in this experiment, as secondary peaks occurred prior to drainage and suspension of infiltrating rainfall.

Conclusion

Implications**:** This study demonstrated that microbes of varying size and taxa were transported through an unsaturated fractured soil during their injection, and mobilization of attenuated microbes occurred when the soil core was subjected to intermittent flow events. The results indicated that while soil matrices may remove large fractions of infiltrating microbes, macropores or preferential flow paths (i.e., soil fractures) can allow microbes to bypass the matrix, and may provide a rapid transport pathway for microbes to reach the subsurface and potentially groundwater aquifers. Therefore, areas vulnerable to heavy rainfall may be at risk for groundwater contamination from microbes originating from agriculture, leaky sewage systems, and wastewater discharge.

While the transport of viruses, bacteria, and protozoa have been studied individually under varying geochemical conditions and in different soils, the impact of size and intermittent flow on their transport and mobilization was lacking. The results of this study suggested that microbe size plays an important role in the degree of transport and mobilization of microbes, and that intermittent rainfall has the potential to mobilize microbes regardless of size or taxa. Greater fractions of larger, spherical-shaped microbes were recovered compared to smaller spherical-shaped microbes, possibly due to increased shear forces with increased size. Spherical-shaped microbes were also recovered to a greater extent than the rod-shaped microbe. Shape was determined to be an important factor in the transport and mobilization potential of microbes. Rod-shaped microbes (i.e., bacteria) have increased contact area with soil grains and therefore an increased likelihood for attachment or removal. Additionally, the numerous points of surface-to-surface contact may limit the mobilization potential of rod-shaped microbes compared to spherical-shaped microbes, as shear forces generated by intermittent flows may not be sufficient to detach them from surfaces. Thus, there may be an increased risk of groundwater contamination from spherical-shaped pathogens in areas prone to heavy rainfall events.

This study also demonstrated the importance of soil physical heterogeneity on microbial transport in fractured media. Flow paths with a higher flux (i.e., macropores or preferential flow paths) allowed for the rapid transport of large fractions of injected microbes; however, the high flux and reduced residence time limited their attachment and therefore their mobilization potential. Conversely, flow paths with a lower flux (i.e., soil matrices) limited the transport of microbes; however, there was a greater degree of mobilization. Water exchange between macropores and the soil matrix has been shown to be important in the mobilization microbes during steady flow. The results of this study suggested that the exchange of water between flow paths may have also contributed to the mobilization of microbes during intermittent flow. Water exchange between flow paths was observed during the application and recovery of the bromide tracer, which indicated that water exchange may have also been important in the mobilization of microbes. Therefore, while macropores or preferential flow paths can provide a rapid transport pathway for pathogenic microbes to migrate toward groundwater aquifers, the soil matrix may act as a long-term source of pathogens, trapping and releasing them slowly.

Future considerations**:** One of the challenges in comparing the effect of microbe size on transport and mobilization potential in this study was that diverse microbes generally have radically different surface chemistries, which affect their attachment and detachment from surfaces. While each of the microbes and the microspheres used in this study have negatively charged surfaces in the near-neutral pH of groundwater, the differences in surface moieties and functional groups could have affected their behavior in subsurface soils. Mohanty et al. (2013a) used two sizes of carboxylated microspheres to demonstrate that an increase in size of microspheres with identical surface chemistries resulted in increased transport and mobilization. However, microspheres are known to behave dissimilarly compared to microbes, and therefore the effect of size should be investigated using actual microbes exhibiting similar or identical surface chemistry. The differences in microbes' surface functionality on their transport and mobilization is an important consideration for future studies, in order to fully understand the effects of microbe size. One idea would be to use several strains of the same microbial species, for example *Pseudomonas* bacteria, that have similar surface functional groups but may cover a range of sizes. An increased understanding of surface chemistry of microbes used in transport studies will allow for better understanding of the mechanisms of microbial removal or attachment in subsurface environments as a function of size.

References

Abudalo, R. A., et al. (2005), Effect of ferric oxyhydroxide grain coatings on the transport of bacteriophage PRD1 and *Cryptosporidium parvum* oocysts in saturated porous media, *Environ Sci Technol.*, *39*, 6412-6419.

Adams, M. H. (1959), Bacteriophages, *Bacteriophages*.

Bales, R. C., et al. (1993), MS-2 and poliovirus transport in porous media: Hydrophobic effects and chemical perturbations, *Water Resour Res*, *29*(4), 957-963.

Bradford, S. A., et al. (2002), Physical factors affecting the transport and fate of colloids in saturated porous media, *Water Resour Res*, *38*(12), doi:10.1029/2002WR001340.

Bradford, S. A., et al. (2004), Straining and attachment of colloids in physically heterogeneous porous media, *Vadose Zone Journal*, *3*(2), 384-394.

Brennan, F. P., et al. (2011), Evaluating E. coli Transport Risk in Soil using Dye and Bromide Tracers, *Soil Sci. Soc. Am. J.*, *76*(2), 663-673.

Bundt, M., et al. (2001), Preferential flow paths: Biological 'hot spots' in soils, *Soil Biology & Biochemistry*, *33*(6), 729-738.

Cey, E. E., et al. (2009), Influence of macroporosity on preferential solute and colloid transport in unsaturated field soils, *Journal of Contaminant Hydrology*, *107*(1-2), 45-57.

Chen, G., and S. L. Walker (2012), Fecal Indicator Bacteria Transport and Deposition in Saturated and Unsaturated Porous Media, *Environmental Science & Technology*, *46*(16), 8782-8790.

Cheng, T., and J. E. Saiers (2010), Colloid-facilitated transport of cesium in vadose-zone sediments: The importance of flow transients, *Environmental Science & Technology*, *44*(19), 7443-7449.

Cumbie, D. H., and L. D. McKay (1999), Influence of diameter on particle transport in a fractured shale saprolite, *Journal of Contaminant Hydrology*, *37*(12), 139-157.

Darnault, C. J. G., et al. (2004), Preferential Flow and Transport of Cryptosporidium parvum Oocysts through the Vadose Zone: Experiments and Modeling, *Vadose Zone Journal*, *3*(1), 262-270.

DeNovio, N. M., et al. (2004), Colloid movement in unsaturated porous media: Recent advances and future directions, *Vadose Zone Journal*, *3*(2), 338-351.

El-Farhan, Y. H., et al. (2000), Mobilization and transport of soil particles during infiltration experiments in an agricultural field, Shenandoah Valley, Virginia, *Environmental Science & Technology*, *34*(17), 3555-3559.

Flury, M., et al. (1994), Susceptibility of soils to preferential flow of water - A field study, *Water Resour Res*, *30*(7), 1945-1954.

Gerba, C. P., and J. E. Smith (2005), Sources of Pathogenic Microorganisms and Their Fate during Land Application of Wastes The opinions expressed in this article are those of the authors and do not necessarily reflect those of the USEPA, *J. Environ. Qual.*, *34*(1), 42-48.

Ginn, T. R., et al. (2002), Processes in microbial transport in the natural subsurface *Advances in Water Resources 25*, 1017-1042.

Glass, R. J., et al. (1988), Wetting front instability as a rapid and far-reaching hydrologic process in the vadose zone, *Journal of Contaminant Hydrology*, *3*(24), 207-226.

Haack, S. K., et al. (2012), Effects on Groundwater Microbial Communities of an Engineered 30-Day In Situ Exposure to the Antibiotic Sulfamethoxazole, *Environmental Science & Technology*, *46*(14), 7478-7486.

Han, J., et al. (2006), Virus Retention and Transport in Chemically Heterogeneous Porous Media under Saturated and Unsaturated Flow Conditions, *Environmental Science & Technology*, *40*(5), 1547-1555.

Harter, T., et al. (2000), Colloid Transport and Filtration of Cryptosporidium parvum in Sandy Soils and Aquifer Sediments, *Environmental Science & Technology*, *34*(1), 62-70.

Harter, T., et al. (2008), Developing Risk Models of Cryptosporidium Transport in Soils from Vegetated, Tilted Soilbox Experiments All rights reserved. No part of this periodical may be reproduced or transmitted in any form or by any means, electronic or mechanical, including photocopying, recording, or any information storage and retrieval system, without permission in writing from the publisher, *J. Environ. Qual.*, *37*(1), 245-258.

Harvey, R., et al. (2011), Differential effects of dissolved organic carbon upon re-entrainment of groundwater bacteria and bacteria-sized microspheres during transport through a contaminated, sandy aquifer, *Environ Sci Technol.*, *45,* 3252-3259.

Harvey, R. W., and J. N. Ryan (2004), Use of PRD1 bacteriophage in groundwater viral transport, inactivation, and attachment studies, *FEMS Microbiology Ecology*, *49*(1), 3-16.

Harvey, R. W., et al. (2008), Assessing the vulnerability of a sole-source, karstic-limestone aquifer. 2. Use of carboxylated polystyrene microspheres to estimate the transport potential of *Cryptosporidium parvum* oocysts in a municipal well field in the Biscayne Aquifer, *Water Resour. Res*, *44*, W08431.

Hijnen, W. A. M., et al. (2005), Transport of MS2 Phage, *Escherichia coli, Clostridium perfringens, Cryptosporidium parvum,* and *Giardia intestinalis* in a Gravel and a Sandy Soil, *Environ Sci Technol., 39*(20), 7860.

Jacobsen, O. H., et al. (1997), Particle transport in macropores of undisturbed soil columns, *Journal of Hydrology*, *196*(1-4), 185-203.

Jardine, P. M., et al. (1990), Unsaturated solute transport through a forest soil during rain storm events, *Geoderma*, *46*(13), 103-118.

Jardine, P. M., et al. (1993), Unsaturated transport processes in undisturbed heterogeneous porous media: I. Inorganic contaminants, *Soil Sci Soc Am J*, *57*(4), 945-953.

Johnson, W. P., et al. (2010), Direct observations of colloid retention in granular media in the presence of energy barriers, and implications for inferred mechanisms from indirect observations, *Water Research*, *44*(4), 1158-1169.

Kenst, A. B., et al. (2008), Virus Transport during Infiltration of a Wetting Front into Initially Unsaturated Sand Columns, *Environmental Science & Technology*, *42*(4), 1102-1108.

Kjaergaard, C., et al. (2004), Colloid mobilization and transport in undisturbed soil columns. II. The role of colloid dispersibility and preferential flow, *Vadose Zone Journal*, *3*(2), 424-433.

Kretzschmar, R., et al. (1999), Mobile Subsurface Colloids and Their Role in Contaminant Transport, in *Advances in Agronomy*, edited, pp. 121-193, Academic Press.

Li, X., and W. P. Johnson (2005), Nonmonotonic Variations in Deposition Rate Coefficients of Microspheres in Porous Media under Unfavorable Deposition Conditions, *Environmental Science & Technology*, *39*(6), 1658-1665.

Li, Y. L., et al. (2012), Removal of Clostridium perfringens, Escherichia coli and F-RNA coliphages by stormwater biofilters, *Ecological Engineering*, *49*(0), 137-145.

Luxmoore, R. J., and C. H. Abner (1987), Field Facilities for Subsurface Transport Research, U.S. Department of Energy, Washington, DC.

Mailloux, B. J., et al. (2003), The role of physical, chemical, and microbial heterogeneity on the field-scale transport and attachment of bacteria, *Water Resour Res*, *39*(6), doi:10.1029/2002WR001591.

Majdalani, S., et al. (2008), Effects of wetting and drying cycles on in situ soil particle mobilization, *European Journal of Soil Science*, *59*(2), 147-155.

Martins, J. M. F., et al. (2012), Role of macropore flow in the transport of Escherichia coli cells in undisturbed cores of a brown leached soil, *Environmental Science: Processes & Impacts*, *15*(2), 347-356.

McCarthy, J. F., and J. M. Zachara (1989), Subsurface transport of contaminants, *Environmental Science & Technology*, *23*(5), 496-502.

McKay, L. D., et al. (1993), A field example of bacteriophage as tracers of fracture flow, *Environmental Science & Technology*, *27*(6), 1075-1079.

McKay, L. D., et al. (2002), Influence of Flow Rate on Transport of Bacteriophage in Shale Saprolite, *J. Environ. Qual.*, *31*(4), 1095-1105.

Mesquita, M. M. F., and M. B. Emelko (2012), Bacteriophages as Surrogates for the Fate and Transport of Pathogens in Source Water and in Drinking Water Treatment Processes.

Metge, D. W., et al. (2007), Use of carboxylated microspheres to assess transport potential of *Cryptosporidium parvum* oocysts at the Russian River water supply facility, Sonoma County, California, *Geomicro. J*, *24*(3), 231 - 245.

Metge, D. W., et al. (2010a), Influence of organic carbon loading, sediment associated metal oxide content and sediment grain size distributions upon Cryptosporidium parvum removal during riverbank filtration operations, Sonoma County, CA, *Water Research*, *44*(4), 1126-1137.

Metge, D. W., et al. (2010b), Influence of organic carbon loading, sediment associated metal oxide content and sediment grain size distributions upon *Cryptosporidium parvum* removal during riverbank filtration operations, Sonoma County, CA, *Water Research*, *44*(4), 1126.

Metge, D. W., et al. (2011), Effects of Sediment-Associated Extractable Metals, Degree of Sediment Grain Sorting, and Dissolved Organic Carbon upon Cryptosporidium parvum Removal and Transport within Riverbank Filtration Sediments, Sonoma County, California, *Environmental Science & Technology*, *45*(13), 5587-5595.

Mishurov, M., et al. (2008), Colloid transport in a heterogeneous partially saturated sand column, *Environmental Science & Technology*, *42*(4), 1066-1071.

Mohanram, A., et al. (2010), Comparison of transport and attachment behaviors of Cryptosporidium parvum oocysts and oocyst-sized microspheres being advected through three minerologically different granular porous media, *Water Research*, *44*(18), 5334-5344.

Mohanty, S. (2011), Colloid-facilitated transport of cations in an unsaturated fractured soil under transient condition, Ph.D. Thesis thesis, 227 pp, University of Colorado at Boulder, Boulder, CO.

Mohanty, S. K., et al. (2013a), Differential transport of two size classes of microspheres through soil: The role of macropores and intermittent flow, edited, p. 25, Stanford University
University of Colorado, Boulder
United States Geological Survey
Engineering Research Center for Re-inventing the Nation's Urban Water Infrastructure.

Mohanty, S. K., et al. (2013b), Engineering Solutions to Improve the Removal of Fecal Indicator Bacteria by Bioinfiltration Systems during Intermittent Flow of Stormwater, *Environmental Science & Technology*.

Nielsen, M. H., et al. (2011), Distribution of bromide and microspheres along macropores in and between drain trenches, *Vadose Zone Journal*, *10*(1), 345-353.

Pace, M. N., et al. (2003), Quantifying the effects of small-scale heterogeneities on flow and transport in undisturbed core from the Hanford formation, *Vadose Zone Journal*, *2*(4), 664-676.

Passmore, J. M., et al. (2010), The utility of microspheres as surrogates for the transport of *E. coli* RS2g in partially saturated agricultural soil, *Water Research*, *44*(4), 1235.

Powelson, D. K., and C. P. Gerba (1994), Virus removal from sewage effluents during saturated and unsaturated flow through soil columns, *Water Research*, *28*(10), 2175-2181.

Ryan, J. N., and P. M. Gschwend (1994a), Effects of ionic strength and flow rate on colloid release: Relating kinetics to intersurface potential energy, *J Colloid Interf Sci*, *164*(1), 21-34.

Ryan, J. N., and P. M. Gschwend (1994b), Effect of solution chemistry on clay colloid release from an iron oxide-coated aquifer sand, *Environmental Science & Technology*, *28*(9), 1717-1726.

Ryan, J. N., et al. (2002), Field and Laboratory Investigations of Inactivation of Viruses (PRD1 and MS2) Attached to Iron Oxide-Coated Quartz Sand, *Environmental Science & Technology*, *36*(11), 2403-2413.

Saiers, J. E., et al. (1994), Colloidal Silica Transport through Structured, Heterogeneous Porous-Media, *Journal of Hydrology*, *163*(3-4), 271-288.

Saiers, J. E., et al. (2003), The role of moving air-water interfaces in colloid mobilization within the vadose zone, *Geophys Res Lett*, *30*(21), doi:10.1029/2003GL018418.

Schelde, K., et al. (2002), Diffusion-limited mobilization and transport of natural colloids in macroporous soil, *Vadose Zone Journal*, *1*(1), 125-136.

Sen, T. K. (2011), Processes in pathogenic biocolloidal contaminants transport in saturated and unsaturated porous media: A review, *Water Air and Soil Pollution*, *216*(1-4), 239-256.

Shen, C., et al. (2011), Surface Roughness Effect on Deposition of Nano- and Micro-Sized Colloids in Saturated Columns at Different Solution Ionic Strengths, *Vadose Zone Journal*, *10*(3), 1071-1081.

Telliard, W. A. (2001), Method 1602: Male-specific (F^+) and Somatic Coliphage in Water by Single Agar Layer (SAL) Procedure, edited by USEPA, United States EPA, Office of Water, Washington D.C.

Tufenkji, N., et al. (2011), Fate and Transport of Microbial Contaminants in Groundwater, in *Encyclopedia of Environmental Health*, edited, pp. 715-726, Elsevier, Burlington.

Van den Daele, G. F. A., et al. (2007), Unsaturated flow and solute transport through the Chalk: Tracer test and dual permeability modelling, *Journal of Hydrology*, *342*(1â€“2), 157-172.

Van Duin, J., and R. Calendar (1988), Single-Stranded RNA Bacteriophages, in *The Bacteriophages*, edited, pp. 117-167, Springer US.

Wan, J. M., and J. L. Wilson (1994), Visualization of the role of the gas-water interface on the fate and transport of colloids in porous-media, *Water Resour Res*, *30*(1), 11-23.

Wan, J. M., and T. K. Tokunaga (1997), Film straining of colloids in unsaturated porous media: Conceptual model and experimental testing, *Environmental Science & Technology*, *31*(8), 2413-2420.

Wang, L., et al. (2011), Effects of phosphate on the transport of *Escherichia coli O157:H7* in saturated quartz sand, *Environmental Science & Technology*, *45*(22), 9566-9573.

Weisbrod, N., et al. (2013), Virus transport in a discrete fracture, *Water Research*, *47*(5), 1888-1898.

Williams, F. P., et al. (2001), USEPA Manual of Methods for Virology
Chapter 16, *EPA 600/4-84/013 (N16)*, 9.

Wilson, G. V., et al. (1990), Hydrology of a forested hillslope during storm events, *Geoderma*, *46*(1-3), 119-138.

Zhuang, J., and Y. Jin (2003), Virus retention and transport through Al-oxide coated sand columns: effects of ionic strength and composition, *Journal of Contaminant Hydrology*, *60*(34), 193-209.

Zhuang, J., et al. (2007), In situ colloid mobilization in hanford sediments under unsaturated transient flow conditions: Effect of irrigation pattern, *Environmental Science & Technology*, *41*(9), 3199-3204.

Zvikelsky, O., and N. Weisbrod (2006), Impact of particle size on colloid transport in discrete fractures, *Water Resour Res*, *42*(12), W12S08.

Appendix 2.A

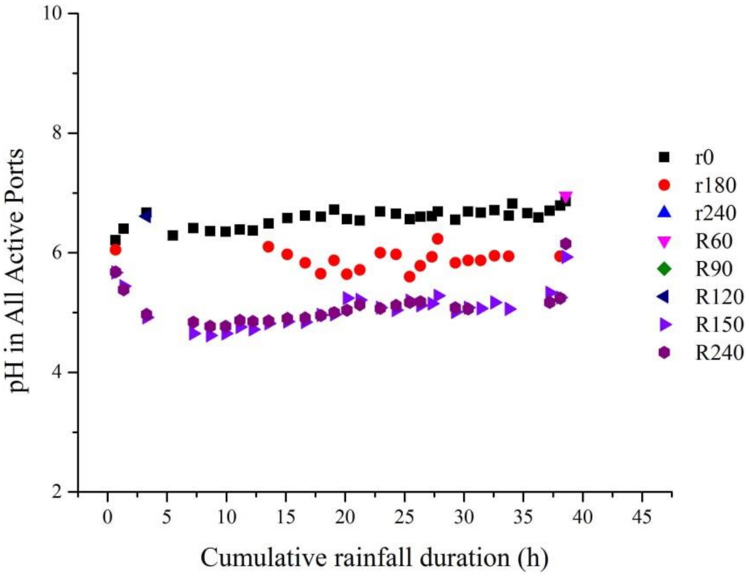

Figure 2.13. pH in all active ports throughout the microbe injection.

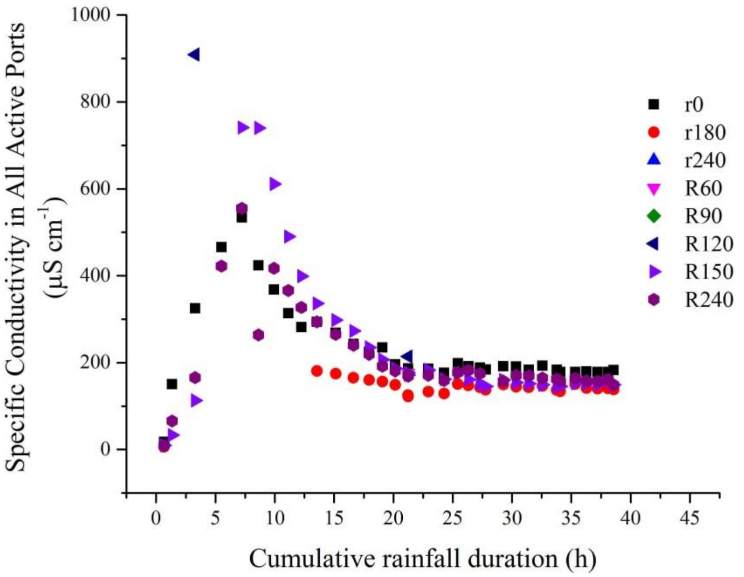

Figure 2.14. Specific conductivity in all active ports throughout the microbe injection.

CHAPTER 3

EFFECT OF REDOX CONDITIONS ON THE RELEASE OF TRACE ELEMENTS FROM SUBMERGED COAL ASH NEAR THE KINGSTON FOSSIL PLANT

To be submitted as a manuscript with the same title to *Environmental Science & Technology*

with co-author Joseph N. Ryan[1]

[1]Department of Civil, Environmental and Architectural Engineering, University of Colorado, Boulder, CO

Abstract

The release of coal ash because of a storage pond dike failure at the Tennessee Valley Authority's Kingston Fossil Plant in December 2008 is a concern because of the potential ecological and human health risks posed by the release of toxic elements from the coal ash into surrounding waters. The effects of redox conditions on the release of elements from coal ash were examined in this study, which focused specifically on how the differences between elements affect their release as a function of varied redox conditions. Using Emory River sediments and water, and fresh coal ash produced at the Kingston Fossil Plant in Kingston, Tennessee, a batch reactor system was created to assess trace element release from the coal ash. Triplicate coal ash-containing batch reactors were used to characterize the release behavior of elements and determine their aqueous concentrations. A control batch reactor containing only Emory River sediment was used to determine baseline chemical conditions and elemental concentrations in the system, and to ascertain which elements were released from the Kingston coal ash. This experiment was conducted in three stages – oxidizing, transition, and reducing – in order to simulate redox changes that might occur during accumulation and weathering of the released coal ash on riverbed sediments. The concentration and release of a wide range of trace elements varied as a function of the redox potential, pH, and dissolved organic matter concentration and aromaticity. The results suggest that the release of several trace elements, including antimony, barium, cadmium, europium, molybdenum, nickel, rhodium, ruthenium, rubidium, samarium, selenium, strontium, and uranium, from the Kingston coal ash may present water quality issues based on their increasing concentrations during the reducing stage. The differences in release of each element can be attributed to changes in chemical properties of the batch reactors (e.g., pH, redox potential), presence and aromaticity of DOC, dissolution of

mineral phases, competition or interaction with other elements and/or anions, precipitation of immobile phases, or release of mobile phases.

Introduction

Problem**:** Just before 1 a.m. on December 22, 2008 a containment dike failed at the Tennessee Valley Authority (TVA) Kingston Fossil Plant and over 4 million cubic meters of coal ash slurry was released near the confluence of the Emory and Clinch Rivers (Bednar et al., 2010). The Kingston Fossil Plant spill was the largest release of coal ash in the United States (TVA, 2009; USEPA, 2009). The ash contains potentially harmful elements that could be released into surrounding waters and could damage to the ecosystem and human health. Trace elements such as arsenic, selenium, mercury, chromium, and uranium are concentrated in the ash during combustion (Wadge et al., 1986; Fernandez-Turiel et al., 1994; Hower et al., 2005; Izquierdo et al., 2012). These elements can be released and transported in aqueous systems (Jegadeesan et al., 2008; Gitari et al., 2009; Kim et al., 2009). Additionally, the weathering of coal ash can cause long-term water quality issues and environmental effects (Akinyemi et al., 2011; Akinyemi et al., 2012). Therefore, it is important to understand the effect of weathering processes on the release of elements from coal ash so that their risk to human health and the environment can be assessed.

Coal ash contains many elements that are available for release, but amounts of the "available" elements may vary with coal ash types, water chemistry conditions, and leaching procedures (Gitari et al., 2009; Kim et al., 2009; Akinyemi et al., 2012). The pH and redox conditions affect elemental release from coal ash because of changes in surface electronegativity and electrostatic attraction, alteration of chemical speciation, and dissolution or precipitation of soluble or insoluble compounds. Coal ash consists primarily of an aluminosilicate core, or matrix, and often contains high concentrations of calcium and sulfate depending on the origin of the coal. Calcium and sulfate are easily released from the coal ash under a range of conditions, as are aluminum, magnesium, sodium, and potassium, due to their solubility or association with the surface of the ash particles (Gitari et al., 2009; Izquierdo et al., 2012). Trace elements, such as arsenic, barium, cadmium, copper, nickel, mercury, molybdenum, selenium, strontium, uranium, and zinc, are concentrated in the less-soluble coal ash matrix (Fernandez-Turiel et al., 1994; Hower et al., 2005). Changes in pH and redox can cause release of the elements in the coal ash matrix because of mineral dissolution, precipitation of immobile phases, release of mobile phases, and competitive effects on adsorption (Brownfield et al., 2005; Jegadeesan et al., 2008; Kim et al., 2009; Izquierdo et al., 2012; Jones et al., 2012). Conversely, these studies have also demonstrated that several elements, such as cobalt, chromium, and vanadium, can also be sequestered by similar mechanisms over the same range of pH values and redox conditions.

***Background*:** Calcium can inhibit the release of several elements from coal ash, including aluminum, arsenic, copper, mercury, selenium, and phosphate (Dubikova et al., 2006; Suess, 2006; Langner, 2009; Wang et al., 2009; Craven, 2012), as it inhibits the release of release of elements from other geomedia. For instance, previous studies showed that calcium inhibited the release of strontium from sludge-amended soils (McBride et al., 1999) and of molybdate from suspended sediments (Ye et al., 2013). Several mechanisms have been suggested to explain this inhibition processes. The inhibition of aluminum, copper, and mercury release from coal ash by calcium has been attributed to Ca^{2+} occupation of binding sites in dissolved organic matter (DOM) (Craven, 2012). While calcium inhibits release of these elements, it inhibits and enhances the release of other elements, such as arsenic and selenium, based on pH. It has been suggested that metal bridging by cations such as calcium may be important in forming soluble DOM-arsenic complexes (Redman et al., 2002; Lin et al., 2004; Wang et al., 2006), which could cause calcium addition to increase arsenic release from the coal ash. However, Wang et al.

(2009) suggested that calcium in coal ash can reduce the leaching of arsenic and selenium under alkaline pH, with a stronger impact on arsenic than selenium. Calcium was thought to inhibit the release of arsenate (AsO_4^{3-}) and selenite (SeO_3^{2-}) due to the formation of insoluble Ca-As compounds and $CaSeO_3$ precipitates at high pH (Wang et al., 2009).

Competitive effects between anions may result in the release of elements from coal ash. This competitive adsorption could be caused by direct competition for sorption sites and from electrostatic effects due to the change in charge of the solid upon adsorption. Phosphate and sulfate are known to compete for adsorption sites on surfaces and can influence the charge of those surfaces, which in turn affects the sorption capability of other species. On goethite surfaces, the influence of phosphate on sulfate adsorption was stronger than that of sulfate on phosphate, which reflected the greater affinity of phosphate for the goethite surface (Geelhoed et al., 1997). In addition to phosphate and sulfate, several other species released from coal ash are known to form oxyanions, including arsenic, antimony, chromium, molybdenum, selenium and vanadium. Anions with high affinity for metal oxides, such as phosphate, decrease the adsorption of inorganic anions with lower affinity, such as arsenate, selenite, molybdate, selenate, and sulfate, over a wide pH range (Ryden et al., 1987; Manning et al., 1996). In the case of molybdate, it has been shown that its adsorption was not influenced by sulfate, but sulfate adsorption was inhibited by molybdate (Wu et al., 2000; Wu et al., 2001) due to molybdate forming an inner-sphere complex with soils, while sulfate formed a weaker outer-sphere complex (Goldberg et al., 1996). On the other hand, phosphate has been demonstrated to effectively compete with molybdate at low concentrations because phosphate had a higher affinity for goethite and pyrite over a wide pH range (3-10) (Xu et al., 2006).

Surface-associated elements are more susceptible to initial leaching when first exposed to an aqueous environment (Izquierdo et al., 2012); however, elements contained in the less soluble core of the coal ash can only be released through long-term weathering processes (Gitari et al., 2009), such as changes in pH and redox potential. The release of soluble buffering constituents in coal ash due to weathering has been shown to significantly affect the pH, metal mobility, and mineralogical transformation of weathered coal ash (Akinyemi et al., 2011), which in turn can affect water quality and facilitate the release of other trace metals and elements. Several studies have shown that the acid-neutralizing capacity (ANC) of coal ash is mostly due to the release of calcium, magnesium, potassium, and sodium (Mizutani et al., 1996; Yan et al., 1999; Seferinoglu et al., 2003). Thus, the release of these alkali metals can increase the pH of solution, which can contribute to additional weathering, as well as affect the release or retention of elements or trace metals from the coal ash (Akinyemi et al., 2012). The pH is often observed as the most important variable affecting the leaching of elements from coal ash (de Groot et al., 1989; Akinyemi et al., 2012; Izquierdo et al., 2012). However, redox conditions can also affect the dissolution of coal ash and the subsequent release of elements (Izquierdo et al., 2012), as well as their speciation (Schweitzer et al., 2010), which in turn affects their mobility. Many trace metals and elements are redox-sensitive (Smith, 2007); therefore, changes in redox conditions can affect their speciation and release from coal ash, as well as precipitation and sorption processes.

Dissolved organic matter (DOM) may affect the concentration of trace elements released from the coal ash. DOM can facilitate the release of elements by binding elements in the ash and stimulating their dissolution into water (Harris et al., 1983; Janos et al., 2002). Changes in aromaticity affect the binding capability of the DOM; thus, the release or dissolution depends on the ligand and element type, and the affinity between them. Previous studies have shown that cinnabar (HgS) dissolution is correlated with the presence of DOM and its aromaticity (Ravichandran et al., 1998; Ravichandran, 2004; Waples et al., 2005). Mercury concentration and release from coal ash has also been shown to increase with increased DOM concentration and aromaticity (Craven, 2012). Several other studies have shown that the presence of organic ligands, such as EDTA and citric acid, enhance the release of trace metals (e.g. copper, iron, lead, zinc) from coal ash (Harris et al., 1983; Van der Bruggen et al., 1998; Janos et al., 2004; Jegadeesan et al., 2008). DOM may also be important for the release of oxyanion-forming elements (i.e., arsenic, chromium, molybdenum, selenium, and vanadium) from coal ash. DOM forms aqueous complexes with arsenic and selenium oxyanions and is also known to compete for surface adsorption sites, which may result in displacement of oxyanions (Buschmann et al., 2006; Wang et al., 2006; Wang et al., 2009). Based on the enhanced release of aluminum, copper, lead, and mercury from coal ash in the presence of DOM (Craven, 2012), similar effects on release are expected in this study.

In river systems, the hyporheic zone likely plays an important role in the release or attenuation of elements in coal ash. The hyporheic zone is defined as the water-saturated transitional zone between surface water and groundwater, across which there is an exchange of water (Bencala, 2005; Smith et al., 2005). This exchange of surface water and groundwater causes changes in geochemical processes, namely gradients in redox potential that control chemical transformations occurring on particle surfaces (Boulton et al., 1998). Redox conditions in the hyporheic zone are of particular importance because precipitation and adsorption processes are dependent on redox conditions (Gandy et al., 2007). Redox potential decreases with depth due to the depletion of oxygen and causes a shift from oxidizing to reducing conditions (Franken et al., 2001).

Under reducing conditions in the hyporheic zone, manganese and iron-oxides dissolve due to redox transformation of Fe(III) to Fe(II) or Mn(IV) to Mn(III), releasing any elements associated with the oxides (Gandy et al., 2007). Manganese and iron oxidation continuously produce new sorption sites in the form of oxide coatings on sediments, which enhance the removal of trace elements (Fuller et al., 2000). However, the reduction of these surface oxides can release any sorbed elements into solution. In a large river system where seasonal deposition of fresh detritus continually covers underlying layers of sediment, it is expected that the river sediments become buried deeper in the hyporheic zone and oxygen is depleted. Over time, these sediments will become increasingly more reduced, which in turn could cause dissolution of oxides or changes in chemical speciation, either of which could cause release of trace metals or elements. A recent review of pollutant dynamics in the hyporheic zone concluded that the boundaries of iron and manganese stability (i.e., the point at which ferric iron and manganese oxides dissolve) lie between the hyporheic zone and groundwater, and the surface water and hyporheic zone, respectively (Gandy et al., 2007). Therefore, manganese oxides would dissolve first, followed by ferric iron oxides, as predicted by the sequence of redox processes. As the manganese and ferric iron oxides are reduced and dissolve, they can release a wide variety of sorbed or co-precipitated toxic metals, such as arsenic and uranium (Nagorski et al., 1999; Wielinga et al., 1999; Winde et al., 2004).

Aside from the dissolution of oxides, it is most important to note that reducing conditions become more pronounced with depth (Franken et al., 2001), and therefore layers of sediment deeper in the hyporheic zones of rivers can become progressively more reduced. This is of particular importance in considering the effects of coal ash spills in river systems. The initial spill of Kingston coal ash created a mixed layer of ash and sediment, and this layer, over time, will be buried progressively deeper in the Emory River under layers of fresh detritus, eventually reaching a depth in the hyporheic zone where oxygen is fully depleted and reducing conditions dominate. Human inputs, such as heavy metals associated with mining, have been shown to be affected by hyporheic zone geochemistry (Hancock, 2002). Therefore, the Kingston Fossil Plant spill will also likely be affected by the chemical and physical properties of the hyporheic zone.

The weathering of coal ash released from the Kingston Fossil Plant spill is of concern because weathered coal ash can release less-soluble elements locked in the aluminosilicate matrix of the ash over time (Kukier et al., 2003; Gitari et al., 2009; Akinyemi et al., 2011). Although extensive hydraulic dredging and mechanical excavation was undertaken to remove the coal ash from the Emory and Clinch Rivers (Bednar et al., 2010; Bednar et al., 2013), it is unlikely that the entirety of the coal ash spill was removed from the waters. The remaining coal ash in the rivers could weather under natural condition and release elements contained in the ash. Several studies have suggested that natural weathering of coal ash is similar to the weathering of volcanic ash (Warren et al., 1985; Zevenbergen et al., 1994; Zevenbergen et al., 1999); however, volcanic ash requires several thousand years for weathering to produce clay mineral development, while it has been shown that clay-like amorphous material can be formed throughout the coal ash after only 8 y of natural weathering (Zevenbergen et al., 1996; Zevenbergen et al., 1999). This transformation of coal ash to clay and clay-like compounds is important in the mobilization or retention of both lithophilic elements and metals (Zevenbergen et al., 1994). Thus, the release of metals and elements locked in the aluminosilicate matrix of the coal ash could occur from the progressive weathering of the ash.

The long-term release of elements from coal ash in the Emory River after the Kingston Fossil Plant spill remains in question. Several studies have investigated the release of trace elements in the Emory River after the Kingston Fossil Plant spill; however, these studies focused on the initial ecological effects on the river system (Ruhl et al., 2009; Bednar et al., 2010) or the characterization of metals released from the coal ash during dredging activities (Bednar et al., 2013). Other studies have investigated the release of elements from coal ash using different leaching procedures (Fernandez-Turiel et al., 1994; Otero-Rey et al., 2005; Gitari et al., 2009; Wang et al., 2009; Bednar et al., 2010; Jones et al., 2012), in the presence of DOM of varying aromaticity (Craven, 2012), and when exposed to natural weathering (Akinyemi et al., 2011; Akinyemi et al., 2012).

***Purpose of this Study*:** The purpose of this study was to simulate the weathering of Kingston coal ash in the Emory River and to identify which elements may cause water quality problems. This experiment was designed so that the first stage simulated a situation where a spill had deposited fresh coal ash into the Emory River. The second stage was designed to simulate the progressive decrease in redox conditions of the coal ash layer in the hyporheic zone, where oxygen would become increasingly more depleted with depth. The third and final stage of this experiment was intended to simulate the firm establishment of reducing conditions in the hyporheic zone, where oxygen was completely depleted. Dissolved concentrations of numerous elements, dissolved organic matter, and anionic species, as well as chemical properties – pH and redox potential – were measured continually throughout the experiment to categorize and determine the release behavior from Kingston coal ash throughout the simulated weathering processes.

Experimental Materials and Methods

***Characterization of Coal Ash*:** The coal ash was a freshly-produced sample collected from the electrostatic precipitator at the Kingston Fossil Plant in Kingston, TN, on December 12, 2012. Elemental composition of the whole coal ash was determined by a hydrochloric acid/nitric acid/hydrofluoric acid digestion at the Laboratory for Environmental and Geological Studies (LEGS) at the University of Colorado, Boulder. The digest was analyzed for concentrations of major elements (Al, Ca, Fe, K, Mg, Mn, Na, P, Si, Ti) using inductively coupled plasma-atomic emission spectrometry (ICP-AES; Applied Research Laboratories, Model 3410+) and concentrations of trace elements (As, Ba, Cd, Co, Cr, Cs, Cu, Ge, Mo, Ni, Pb, Pd, Rb, Rh, Sc, Sb, Sm, Sn, Sr, V, T, Zn, Zr), rare earth elements (REE), lanthanides, and actinides (Ce, Dy, Er, Eu, Gd, Ho, La, Lu, Nd, Pr, Tb, Te, Th, Tm, U, Yb) using inductively coupled plasma-mass spectrometry (ICP-MS; Varian 810MS). Solid phase mercury (Hg) concentration in the coal ash was measured using a thermal decomposition method with a gold trap and atomic adsorption detector on a direct mercury analyzer (Milestone DMA-80). Selenium (Se) concentration in the coal ash was measured using inductively coupled plasma dynamic reaction cell mass spectrometry (ICP-DRC-MS), a technique that removes argon interference by using methane as a reactive cell gas in a dynamic reaction cell. The organic matter content of the coal ash was determined previously by loss on ignition (LOI) (Craven, 2012). Coal ash mineralogy was characterized using x-ray diffraction (XRD).

***Characterization of Emory River Sediment*:** Riverbed sediment samples were collected from the Emory River (35.94752912°N, 84.53179222°W) upstream from the Kingston Fossil Plant in Kingston, TN, and the downstream water affected by the coal ash spill (Figure 3.1). Fresh sediment samples were collected on December 11, 2012, at Emory River marker (ERM)

10.0, a reference sampling location, by Tennessee Valley Authority personnel and shipped on ice overnight to our laboratory in Boulder, CO. Sediment samples were collected using a grab sampler (Wildco, model Ponar) according to a standard operating procedure (TVA, KIF-SOP-05). Organic detritus was removed from samples prior to placing the sediment into trace metal clean sample containers, leaving the upper 15-20 cm of Emory River sediment available for analysis. The wet sediment was air-dried in a fume hood using trace metal-clean high-density polyethylene (HDPE) containers and mixed daily to prevent caking. The sediment drying containers were weighed daily until a consistent mass was observed, at which point the sediment was considered dried. The dry sediment was returned to trace metal-clean sample jars after being sieved (2 mm) to remove any large particles or remaining detritus. The elemental composition and mineralogy of the bulk Emory River sediment was determined using the same methods employed for the Kingston coal ash.

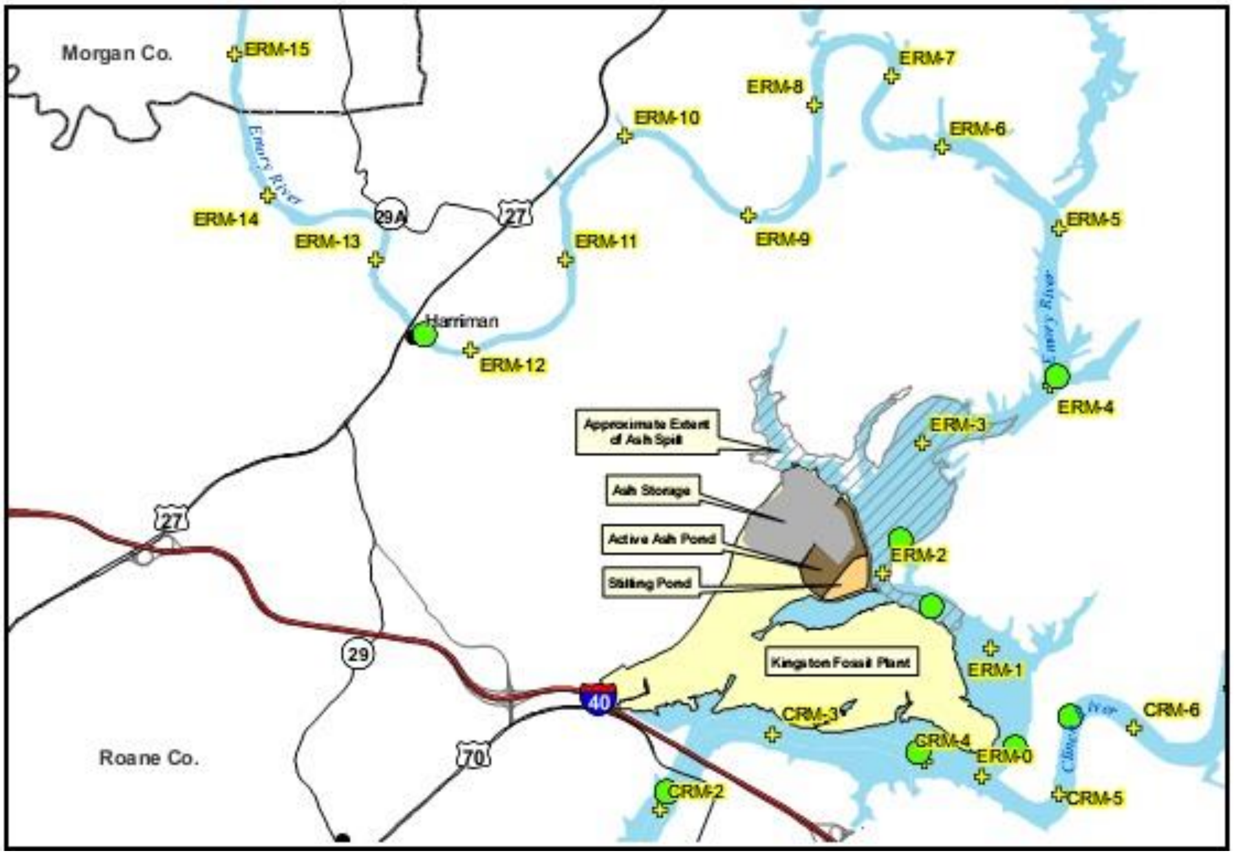

Figure 3.1. Map of the Tennessee Valley Authority surface water sampling sites. Emory River sediment was collected from mile marker 10.0 (ERM 10), and Emory River water was collected from mile marker 9.0 (ERM 9). These sampling locations are located upstream of the Kingston Fossil Plant.

Surface Water Samples**:** Surface water samples (50 L) were collected from the Emory River (39.93923100°N, 84.51636750°W) upstream from the Kingston Fossil Plant in Kingston, TN (Figure 2.1). Fresh water samples were gathered on December 12, 2012 at sampling location ERM 9.0 by Tennessee Valley Authority personnel, and shipped on ice overnight to our laboratory in Boulder, CO. Upon their arrival, water samples were filtered (0.45 µm membrane capsule filter; Geotech Environmental Equipment Inc.) and stored in darkness at 4°C.

Analysis of Water Samples**:** Water samples were removed from the batch reactors with a syringe (BD, 60 mL) filtered through filters (0.45 µm, Pall Acrodisc, Supor$^{\circledR}$ membrane) and analyzed for pH, specific conductivity, oxidation-reduction potential (ORP), dissolved organic carbon (DOC), and Ultraviolet absorbance. The pH was measured using a pH meter (Orion 3-Star Plus pH Benchtop Meter) and pH electrode (Orion 9157BNMD). The specific conductivity was measured using a conductivity meter (Oakton pH/CON 300) and electrode (Accumet Conductivity Probe). Oxidation-reduction potential (ORP) was measured using a millivolt meter (Orion 3-Star Plus pH Benchtop Meter) and ORP electrode (Orion 9180BN). The ORP meter was calibrated to the E_H mV values that would be obtained using a Standard Hydrogen Electrode. Dissolved organic carbon (DOC) was measured using persulfate oxidation (Oceanography International, model 700) and calibrated using 0.2, 0.7, 2.5, 5.2, 10.2, 15.2, 20.2, and 30.2 $mg_{carbon}\ L^{-1}$ standards. Ultraviolet absorbance at 254 nm was measured using an ultraviolet/visible spectrophotometer (Hewlett Packard, model 8453). The dissolved organic carbon concentration and absorbance of ultraviolet light at 254 nm was used to calculate the specific ultraviolet absorption at 254 nm ($SUVA_{254}$). DOC and UV absorbance were measured in samples collected in 40 mL trace metal-clean amber bottles. Analysis of oxic samples was conducted open to the atmosphere with no additional preparation necessary. For anoxic samples, the samples were prepared in a controlled nitrogen atmosphere within a separate glove box (Coy Laboratories Inc.; 95% N_2, 5% H_2). $SUVA_{254}$ samples were sealed in capped cuvettes prior to UV absorbance measurements, and DOC samples were placed immediately into the carbon analyzer to prevent exposure to air.

Aqueous mercury samples were analyzed in duplicate by cold vapor atomic fluorescence spectrophotometry (CVAFS; Tekran® Series 2600 Ultra-Trace Mercury Analysis System) following EPA method 1631. Samples were preserved in 1% BrCl by volume in trace metal-clean glass vials (I-Chem 200 series). Calibration standards for the CVAFS were prepared by serially diluting a $Hg(NO_3)_2$ standard (National Institute of Standards and Technology). The analytical detection limit was determined to be 0.5 ng L^{-1}. Any sample with concentrations below the detection limit (BDL) were considered unreliable and reported as such.

The major, trace metal, rare earth, lanthanide, and actinide elements were analyzed in the water samples using ICP-OES and ICP-MS. Water samples were collected in trace metal clean HDPE bottles and preserved with 1% by volume trace metal-grade nitric acid. The samples were analyzed for the same elements as reported in sediment analysis. Analysis of oxic samples was conducted open to the atmosphere and anoxic water samples were analyzed within 2 d.

Water samples were analyzed for anions including F^-, Cl^-, Br^-, NO_2^-, NO_3^-, PO_4^{3-}, and SO_4^{2-} by ion chromatography (IC; Dionex Series 4500I Liquid Ion Chromatography). Water samples were stored in 40 mL trace metal-clean glass amber bottles to prevent any degradation from light, stored at 4°C, and analyzed within 2 d.

Instrument detection limits of all elements, as well as anions are listed in Table 3.1 below. All elements measured at concentrations equal to or below the detection limit were not considered in this study.

Table 3.1. Instrument detection limits for liquid ICP-MS, ICP-DRC-MS, and ICP-OES analysis.

Analysis	Element	Unit	DL	Analysis	Element	Unit	DL	Analysis	Element	Unit	DL
ICP-OES	Si	ppm	0.032	ICP-MS	Ce	ppb	0.144	ICP-MS	Rb	ppb	0.009
	Mn	ppm	0.002		Co	ppb	0.005		Rh	ppb	0.003
	Fe	ppm	0.007		Cr	ppb	0.230		Ru	ppb	0.009
	Mg	ppm	0.020		Cs	ppb	0.006		Sc	ppb	0.801
	Ca	ppm	0.024		Cu	ppb	0.026		Sb	ppb	0.036
	Na	ppm	0.015		Dy	ppb	0.004		Se	ppb	0.210
	K	ppm	0.122		Er	ppb	0.006		Sm	ppb	0.003
IC	F	ppm	0.020		Eu	ppb	0.003		Sn	ppb	0.088
	Cl	ppm	0.020		Gd	ppb	0.003		Sr	ppb	0.003
	NO2	ppm	0.030		Hf	ppb	0.004		Ta	ppb	0.026
	Br	ppm	0.050		Ho	ppb	0.002		Tb	ppb	0.009
	NO3	ppm	0.050		La	ppb	0.082		Te	ppb	0.097
	PO4	ppm	0.200		Lu	ppb	0.002		Th	ppb	0.013
	SO4	ppm	0.200		Mo	ppb	0.685		Ti	ppb	0.564
ICP-DRC-MS	Se	ppb	0.110		Nb	ppb	0.066		Tl	ppb	0.035
ICP-MS	Ag	ppb	1.000		Nd	ppb	0.024		Tm	ppb	0.002
	Al	ppb	0.444		Ni	ppb	0.017		U	ppb	0.004
	As	ppb	0.881		P	ppb	4.060		V	ppb	4.375
	Ba	ppb	0.008		Pb	ppb	0.008		Y	ppb	0.005
	Cd	ppb	0.041		Pd	ppb	0.012		Yb	ppb	0.002
					Pr	ppb	0.009		Zn	ppb	0.147
					Pt	ppb	0.011		Zr	ppb	0.003

***Water sample concentration correction factor*:** After collecting water samples from each reactor, the same volume of Emory River water was added to the respective reactor to maintain a constant solid:solution ratio. This addition caused dilution of the remaining water in the reactor. To account the dilution factor, the concentrations of measured species or parameters were corrected using the following equation.

$$C_{corrected}=\frac{C_{m,0}V_s+C_{m,1}(V_0-V_s+V_a)}{(V_0-V_s+V_a)}$$

where $C_{corrected}$ is the concentration corrected for the dilution, $C_{m,0}$ is the concentration measured in the previous sample, $C_{m,1}$ is the concentration measured in the following sample, V_0 is the initial volume in the control or coal ash reactors, V_s is the volume of the sample removed, and V_a is the volume of the Emory River water added to replace the sample. The exact volumes removed and added were measured by the differences in masses of the filled and empty syringe (Ryan et al., 2011).

Experimental Setup**:** Coal ash weathering experiments were conducted using three batch reactors containing Kingston coal ash, Emory River sediment, and Emory River water and a control batch reactor with only river sediment and water.

To simulate the weathering processes of coal ash, the batch experiments were first conducted with solution exposed to open atmosphere. This portion of the experiment represents the condition when fresh ash is deposited on the riverbed surface, exposed to oxygenated water, and mixed slightly with the upper sediment layer. To simulate weathering under reducing conditions, the batch reactors were then closed to the atmosphere. This portion of the experiment represents the condition when coal ash has been covered by layers of fresh sediment and detritus, and becomes entrenched in the hyporheic zone depleted of oxygen.

Batch Experiment – Oxidizing Stage**:** One control reactor with only Emory River sediment and water was used to determine the release of elements from the sediment, while batch reactors with an ash-sediment mixture were conducted in triplicate. Each of the three coal ash reactors were comprised of a 4 L trace metal-clean jar, 500 g of dried Emory River sediment, 500 g of Kingston coal ash, and 3 L of Emory River water (Figure 3.2). The ash-sediment-water mixture was prepared by suspending 250 g of sediment in 1.5 L of river water, mixing by hand, adding 250 g of coal ash, mixing by hand, and then repeating the process. The mixture was allowed to settle for 3 h, which formed an ash-sediment layer at the bottom of the reactor. Floating particles (< 5 g) were removed from the air-water interface. Batch reactors with an ash-sediment mixture were conducted in triplicate to ensure statistical significance of the results. The control reactor consisted of a 4 L trace metal clean jar, 500 g of dried Emory River sediment, and 3 L of Emory River water.

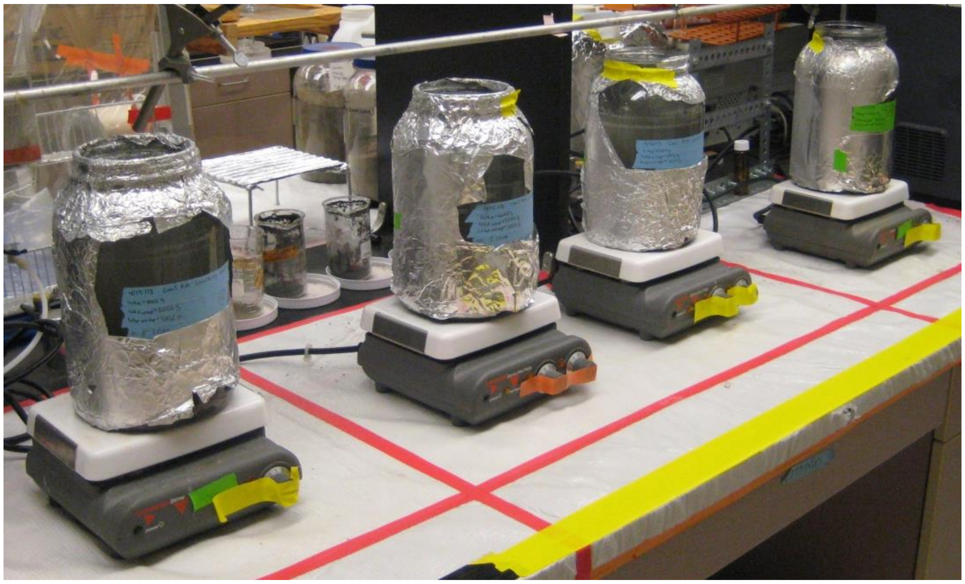

Figure 3.2. Experimental setup to release elements from coal ash under oxic condition. The three coal ash reactors are colored blue, and the control reactor is colored green.

Floating magnetic stir bars were placed in the water layer without touching the solid layer. Floating magnetic stir bars allow water to be circulated above a solid layer at a desired speed, without disturbing the solid layer. In this experiment, floating stir bars were rotated at the lowest speed (45 rpm) to stimulate exchange between surface water and groundwater and to promote mixing of the river water.

The reactors were sampled at intervals of 0.5, 1, 2, and 4 h, and then daily for 7 d. Sampling frequency was high during the first day in order to thoroughly categorize elemental behavior and water quality during the initial deposition of coal ash.

Batch Experiment – Reducing Stage**:** Upon completion of oxic sampling, the triplicate coal ash reactors and the control reactor were transferred to a glove box (AirScience, Purair® Flex™) for the anoxic portion of the experiment. To maintain reducing condition, nitrogen gas (ultra-high purity) was pumped through fritted glass diffusers into the batch reactors to displace oxygen (Figure 3.3). Magnetic stir plates were placed underneath the glove box to continue the slow rotation of the floating stir bars within the batch reactors during the anoxic experiments. The reactors were inspected prior to sampling to ensure the nitrogen gas bubbles did not disturb the ash-sediment or sediment-only layers or cause interference with the rotation of the floating stir bar.

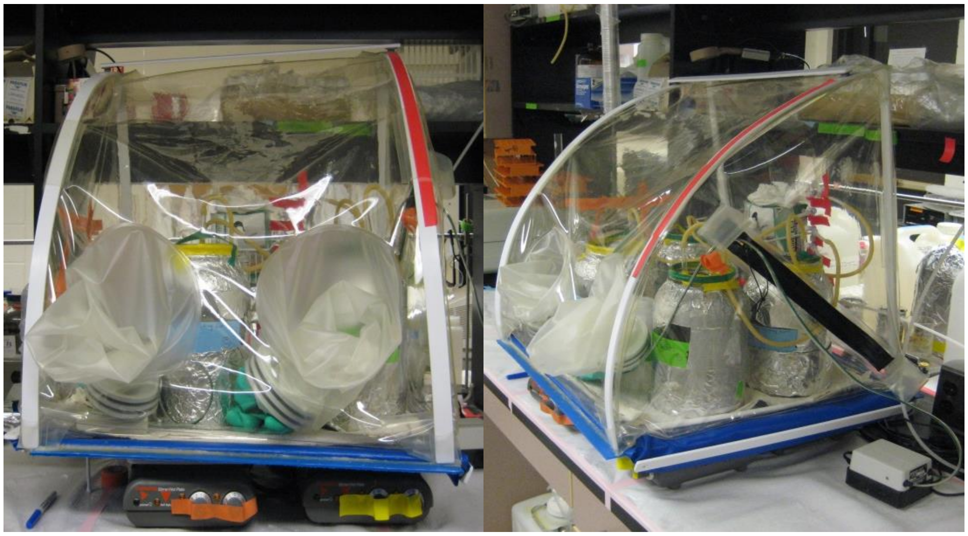

Figure 3.3. Experimental setup to release elements from coal ash under anoxic condition. The three coal ash reactors are colored blue, and the control reactor is colored green.

Nitrogen gas was allowed to diffuse into each reactor for 2 h prior to the commencement of sampling. Several initial redox potential measurements were taken in each batch reactor to ensure that the system was transitioning to reducing conditions. Afterwards, the first anoxic water samples were collected from the coal ash and control reactors.

Sequential water samples were collected over one month. The reactors were sampled at intervals of 0.5, 1, 2, and 4 h, daily for 7 d, and then once per week for the final three weeks. Sampling frequency was high during the first day of the anoxic experiment in order to monitor the elemental release and effects on water quality during the change to reducing conditions.

Mineralogical Analysis**:** Mineral composition of the sediment and the coal ash were analyzed using x-ray powder diffraction (XRD; Siemens Kirstalloflex 805). One gram of dried solid sample were mixed separately with corundum (0.25 g), milled, and analyzed at 2Θ angles between 5 and 65° at 0.02° steps with a 2 s count per step to measure peak intensities using copper K_α radiation. Measured peak intensities were then fitted with known mineral peaks (Brown et al., 1980) to determine the mineralogy of the sample using RockJock (Eberl, 2003). The goodness of fit between the measured and calculated XRD peaks is indicated by the 'degree of fit' parameter, where values below 0.10 signify the reliability of the analysis (Eberl, 2003). Several clay minerals are often indistinguishable from one another at low 2Θ angles of 25° or less (e.g., smectite, illite, chlorite, biotite, vermiculite); therefore, the low angle region of the diffractogram was inspected to see if clay minerals with peaks in this region should be included in the analysis (Eberl, 2003). Indistinguishable clay minerals present in the low angle region required chemical alteration of samples to separate clay mineral peaks. However, alteration of samples to distinguish clays prevented any quantitative analysis of the fine clay fraction mineralogy in the low angle region.

Emory River sediment was first analyzed in the bulk fraction followed by the fine clay fraction. The bulk sediment was sieved to less than 500 µm, as required by XRD, and analyzed on a randomly-oriented powder mount to measure the peak intensities between 2Θ angles of 5 and 65°. The 2Θ angles were then converted to *d*-spacings, the distance between adjacent planes of atoms, using Bragg's Law (Brown et al., 1980; Eberl, 2003). Quantitative analysis of bulk Emory River sediment was possible because the mass of the sample being analyzed was known, which allowed RockJock to determine the percentage of each mineral by weight.

Fine clays were mixed with de-ionized (DI) water, sonicated, and centrifuged (1000 rpm, 2 min) to separate from fines from the bulk sediment. The supernatant, containing the <2 µm clay fines, was then pipetted onto silicon wafers and dried in air. The fine clay fraction of the Emory River sediment was analyzed using an oriented aggregate mount, containing the silicon wafer, to determine the peak intensities between low 2Θ angles of 2 and 19°. Results from the fine clay fraction revealed that additional analysis was required to differentiate minerals with similar peaks in the low angle region. To separate indistinguishable fine clay peak intensities from one another, ethylene glycol was applied to the oriented mount to expand clay layers (Eberl, 2003). The addition of ethylene glycol to the sample altered the peak intensities, their locations, and the sample mass, which prevented any quantitative mineral determination in the fine clay fraction of sediment. Kingston coal ash was analyzed on a randomly-oriented powder mount to quantify the mineral content of the ash. No clay minerals were detected in the Kingston coal ash, thus a fine clay fraction analysis was not required.

Statistical calculations**:** A Spearman's rank correlation coefficient matrix was used to find correlations between water quality parameters measured in this study. Spearman's rank correlation coefficient measures the tendency of one variable to increase as another variable increases, without requiring that increase to be linear. Conversely, the correlation coefficients will be negative if one variable decreases and another increases. The Spearman's rank correlation coefficient, ρ, ranges from -1 to 0 to 1, denoting perfect negative correlation, no correlation, and perfect positive correlation, respectively (Dytham, 2011). Each of the variables were analyzed in a correlation matrix using OriginPRO (OriginLab®). The Spearman's correlation coefficient matrix allowed for correlations to be determined between all variables in this study simultaneously.

In addition to the ρ parameter, the level of significance, *P*, was also used to examine the results for correlations. In order to determine if the obtained Spearman's ρ values are sufficient to be deemed statistically significant, the level of significance was set at 0.05. Using the correlation matrix function in OriginPRO allowed for the significant correlations to be highlighted with an asterisk. Only significant correlations were considered in this study.

Pearson's product-moment correlation was not viable for this experiment because the data was not normally distributed, nor was it measured on a continuous scale. Because these conditions did not apply, Spearman's rank correlation coefficient was used instead (Dytham, 2011). Spearman's correlations are much more conservative than Pearson's, thus they may give a more realistic interpretation of the correlations found in the data.

***Error calculations*:** Errors in measurements were calculated for all water quality parameters in each of the three coal ash reactors and for the characterization of Kingston Fossil Plant coal ash and Emory River sediment. For the water quality parameters, standard deviations were estimated from measurements on triplicate samples, with each sample analyzed twice. Standard deviations of water quality parameters and major and trace element concentrations in solid coal ash and sediment were then divided by the square root of the number of replicate samples to obtain standard error. Because the control reactor had only one measurement per sample, no standard deviation or standard error calculations were made. Standard error between triplicate coal ash reactor water samples are shown as error bars in all figures.

Results

Characterization of Emory River sediment**:** The major constituent of the Emory River sediment was silica and the minor constituents included alumina and organic matter in the bulk sediment sample (Table 3.2). The Emory River sediment was sieved to contain grains less than 500 µm in diameter for XRD. The major minerals in the Emory River sediment were quartz and clay minerals (Table 3.3). In the XRD analysis and curve fitting of Emory River sediment, the degree of fit between measured and calculated peak intensities was 0.08, which indicated a good degree of fit (Figures 3.4, 3.5). The non-clay fraction of the sediment was 87.3% quartz, 1.2% plagioclase (labradorite), and 1.0% potassium-feldspar (K-feldspar, ordered microcline). The clay mineral fraction made up 10.5% of the bulk sediment, including 6.1% smectite, 2.4% illite, and 2.1% kaolinite. The clay-sized fraction of the Emory River sediment consisted of chlorite, biotite, and kaolinite.

Table 3.2. Emory River sediment characterization by total acid digestion and ICP-MS (trace elements), ICP-DRC-MS (Se), ICP-OES analysis (major elements), and thermal decomposition (Hg). Standard error between replicate samples is shown next to each measurement.

Major Elements (mass % oxides)		Trace Elements (ng g^{-1})			
SiO_2	84.6 ± 2.43	Ag	BDL	Pd	BDL
Al_2O_3	4.43 ± 0.29	As	11,500 ± 800	Pr	4650 ± 366
Fe_2O_3	1.86 ± 0.17	Ba	132,000 ± 11,000	Pt	BDL
K_2O	0.65 ± 0.04	Cd	294 ± 16	Rb	27,300 ± 2060
TiO_2	0.34 ± 0.02	Ce	38,700 ± 3,200	Rh	BDL
CaO	0.29 ± 0.04	Co	8850 ± 769	Ru	BDL
MgO	0.24 ± 0.02	Cr	19,400 ± 1820	Sc	53,400 ± 1900
P_2O_5	0.23 ± 0.019	Cs	1319 ± 110	Sb	410 ± 37.4
Na_2O	0.077 ± 0.0112	Cu	8860 ± 856	Se	BDL
MnO	0.029 ± 0.0018	Dy	2130 ± 228	Sm	3450 ± 297
LOI[a]	4.77 ± 0.06	Er	1230 ± 129	Sn	3450 ± 297
Total	97.5	Eu	717 ± 63.5	Sr	BDL
		Gd	3480 ± 348	Ta	12,300 ± 2520
		Ge	1050 ± 48.6	Tb	12,300 ± 2520
		Hf	2870 ± 252	Te	BDL
		Hg[b]	45.0 ± 0.29	Th	5670 ± 284
		Ho	392 ± 42.6	Tl	BDL
		La	18,600 ± 1460	Tm	BDL
		Lu	217 ± 0.0	U	1680 ± 160
		Mo	BDL	V	59,300 ± 7610
		Nb	8850 ± 656	Y	10,100 ± 1080
		Nd	17,900 ± 1200	Yb	1190 ± 84.2
		Ni	17,700 ± 1520	Zn	58,300 ± 3700
		Pb	295,000 ± 33,700	Zr	75,300 ± 7040

[a] Loss on ignition at 550°C

[b] Mercury concentration determined previously (Ruhl et al., 2009)

Table 3.3. Emory River sediment mineralogy. Mineralogical content is expressed as the weight percent of each mineral present in the sample (%).

Mineral	Weight percent (%)
NON-CLAYS	
Quartz	87.3
K-feldspar (ordered microcline)	1.0
Plagioclase (labradorite)	1.2
Total non-clays	89.5
CLAYS	
Kaolinite (Dry Branch)	2.1
Smectite (Ca-Kinney montmorillonite)	6.1
Illite (1M; RM30)	2.4
Total clays	10.5
TOTAL	100.0
Full pattern degree of fit:	0.08

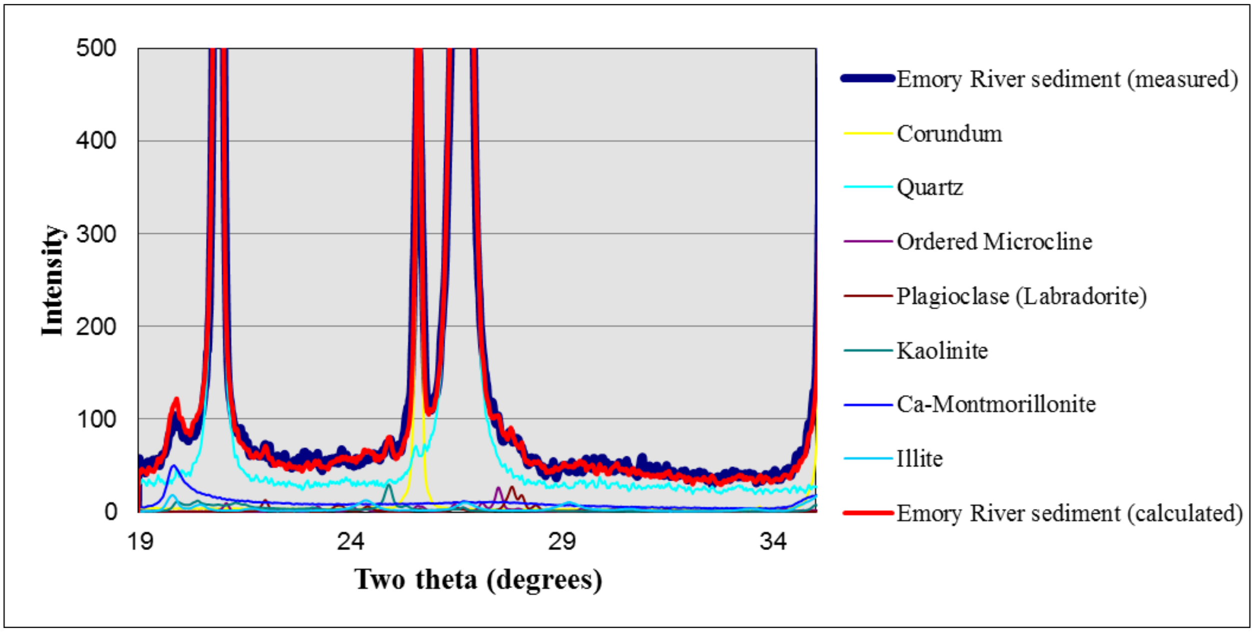

Figure 3.4. XRD diffractogram of bulk Emory River sediment from 2Θ angles between 19 and 34° as analyzed in RockJock. The measured sediment diffraction pattern and peak intensities are shown in blue and the calculated diffraction pattern is displayed in red. Standard minerals used to create the calculated diffraction pattern are shown in the legend.

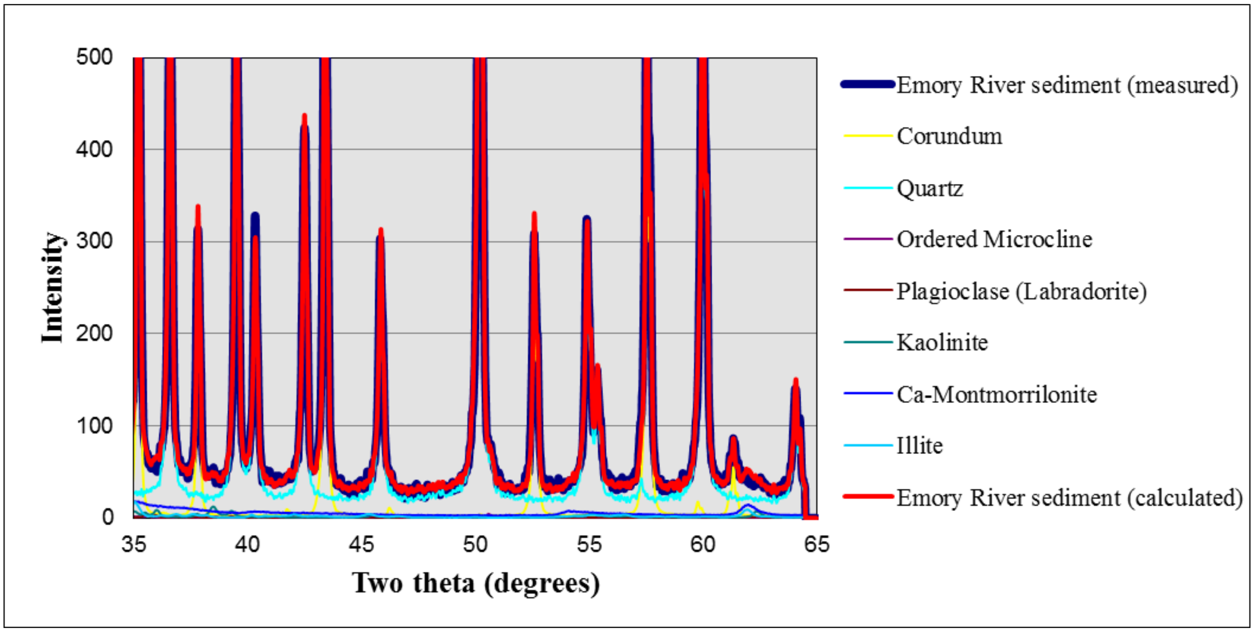

Figure 3.5. XRD diffractogram of bulk Emory River sediment from 2Θ angles between 35 and 65° as analyzed in RockJock. The measured sediment diffraction pattern and peak intensities are shown in blue and the calculated diffraction pattern is displayed in red. Standard minerals used to create the calculated diffraction pattern are shown in the legend.

***Characterization of coal ash*:** The chemical characterization of Kingston coal ash showed that it consisted primarily of silica and alumina in the bulk ash sample (Table 3.4). The Kingston coal ash was sieved to contain grains less than 500 µm in diameter for XRD. The major minerals were identified as tephra, quartz, sillimanite, and ferric oxyhydroxides (Table 3.5). In the XRD analysis and curve fitting of Kingston coal ash, the degree of fit between measured and calculated peak intensities was 0.09, which indicated a good degree of fit (Figures 3.6 and 3.7). No clay minerals were detected in the Kingston coal ash.

Table 3.4. Kingston coal ash characterization by total acid digestion and ICP-MS (trace elements), ICP-DRC-MS (Se), ICP-OES analysis (major elements), and thermal decomposition (Hg). Standard error between replicate samples is shown next to each measurement.

Major Elements (mass % oxides)		Trace Elements (ppb or ng g^{-1})			
SiO_2	48.8 ± 1.65	Ag	BDL	Pd	41.9 ± 1.22
Al_2O_3	25.1 ± 0.22	As	145 ± 0.96	Pr	42.2 ± 1.14
CaO	7.48 ± 0.04	Ba	4420 ± 29.1	Pt	0.45 ± 0.18
Fe_2O_3	5.23 ± 0.01	Cd	2.72 ± 0.059	Rb	182 ± 1.54
MgO	1.93 ± 0.02	Ce	350 ± 2.18	Rh	0.71 ± 0.029
K_2O	1.79 ± 0.07	Co	130 ± 1.49	Ru	1.05 ± 0.046
TiO_2	1.39 ± 0.01	Cr	281 ± 1.94	Sc	343 ± 3.28
Na_2O	0.65 ± 0.01	Cs	13.7 ± 0.12	Sb	13.6 ± 0.25
P_2O_5	0.62 ± 0.04	Cu	353 ± 2.14	Se	15,100 ± 612
MnO	0.023 ± 0.00033	Dy	31.4 ± 0.35	Sm	42.4 ± 0.40
LOI[a]	6.20 ± 0.0002	Er	19.2 ± 0.21	Sn	13.1 ± 0.57
Total	99.2	Eu	13.1 ± 0.17	Sr	2540 ± 17.7
		Gd	52.5 ± 0.53	Ta	16.0 ± 3.49
		Ge	30.4 ± 0.17	Tb	6.32 ± 0.05
		Hf	14.3 ± 0.39	Te	BDL
		Hg	407 ± 21.6	Th	55.8 ± 0.88
		Ho	6.09 ± 0.055	Tl	6.64 ± 0.11
		La	171 ± 1.03	Tm	2.45 ± 0.031
		Lu	2.29 ± 0.02	U	24.9 ± 0.15
		Mo	24.4 ± 1.78	V	711 ± 10.1
		Nb	62.8 ± 0.94	Y	167 ± 1.25
		Nd	160 ± 0.71	Yb	15.8 ± 0.09
		Ni	267 ± 0.71	Zn	332 ± 2.40
		Pb	130 ± 63.1	Zr	474 ± 2.68

[a] Loss on ignition at 550°C (Craven, 2012)

Table 3.5. Kingston Fossil Plant coal ash XRD mineralogy results, as calculated by RockJock. Mineralogical content is expressed as the weight percent of each mineral present in the sample (%).

Mineral	Weight Percent (%)
NON-CLAYS	
Quartz	9.6
Kspar (ordered Microcline)	0.5
Hematite	1.2
Goethite	1.3
Sillimanite	9.1
Tephra (White River)	78.2
Total non-clays	100.0
CLAYS	
Total clays	0.0
TOTAL	100.0
Full pattern degree of fit:	0.09

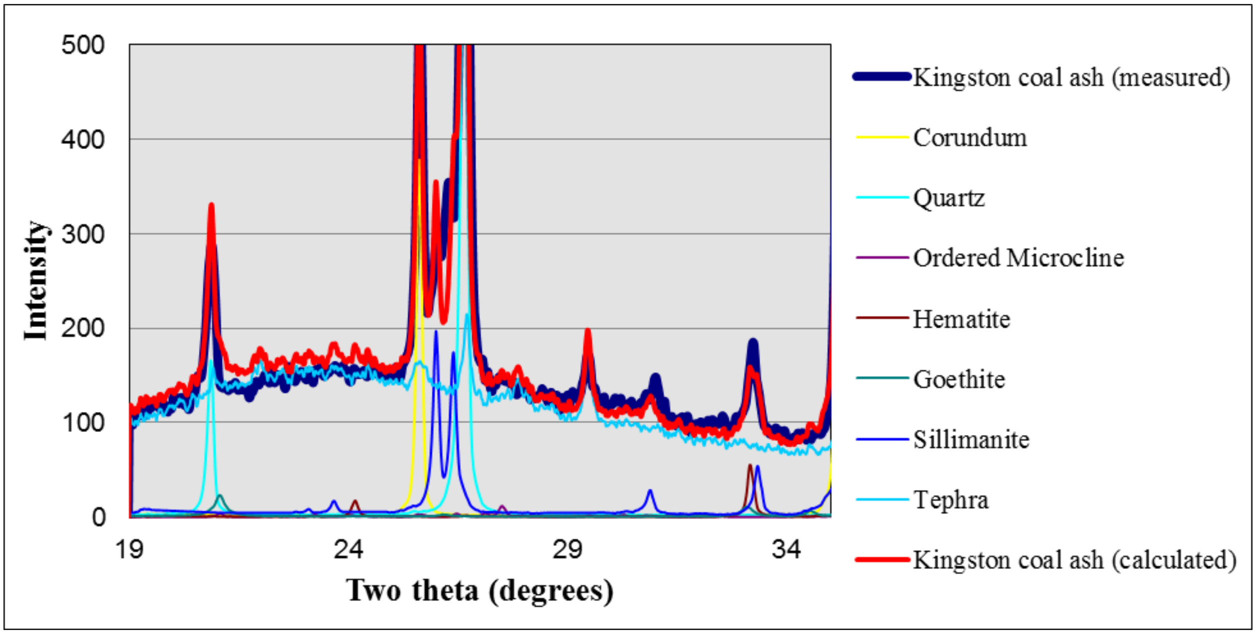

Figure 3.6. XRD diffractogram of bulk Kingston coal ash from 2Θ angles between 19 and 34°, as analyzed in RockJock. The measured sediment diffraction pattern and peak intensities are shown in blue and the calculated diffraction pattern is displayed in red. Standard minerals used to create the calculated diffraction pattern are shown in the legend.

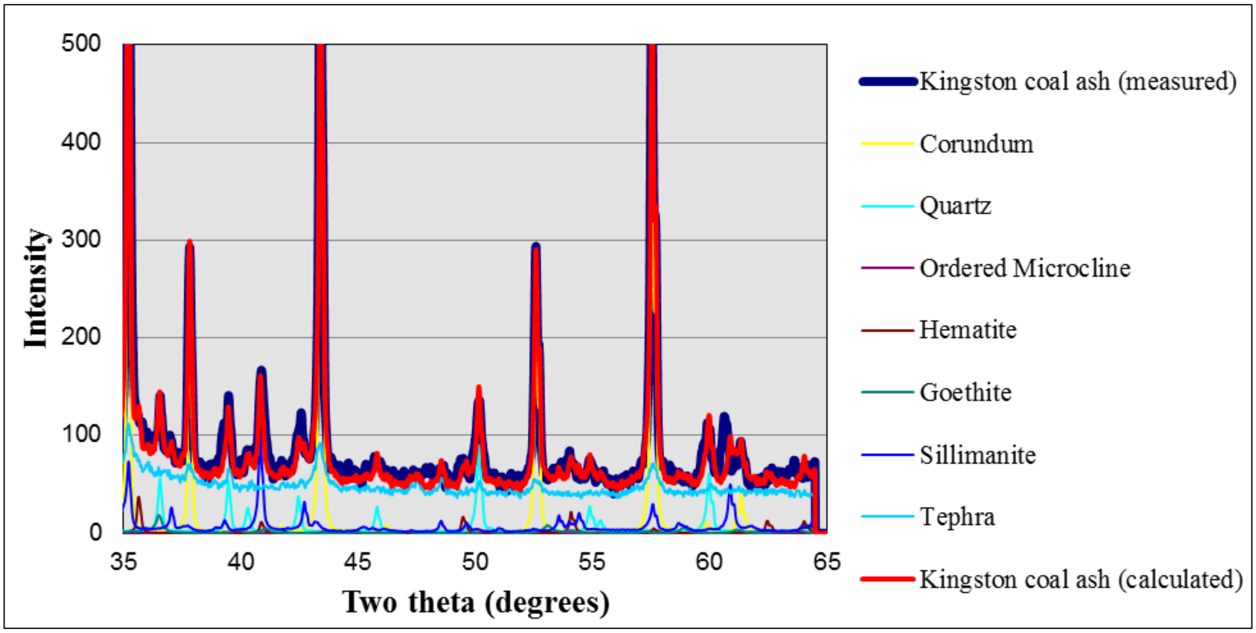

Figure 3.7. XRD diffractogram of bulk Kingston coal ash from 2Θ angles between 35 and 65°, as analyzed in RockJock. The measured sediment diffraction pattern and peak intensities are shown in blue and the calculated diffraction pattern is displayed in red. Standard minerals used to create the calculated diffraction pattern are shown in the legend.

***Redox potential in batch reactors*:** Redox potential behaved similarly in the control and coal ash reactors (Figure 3.8). Open to the atmosphere, redox potential increased initially before reaching a plateau at about 50 h. At 166 h, nitrogen gas was pumped into the reactors and the redox potential decreased to 0.0 mV at about 250 h and to about -600 mV at about 650 h. The control reactor reached reducing conditions more rapidly that the coal ash reactors. The redox potential measurements were used to designate three stages of the experiment: (1) oxidizing (0 to 166 h), (2) transition (166 to 222 h), and (3) reducing (222 to 895 h).

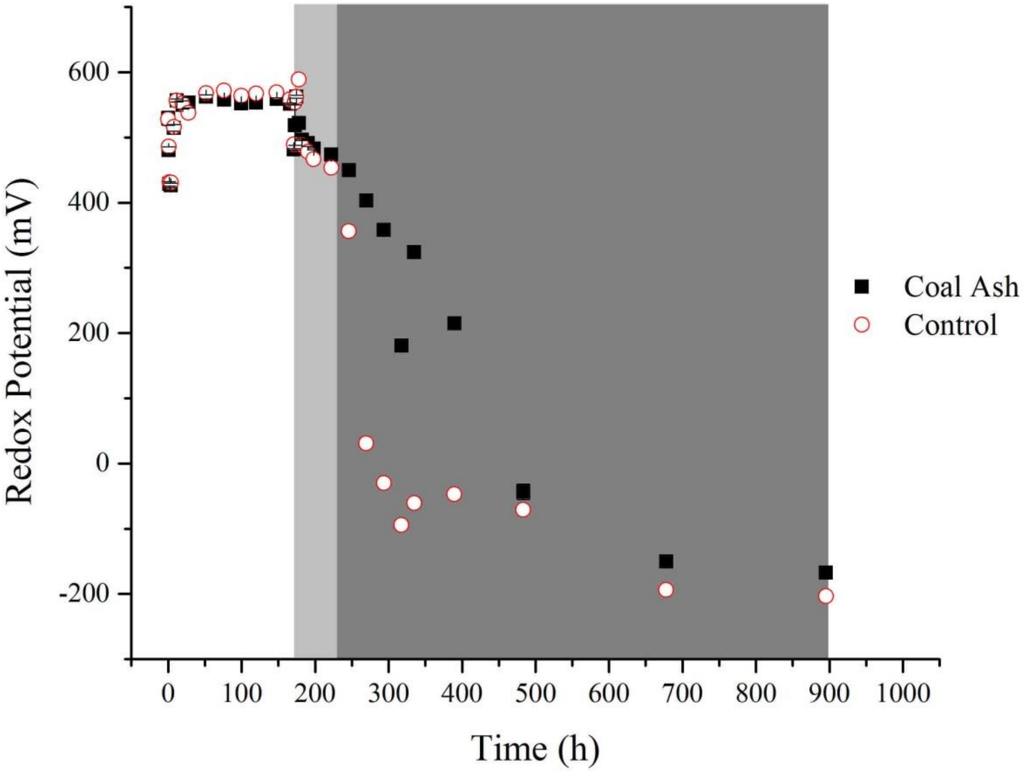

Figure 3.8. Redox potential measurements in coal ash and control batch reactors as a function of time. Closed symbols correspond to samples taken in coal ash reactors. Open symbols represent samples taken from the control reactor. The oxidizing, transition, and reducing stages are shown in white, light grey and dark grey, respectively. Error bars in coal ash reactor samples represent the standard error between triplicate sample measurements.

***Conductivity in batch reactors*:** The conductivity profile for the control reactor was stable over the course of the experiment; however, conductivity in the coal ash reactors varied greatly (Figure 3.9). In the coal ash reactors, the conductivity was highest initially and decreased over the oxic stage. During the transition stage, conductivity decreased from nearly 1,400 to roughly 900 µS. Conductivity continued to decrease to a minimum around 350 h, beyond which conductivity increased slowly until the end of the experiment. In the control reactor, conductivity was steady during the transition and reducing stages; however, a slight decrease in conductivity occurred after 350 h.

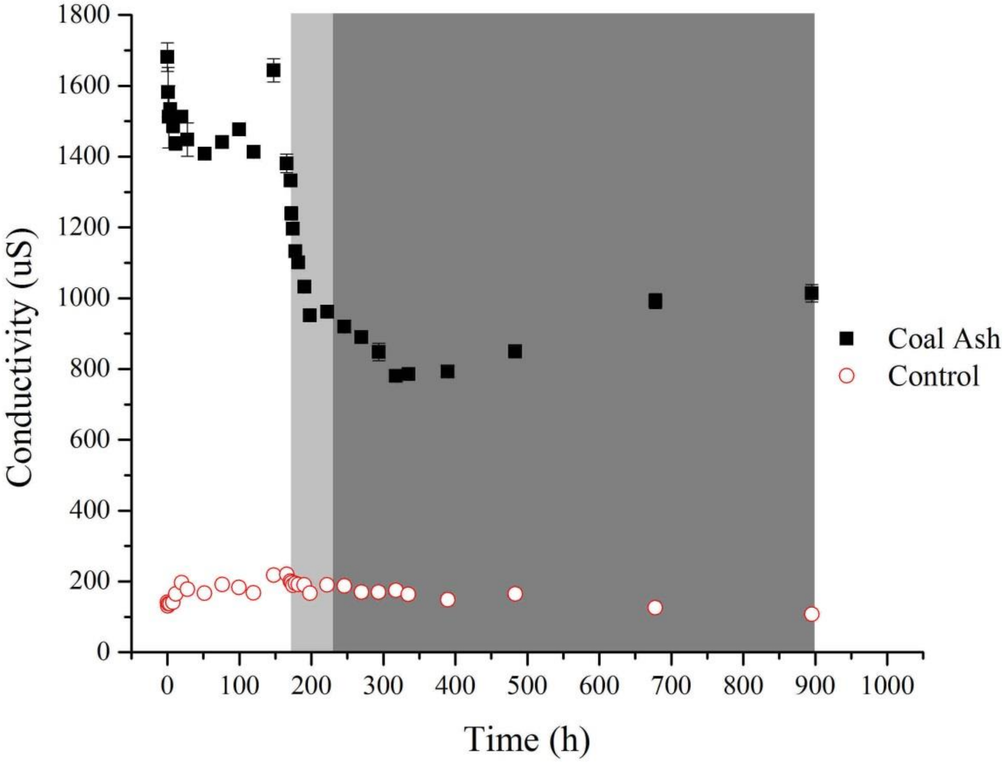

Figure 3.9. Conductivity measurements in coal ash and control batch reactors as a function of cumulative experiment time. Closed symbols correspond to samples taken in coal ash reactors. Open symbols represent samples taken from the control reactor. The oxidizing, transition, and reducing stages are shown in white, light grey and dark grey, respectively. Error bars in coal ash reactor samples represent the standard error between triplicate sample measurements.

pH in batch reactors**:** In the control and coal ash reactors, pH behaved similarly (Figure 3.10). The pH of water samples in the reactors decreased initially from around pH 8 to near pH 7 over the first 2 d of the experiment. As the oxidizing stage continued, the pH of the reactors was steady until the transition stage, at which point pH increased from near neutral to around 9. During the reducing stage, the pH in the reactors was steady around pH 9.

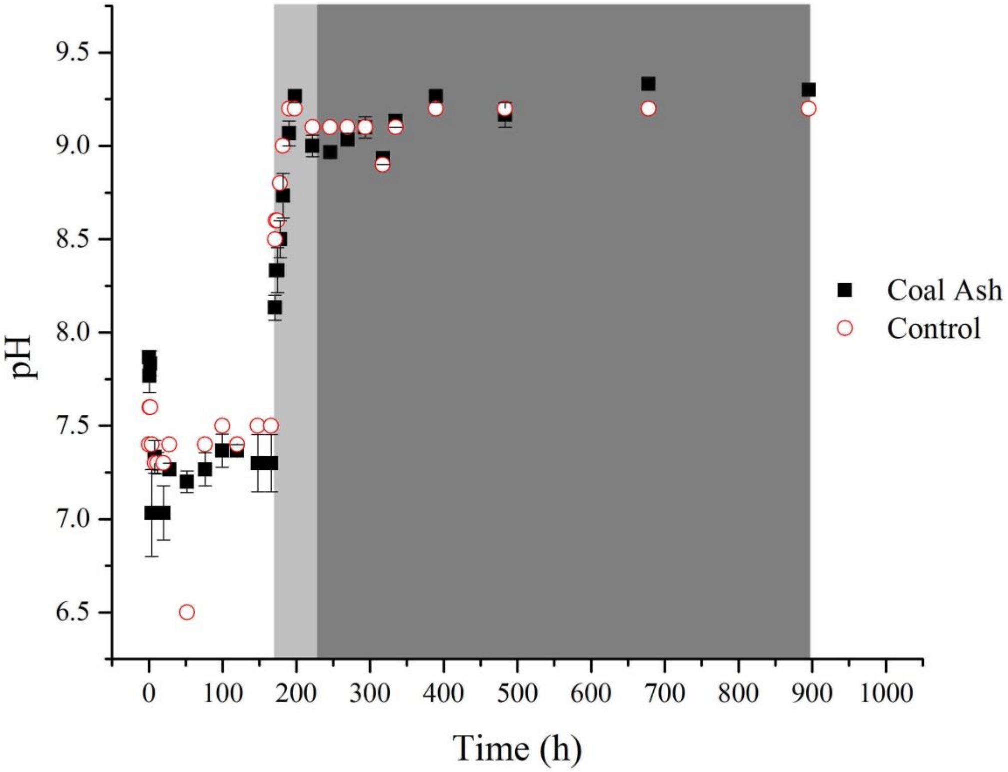

Figure 3.10. Measurements of pH in coal ash and control batch reactors as a function of cumulative experiment time. Closed symbols correspond to samples taken in coal ash reactors. Open symbols represent samples taken from the control reactor. The oxidizing, transition, and reducing stages are shown in white, light grey and dark grey, respectively. Error bars in coal ash reactor samples represent the standard error between triplicate sample measurements.

Elemental water sample results**:** Due to the large number of analyses, elements have been separated and grouped together for reasons relating to their chemical characteristics, location on the periodic table, and similar release behavior. Major elements (Al, Ca, Fe, K, Mg, Mn, Na, Si) were separated in two groups: (1) major cations (Ca, K, Mg, Na) and (2) major elements (Al, Fe, Mn, Si). Trace elements (As, Ba, Cd, Ce, Co, Cr, Cs, Cu, Eu, Ge, Mo, Nb, Ni, P, Pb, Pd, Pt, Rb, Rh, Ru, Sc, Sb, Sm, Sr, U, V, Ta, Ti, Y, Zn, Zr) were separated into several groups: (1) alkali and alkaline earth metals (Ba, Cs, Rb, Sr), (2) oxyanion forming elements (As, Cr, Mo, Se, V), (3) transition metals (Cd, Co, Cr, Cu, Hg, Nb, Ni, Pb, Pd, Pt, Rh, Ru, Sc, Ta, Ti, Y, Zn, Zr), (4) other metals (Sn, Tl), and (5) metalloids (Ge, Sb). Rare earth elements (REE) were separated into two groups: (1) lanthanides (Ce, Eu, Gd, Sm) and (2) actinides (Th, U).

***Release of major cations*:** The release behavior of major cations was similar in coal ash and control reactors over the course of the experiment (Figure 3.11). In coal ash reactors, peak Na, K, Mg, Ca concentrations were measured in the first sample, and subsequently decreased until 50 h. Potassium, Mg, and Na concentrations reached a plateau from 50 to 100 h, and then slowly decreased until the transition stage. Conversely, Ca concentration increased from 50 h to 100 h. All major cations experienced a decrease in concentration after the oxidizing stage was complete, proceeded by a slower decrease in concentration during the reducing stage. Potassium, Mg, and Na concentrations reached a plateau in the reducing portion of the experiment. Calcium concentration, on the other hand, increased in concentration from roughly 325 to 500 h, at which point concentrations reached a plateau.

In the control reactor containing only Emory River sediment, release behavior of all major cations was similar. Calcium, K, and Mg concentrations increased over oxidizing conditions, decreased slightly during the transition stage, and finally decreased slowly until a plateau was reached in the reducing stage. Sodium concentration differed in that release increased during the transition stage before reaching a constant concentration in the reducing stage.

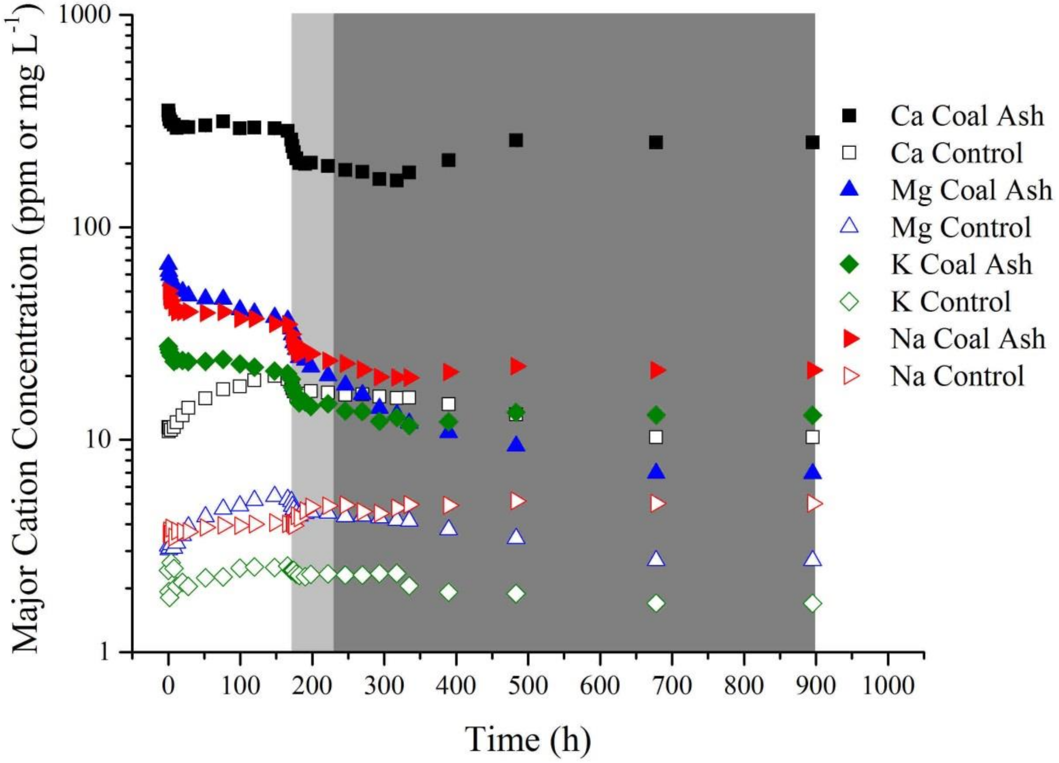

Figure 3.11. Concentration of the major cations Na, K, Mg, and Ca as a function of time. Closed symbols correspond to samples taken in coal ash reactors. Open symbols represent samples taken from the control reactor. The oxidizing, transition, and reducing stages are shown in white, light grey and dark grey, respectively. Error bars in coal ash reactor samples represent the standard error between triplicate sample measurements.

***Release of major elements*:** Release of major elements varied between elements as well as between coal ash and control reactors (Figure 3.12). In coal ash reactors, Si concentration was highest initially and decreased steadily until the transition stage, beyond which concentration of Si increased significantly. In the reducing stage, Si release decreased slowly before reaching an apparent plateau after 650 h. Iron concentrations were below detection limit prior to the transition stage, whereupon Fe release increased by several orders of magnitude. The spike in Fe concentration subsided after roughly 350 h, and was subsequently decreased below detection limit. Concentration of Al in coal ash reactors increased until 350 h, beyond which the concentrations remained constant. Manganese concentration was greatest initially, decreasing under oxidizing conditions and over the transition stage. In the reducing stage, Mn concentrations remained constant until 350 h, at which point a slight increase in concentration was observed before becoming steady.

Initial Mn concentrations in coal ash and control reactors were similar; however, Mn concentration in the control reactor spiked prior to the transition stage. In the control, the transition stage caused increased Mn concentration until the start of the reducing stage, after which Mn concentrations reached a plateau. Concentration of Si in the control batch reactor differed from the coal ash reactor. Silicon concentration was lowest initially and increased gradually until the transition stage; at which point the concentration increased. Subsequently, the concentration of Si decreased until roughly 650 h, when the concentration was steady. In the control reactor, Fe concentration increased over the experimental duration, reached a plateau after roughly 450 h, and experienced only a small decrease in the transition stage. Concentration of Al in the control reactor dipped under oxidizing conditions and later increased several orders of magnitude in concentration over the transition stage. Aluminum concentrations remained relatively constant during the reducing stage in the control reactor.

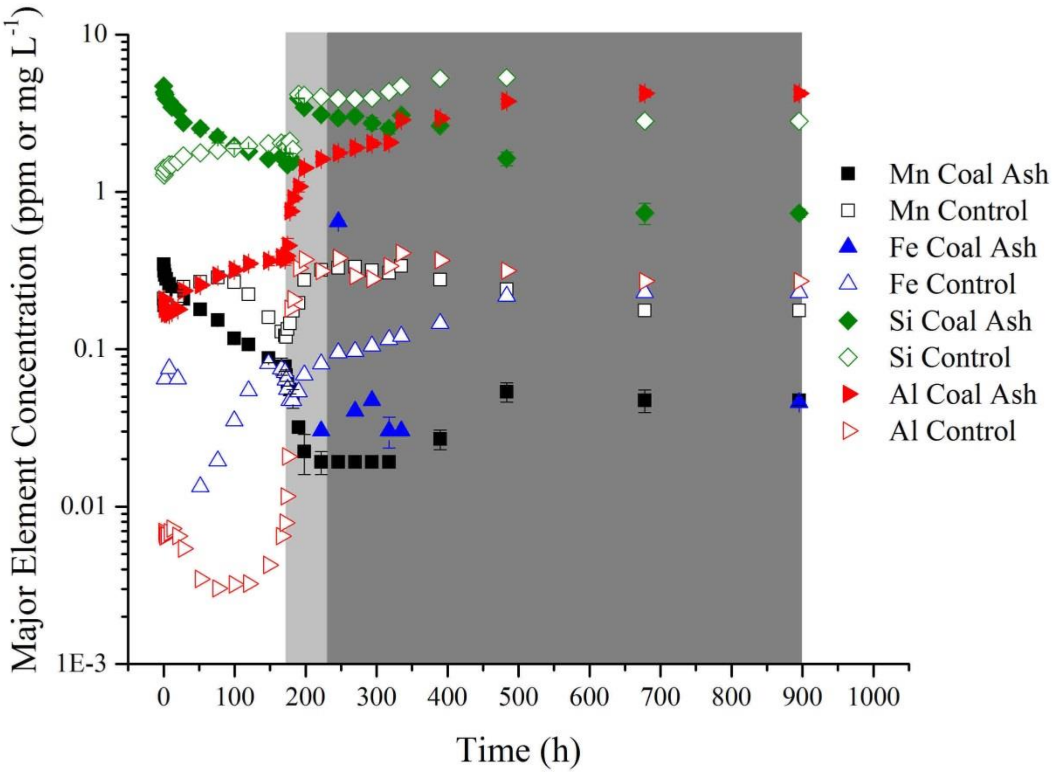

Figure 3.12. Concentration of the major elements Al, Fe, Mn, and Si as a function of time. Closed symbols correspond to samples taken in coal ash reactors. Open symbols represent samples taken from the control reactor. The oxidizing, transition, and reducing stages are shown in white, light grey and dark grey, respectively. Error bars in coal ash reactor samples represent the standard error between triplicate sample measurements.

***Release of alkali and alkaline earth metals*:** Alkali and alkaline earth metals release in coal ash reactors was comparable between elements with similar ionic radius (Figure 3.13). Concentrations of Sr and Rb decreased slightly from their initial values, and remained constant while exposed to oxidizing conditions. During the transition stage, Sr and Rb concentration decreased. Concentrations of Sr and Rb slowly decreased in the reducing stage until roughly 350 h, at which point a slight increase, followed by a plateau in concentration was observed until the culmination of the experiment. In coal ash reactors, concentrations of Ba and Cs initially decreased from the start of sampling and remained constant until the transition stage, at which point a large increase occurred. Barium and Cs concentrations were then constant before increasing slightly at around 350 h. Cesium concentration decreased slightly after 350 h, opposite to Ba, which experienced a small increase in concentration after 350 h. While the trends of Ba and Cs release were similar, Ba concentrations were over two orders of magnitude greater than Cs.

Strontium and Rb concentrations in the control reactor increased under oxidizing conditions. Strontium and Rb concentrations were constant until approximately 350 h, after which point a small decrease was observed. A slight dip in Sr and Rb concentrations occurred during the transition stage. In the control reactor, Ba concentration increased under oxidizing conditions, nearly doubled during the transition stage, and finally remained constant during the reducing stage. Cesium concentration was below the detection limit under oxidizing conditions in the control reactor, but increased nearly two orders of magnitude during the transition stage. Cesium release in control and coal ash reactors was not discernibly different in the reducing stage.

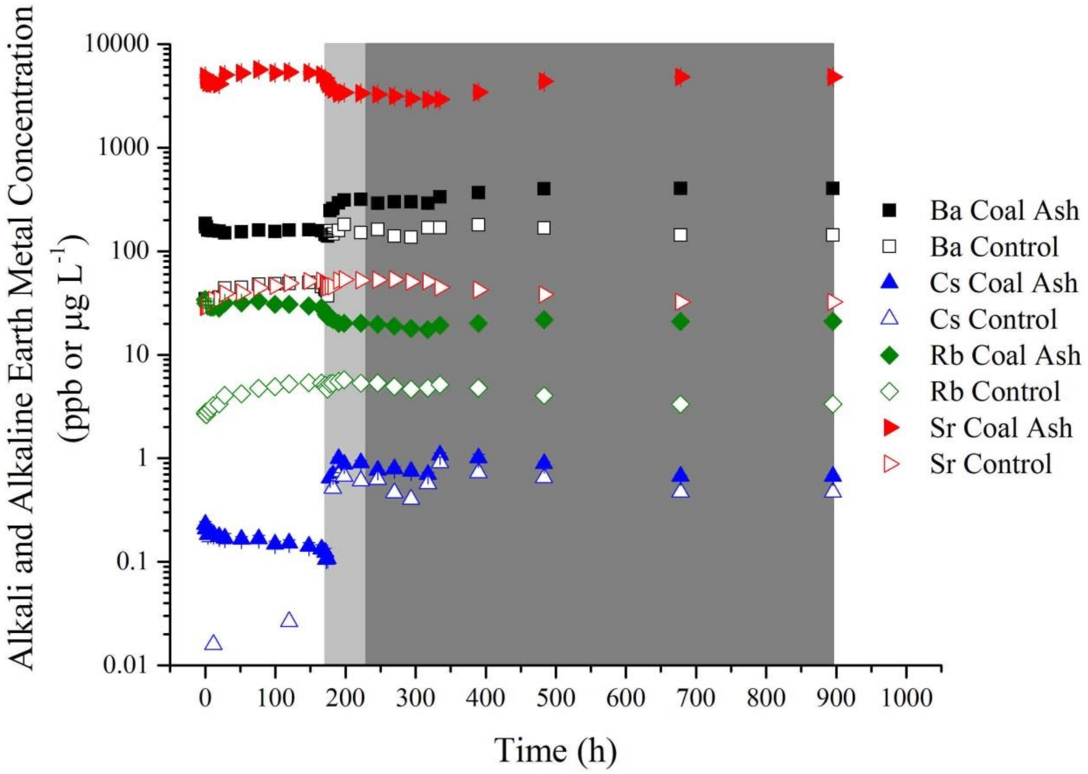

Figure 3.13. Concentration of Rb, Cs, Sr, and Ba as a function of time. Closed symbols correspond to samples taken in coal ash reactors. Open symbols represent samples taken from the control reactor. The oxidizing, transition, and reducing stages are shown in white, light grey and dark grey, respectively. Error bars in coal ash reactor samples represent the standard error between triplicate sample measurements.

***Release of oxyanion-forming elements*:** Release behavior among oxyanion-forming elements (As, Cr, Mo, Se, V) was similar except for As, which behaved differently in the reducing stage (Figure 3.14). In coal ash reactors, Mo concentration increased initially from the start of sampling and remained constant in oxidizing conditions until the transition stage, at which point it decreased rapidly. The decrease in Mo concentration became less pronounced during the reducing stage, and increased after nearly 350 h. Chromium concentration in coal ash reactors decreased rapidly until nearly 350 h, and then reached a plateau. In coal ash reactors, peak Se, As, and V concentrations occurred in the first water sample and decreased under oxidizing conditions. However, Se, As, and V release varied widely after the oxidizing stage.

Se concentration continued to decrease during the transition stage and during the reducing stage until approximately 350 h, when Se concentration increased before reaching a plateau. Vanadium concentration continued to decrease as the experiment entered the reducing stage, before an order of magnitude decrease in concentration occurred between roughly 350 and 450 h. After 450 h, V concentrations remained constant. As release differed from other oxyanion-forming elements after the oxidizing stage of the experiment was complete. The transition stage caused a large increase in As concentration, which remained constant during the reducing stage.

In the control reactor, oxyanion-forming element concentrations were well below their concentrations in the coal ash reactors, except for As. Vanadium was entirely below detection limit in the control reactor. Mo concentration in the control was below detection limit prior to the transition stage. Afterwards, Mo concentration increased before decreasing after nearly 400 h. Selenium concentrations in the control reactor increased in oxidizing conditions and remained at the same levels until around 350 h, when Se concentration increased. Chromium concentration in the control reactor increased until the start of the reducing stage, and subsequently plateaued. Arsenic was below detection limit in the control reactor until the transition stage, beyond which the concentration remained constant.

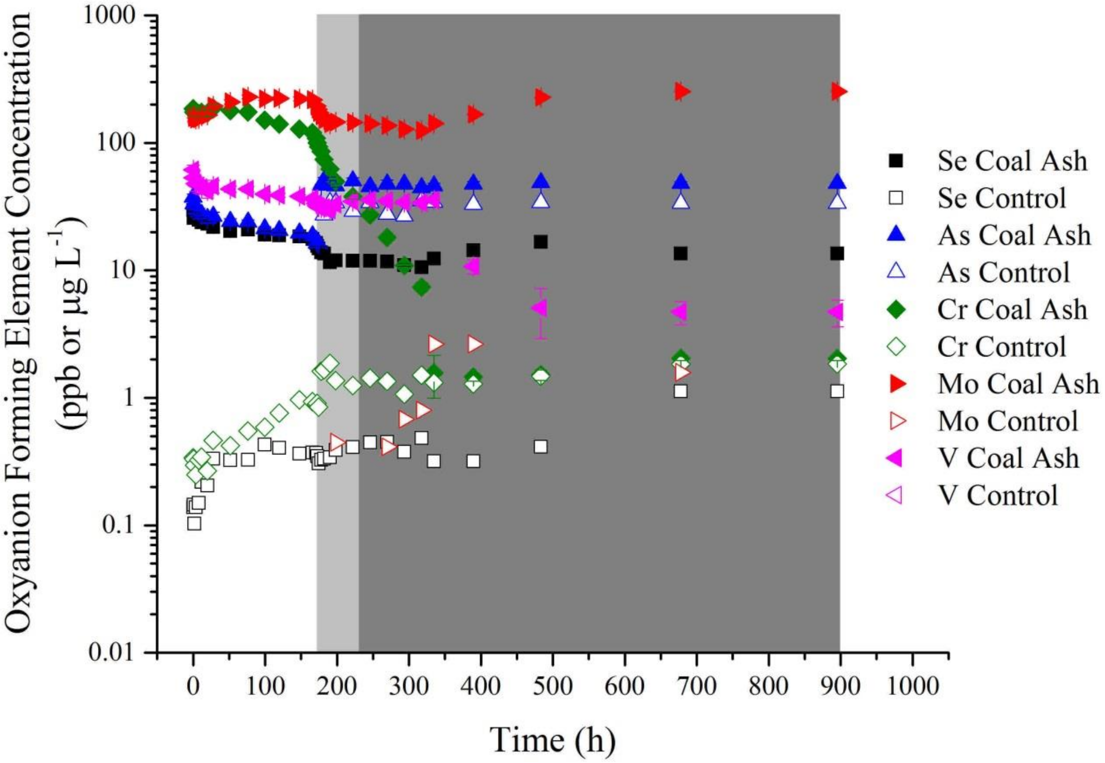

Figure 3.14. Concentration of the oxyanion-forming elements As, Cr, Mo, Se, and V as a function of time. Closed symbols correspond to samples taken in coal ash reactors. Open symbols represent samples taken from the control reactor. The oxidizing, transition, and reducing stages are shown in white, light grey and dark grey, respectively. Error bars in coal ash reactor samples represent the standard error between triplicate sample measurements.

Release of groups 12 and 14 transition metals**:** Elements in the Groups 12 (Figure 3.15) and 14 (Figure 3.16) transition metals (Cd, Hg, Pb, Zn) exhibited variable release among elements and between coal ash and control reactors. Zinc release varied highly among replicate samples, and no trends were discerned; however, Zn release decreased overall throughout the experiment. The standard error of replicate analyses indicated that sequential samples did not have Zn concentrations statistically different from one another. Thus, while Zn concentration seemed to decrease over the oxidizing stage of the experiment, this relationship is not certain. The same was true for the transition and reducing stages; while averaged Zn concentrations between triplicate samples indicated release trends, standard errors between sequential samples showed that the Zn concentrations were not statistically different. Around 350 h, Zn concentrations remained constant until the culmination of the experiment. Cadmium concentrations in coal ash reactors were low; however, error between sequential samples showed that release behaviors could be identified. Cadmium concentration increased under oxidizing conditions, decreased sharply during the transition stage, and decreased slowly during the reducing stage. Cadmium concentration increased after roughly 350 h. In coal ash reactors, Hg concentration increased within the first two hours, and subsequently decreased until around 50 h, before increasing over the remainder of the oxidizing stage. Mercury release behavior during the transition stage through 300 h was indiscernible; Hg concentrations in replicate coal ash reactor samples were highly varied. Standard errors of sequential samples showed that measured concentrations were not statistically different and therefore release trends could not be identified, similar to Zn. After 350 h, however, standard errors decreased, and a trend of increased Hg concentration occurred before reaching a plateau. Lead concentrations were below detection limit under oxidizing conditions, and increased during the transition stage. A dip in Pb concentration occurred during the transition stage through nearly 350 h, after which the concentration was steady.

Release behavior of Group 12 and 14 transitions metals in the control reactor was distinct compared to the coal ash reactors. In the control reactor, Zn appeared to decrease under oxidizing conditions, and then increased during the reducing stage. Zinc release in the control reactor was not noticeably different from coal ash reactors in the reducing stage. Cadmium was below detection limit under oxidizing conditions, and a small increase in concentration occurred in the reducing stage. In the control reactor, Hg concentrations were higher than their coal ash counterparts. Mercury concentration overall increased over the course of the experiment with two caveats. First, the transition stage initially caused an anomalous decrease in Hg which subsequently rebounded. Secondly, after 350 h, the increase in Hg release slowed to a plateau. Pb was also below detection limit under oxidizing conditions, and an increase in concentration of nearly two orders of magnitude was observed after the transition stage. Lead concentration in the control exhibited an increasing trend until after nearly 500 h, at which point Pb concentrations reached a plateau.

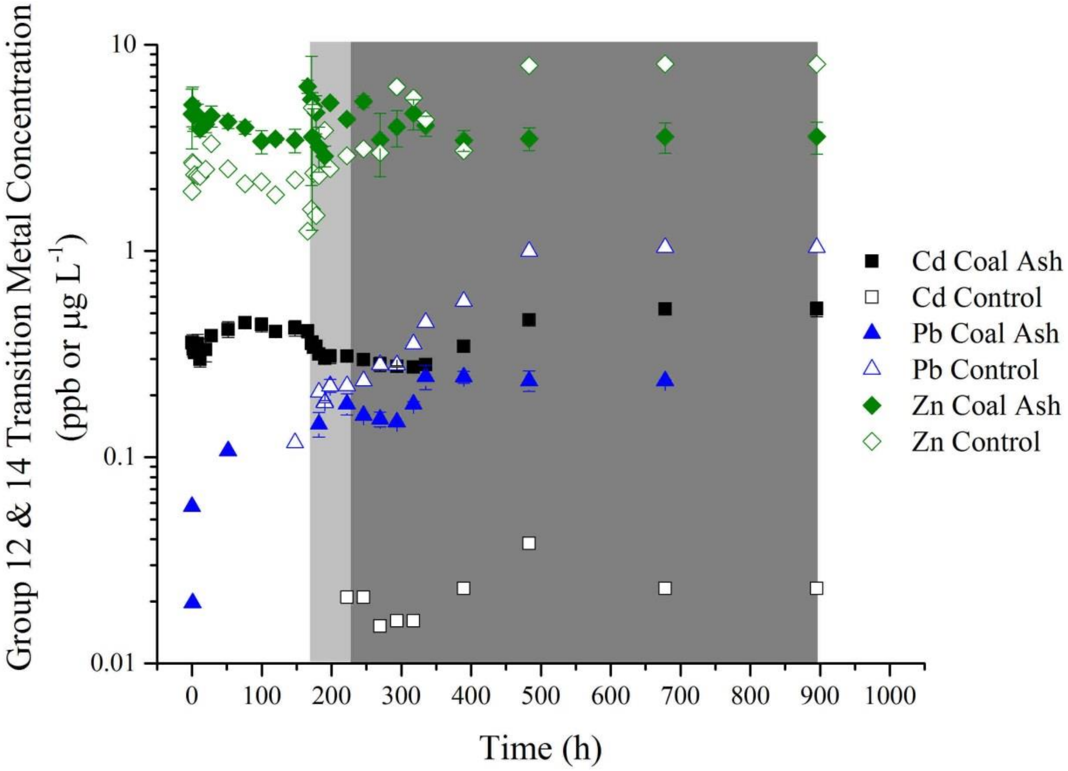

Figure 3.15. Concentration of the Group 12 and 14 transition metals Cd, Pb, and Zn as a function of time. Closed symbols correspond to samples taken in coal ash reactors. Open symbols represent samples taken from the control reactor. The oxidizing, transition, and reducing stages are shown in white, light grey and dark grey, respectively. Error bars in coal ash reactor samples represent the standard error between triplicate sample measurements.

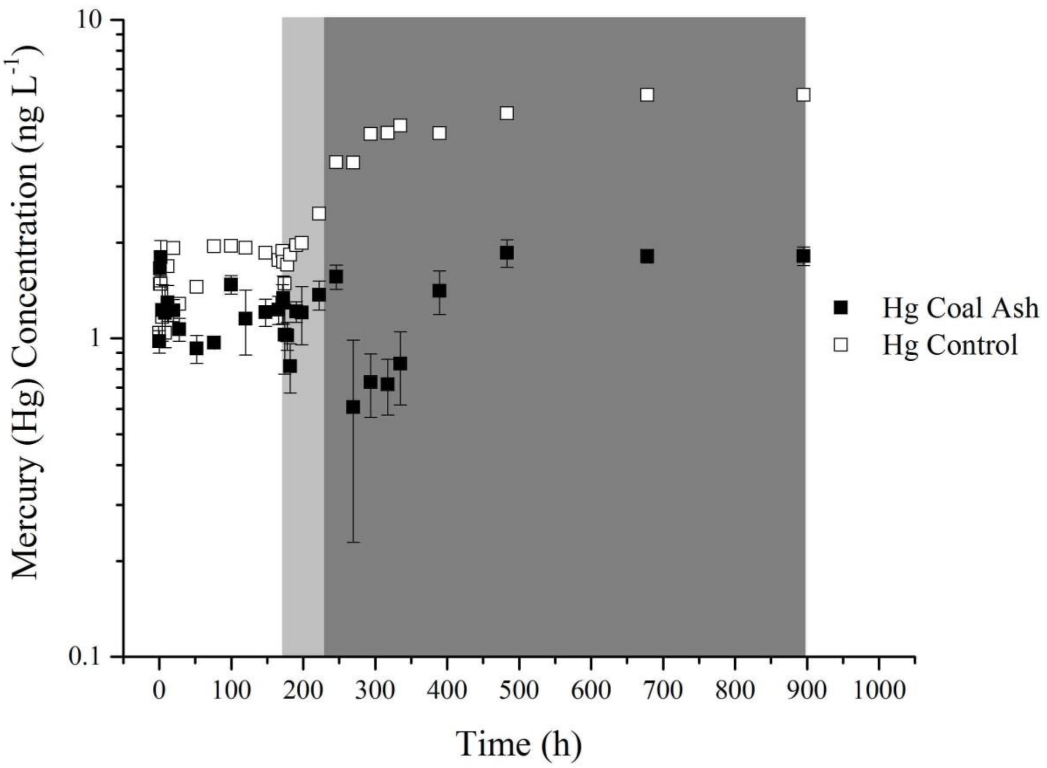

Figure 3.16. Concentration of mercury (Hg) as a function of time. Closed symbols correspond to samples taken in coal ash reactors. Open symbols represent samples taken from the control reactor. The oxidizing, transition, and reducing stages are shown in white, light grey and dark grey, respectively. Error bars in coal ash reactor samples represent the standard error between triplicate sample measurements.

***Release of groups 10 and 11 transition metals*:** Release of Groups 10 and 11 transition metals (Ag, Cu, Ni, Pd, Pt) was irregular, and varied above and below the detection limit, except for Cu and Ni (Figure 3.17). In coal ash reactors, peak Ni concentration was measured in the first sample and subsequently decreased. However, Ni concentration decreased over the first several hours of the transition stage before rebounding. At around 350 h, Ni concentrations increased before reaching a plateau after 450 h. Copper release was similar to Zn, in that sequential samples were not statistically different from one another. The results indicate that Cu concentration decreases over the duration of the experiment in coal ash reactors; however, specific trends during the transition and anoxic stages cannot be determined. Palladium was below detection limit under oxidizing conditions, and Pd concentration increased during the transition stage, before decreasing after 350 h. Gold was below detection limit in the coal ash reactors.

Nickel concentration in the control reactor increased under oxidizing conditions and during the transition stage, subsequently reaching a plateau during the reducing stage. Cu concentration increased under oxidizing conditions, increased sharply during the transition stage, afterwards reaching a plateau. Copper concentration was nearly the same in both coal ash and control reactor samples. Platinum was measured in some oxic coal ash reactor samples; however, Pt was below detection limit for the remainder of the experiment. The limited number of Pt samples above the detection limit, in addition to large standard errors among sequential samples makes deducing Pt release behavior troublesome, similar to Zn and Cu. Gold was below detection limit in the control reactor over the entire experiment.

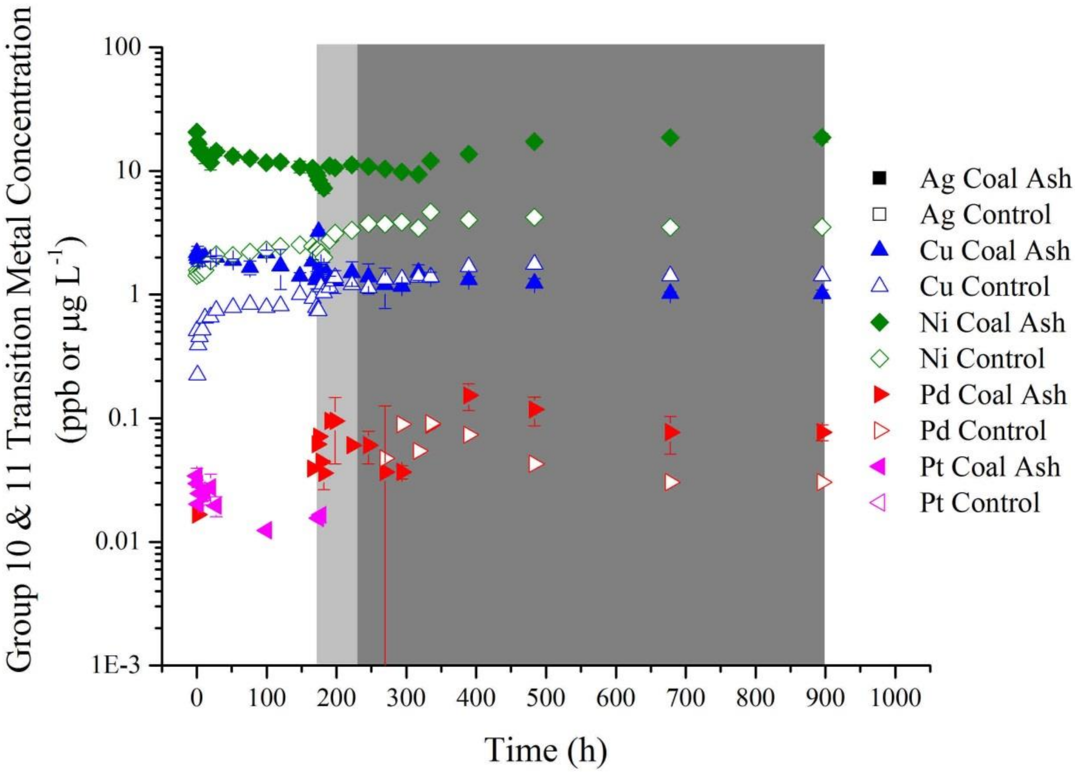

Figure 3.17. Concentration of the Group 10 and 11 transition metals Ag, Cu, Ni, Pd, and Pt as a function of time. Closed symbols correspond to samples taken in coal ash reactors. Open symbols represent samples taken from the control reactor. The oxidizing, transition, and reducing stages are shown in white, light grey and dark grey, respectively. Error bars in coal ash reactor samples represent the standard error between triplicate sample measurements.

***Release of groups 6, 8 and 9 transition metals*:** The release of Groups 8 and 9 transition metals (Co, Rh, Ru) was comparable (Figure 3.18). Rhodium and Ru had similar release characteristics, while Co was unrelated. Cobalt concentration in coal ash reactors was highest initially, and decreased nearly an order of magnitude as the experiment progressed from oxidizing conditions to the reducing stage. However, around 350 h, Co concentration increased and reached a plateau before the end of the experiment. The release behavior of Rh and Ru was identical in coal ash reactors. Rhodium and Ru concentration both increased overall, with two caveats. First, an anomalous decrease in Rh and Ru concentration occurred during the transition stage and subsided around 190 h. Second, Rh and Ru concentration reached a plateau during the reducing stage until nearly 350 h, and afterwards concentration increased.

Release behavior of Group 6, 8 and 9 transitions metals in the control reactor was more distinct compared to the coal ash reactors. Cobalt decreased in concentration under oxidizing conditions, and rapidly increased during the transition stage. During the reducing stage, Co concentration decreased to a plateau after 500 h. Ruthenium release in the control reactor was sporadic; concentrations were below detection limit under oxidizing conditions and after 500 h, and a small spike in Ru concentration occurred from 166 h through 500 h. Rhodium concentration was below the detection limit in the control reactor.

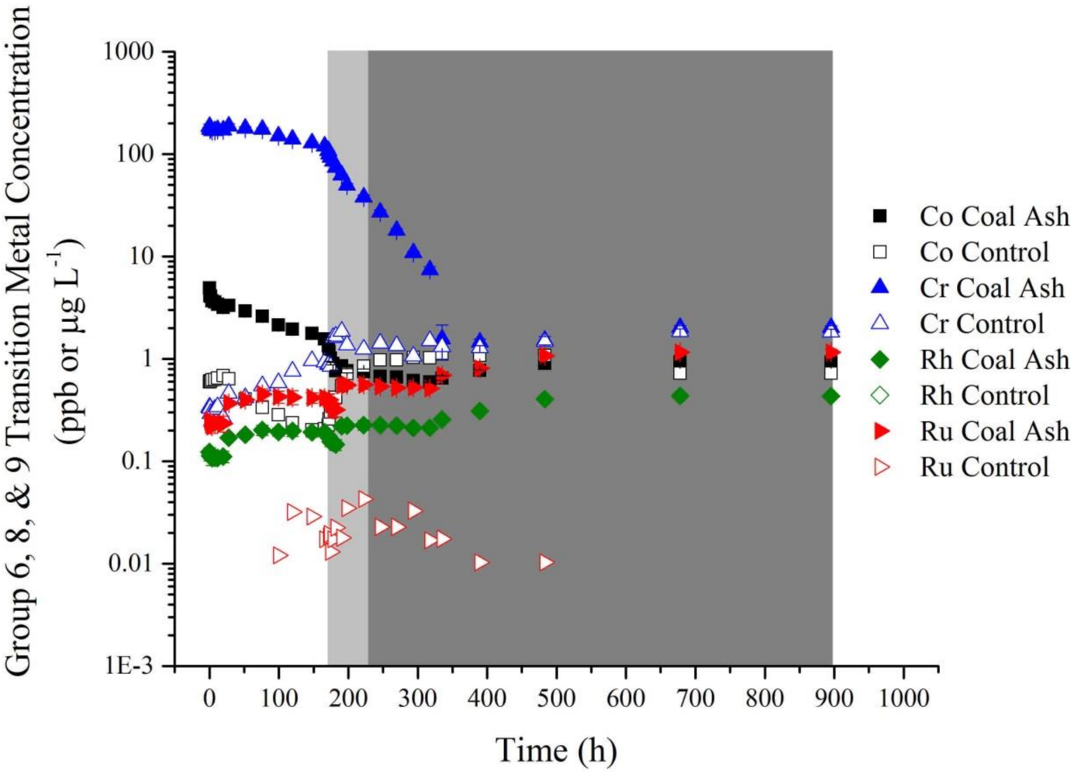

Figure 3.18. Concentration of the Group 6, 8 and 9 transition metals Co, Rh, and Ru as a function of time. Closed symbols correspond to samples taken in coal ash reactors. Open symbols represent samples taken from the control reactor. The oxidizing, transition, and reducing stages are shown in white, light grey and dark grey, respectively. Error bars in coal ash reactor samples represent the standard error between triplicate sample measurements.

Release of groups 4 and 5 transition metals**:** Release of Groups 4 and 5 transition metals (Hf, Nb, Ta, Ti, Zr) was inconsistent, and variations in replicate samples made it difficult to characterize any trends in concentration of these elements in the coal ash reactors (Figure 3.19). Ti concentration in coal ash reactors decreased from the start of sampling until nearly 350 h, after which a small increase occurred before Ti concentration reached a plateau. Behavior of Zr in coal ash reactors during the oxidizing stage could not be determined. Zirconium concentration increased during the transition stage and afterwards decreased. An increase in Zr concentration occurred just prior to 350 h, after which Zr levels reached a plateau. Hafnium appeared to decrease in concentration initially, increase during the transition stage, and decrease over the remainder of the experiment. However, sequential samples were not statistically different, , and therefore trends cannot be identified concretely. Niobium and Ta were below detection limit over the entire experiment.

The variable release of Group 4 and 5 transition metals also made identifying behavior problematic in the control reactor. In the control reactor, Ti was below detection limit under oxidizing conditions. As the experiment proceeded toward reducing conditions, Ti concentration in the control reactor increased to nearly the same as in coal ash reactors. Zirconium concentration was consistently higher in the control reactor compared to the coal ash reactors. Zirconium concentration oscillated as the experiment proceeded, making any behavior difficult to identify in the control reactor; however, after nearly 500 h the Zr concentration reached a plateau. Hafnium concentration in control reactor samples were within the standard error of the coal ash reactor samples, which indicated that Hf was released similar to coal ash reactors. Niobium and Ta concentrations were below detection limit in control reactor samples over the duration of the experiment.

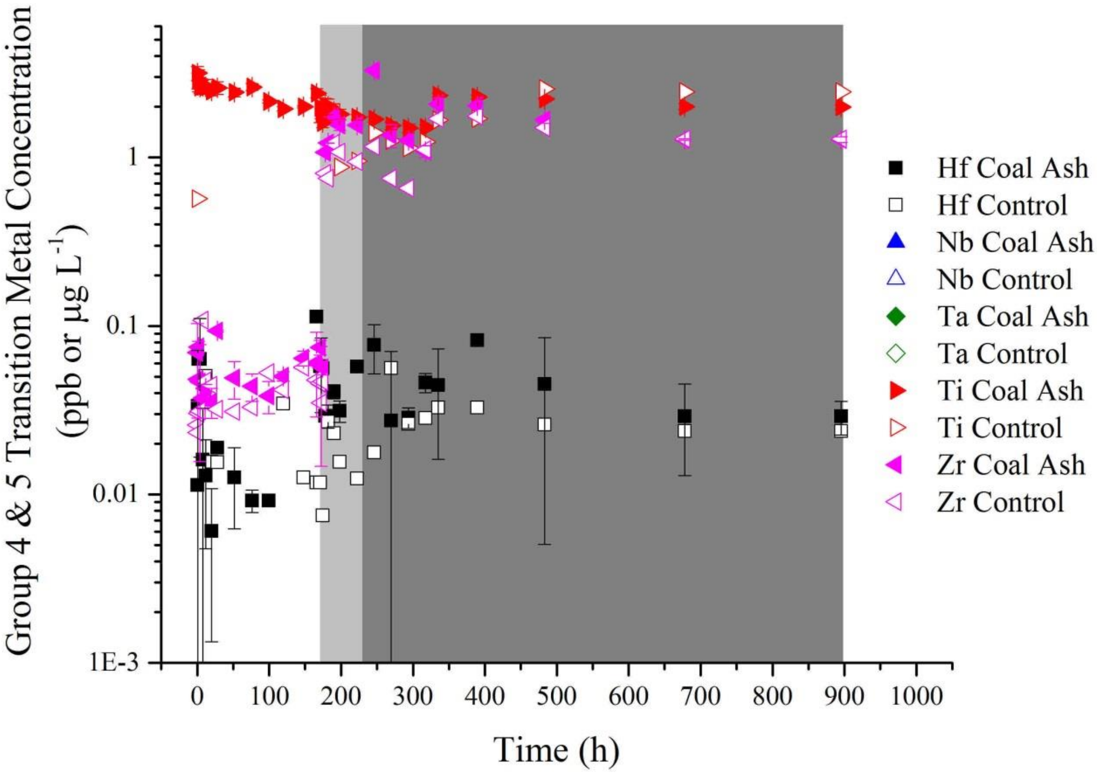

Figure 3.19. Concentration of the Group 4 and 5 transition metals Hf, Nb, Ta, Ti, and Zr as a function of time. Closed symbols correspond to samples taken in coal ash reactors. Open symbols represent samples taken from the control reactor. The oxidizing, transition, and reducing stages are shown in white, light grey and dark grey, respectively. Error bars in coal ash reactor samples represent the standard error between triplicate sample measurements.

***Release of group 3 transition metals*:** Release of Group 3 transition metals (Sc, Y) was different between elements, but the behavior between control and coal ash reactors was similar (Figure 3.20). Scandium concentration in coal ash reactors was highest initially, and decreased slowly under oxidizing conditions. A sharp decrease in Sc concentration during the transition stage was proceeded by a slow decrease in Sc concentration during the reducing stage. Scandium was below detection limit after 500 h. Yttrium concentration in coal ash reactors was relatively constant under oxidizing conditions; however, Y concentration increased roughly an order of magnitude during the transition stage. A slow decrease in Y concentration occurred as the experiment progressed, and after 350 h Y was below detection limit.

The release behavior and concentration of Y in control and coal ash reactors was nearly identical. Scandium in control reactors was below detection limit until the reducing stage, at which point Sc release and concentration was nearly equivalent to the coal ash reactors.

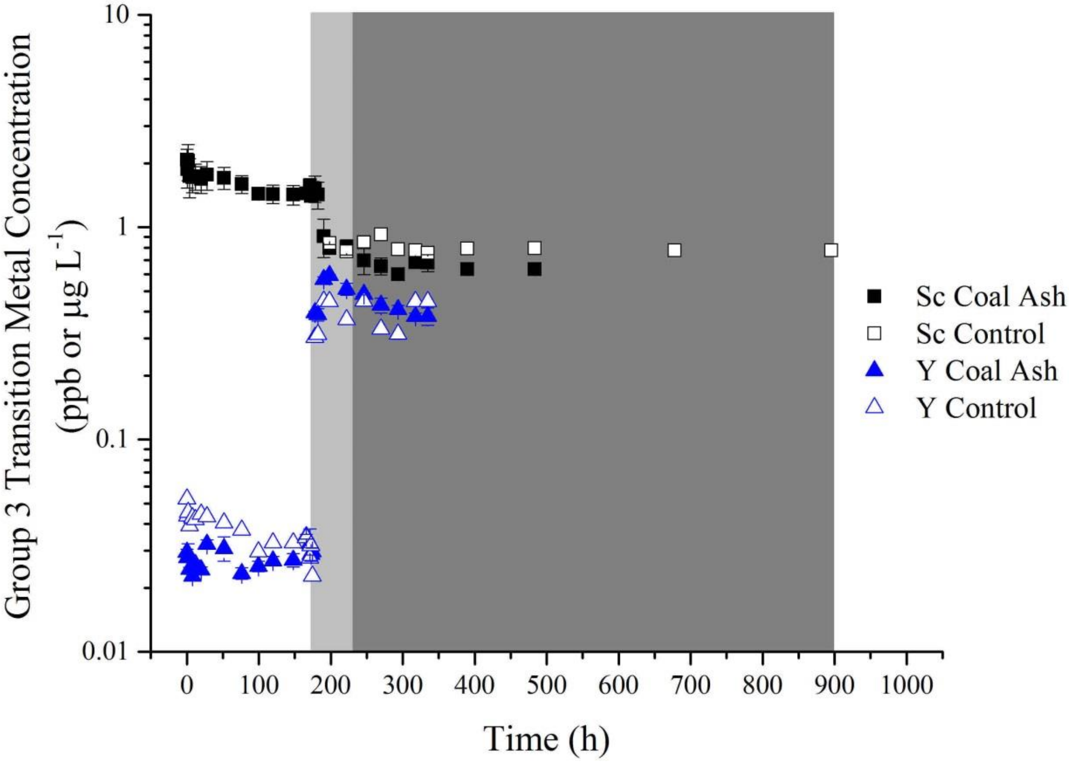

Figure 3.20. Concentration of the Group 3 transition metals Sc, and Y as a function of time. Closed symbols correspond to samples taken in coal ash reactors. Open symbols represent samples taken from the control reactor. The oxidizing, transition, and reducing stages are shown in white, light grey and dark grey, respectively. Error bars in coal ash reactor samples represent the standard error between triplicate sample measurements.

***Release of other metals*:** Tin and Tl release characteristics were not clear (Figure 3.21). In both coal ash and control reactors, Sn was below detection limit. Thallium was measured under oxidizing conditions, but decreased below detection limit after 100 h. Based on the limited number of samples, no release behavior can be adequately described. Thallium was below detection limit in the control reactor.

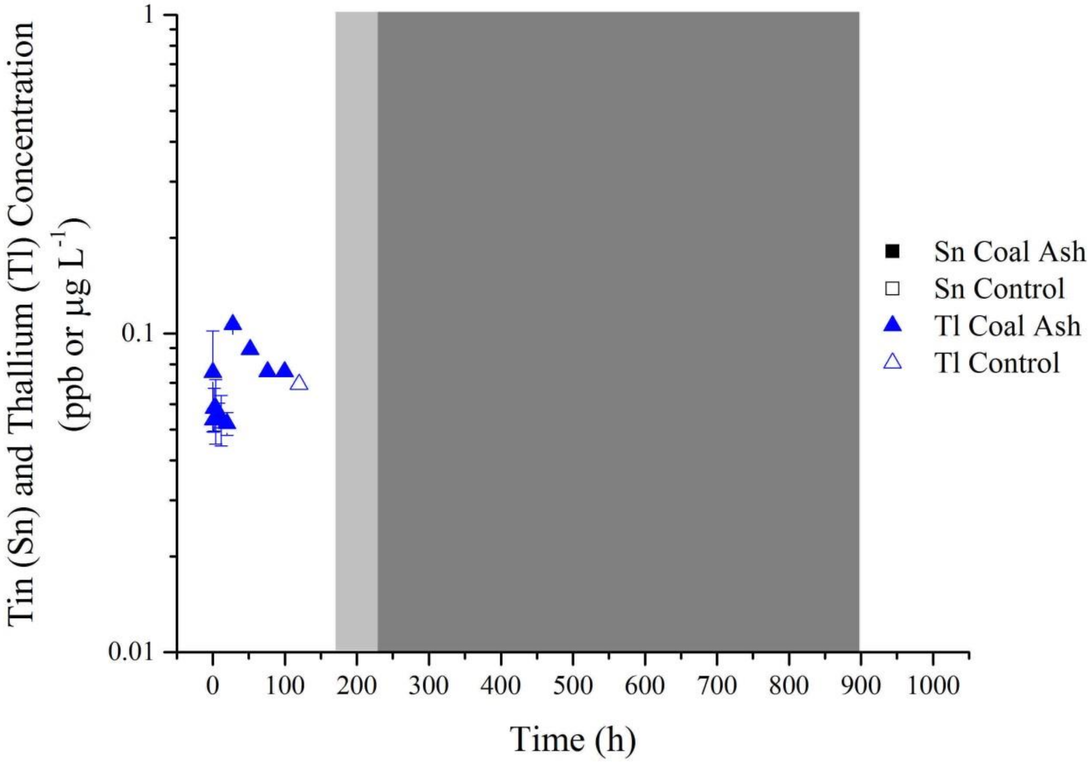

Figure 3.21. Concentration of the other metals Sn and Tl as a function of time. Closed symbols correspond to samples taken in coal ash reactors. Open symbols represent samples taken from the control reactor. The oxidizing, transition, and reducing stages are shown in white, light grey and dark grey, respectively. Error bars in coal ash reactor samples represent the standard error between triplicate sample measurements.

***Release of metalloids*:** Metalloids (Ge, Sb, Te) exhibited variable release among elements and between coal ash and control reactors (Figure 3.22). Germanium concentration was highest initially, and decreased over the experiment until nearly 350 h, at which point Ge concentration increased slightly before reaching a plateau. Antimony release differed from Ge in that the concentration increased during the oxidizing stage. Antimony concentration subsequently decreased during the transition stage, and the concentration remained essentially invariable until nearly 350 h. Around 350 h, Sb concentration increased and plateaued to its peak concentration (6.5 ppb). Tellurium was below detection limit in coal ash reactors.

In the control reactor, Ge release behavior was difficult to ascertain prior to reducing conditions. However, Ge concentration increased during the reducing stage before reaching a steady concentration. Antimony release in the control reactor increased under oxidizing conditions and during the transition stage; however, Sb concentration decreased during the reducing stage. After 350 h, Sb concentration was below detection limit in the control reactor. Tellurium was below detection limit in the control over the duration of the experiment.

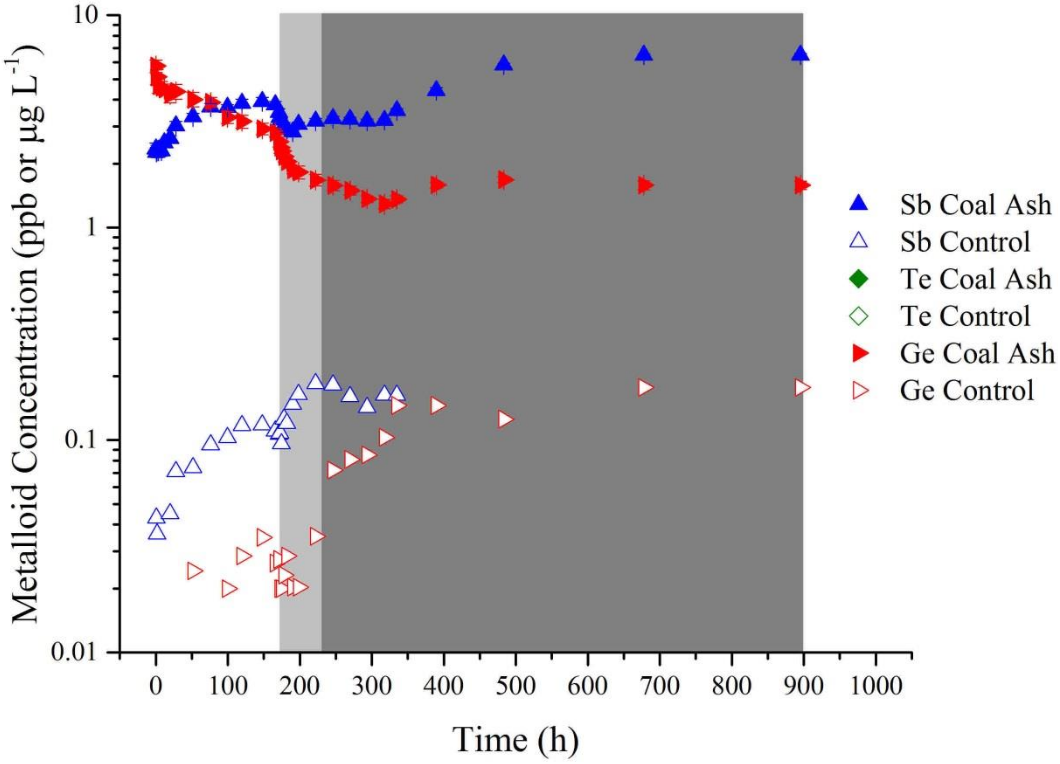

Figure 3.22. Concentration of the Metalloids Ge, Sb, and Te as a function of time. Closed symbols correspond to samples taken in coal ash reactors. Open symbols represent samples taken from the control reactor. The oxidizing, transition, and reducing stages are shown in white, light grey and dark grey, respectively. Error bars in coal ash reactor samples represent the standard error between triplicate sample measurements.

***Release of actinides*:** The release behavior of Actinides (Th, U) was similar in coal ash and control reactors (Figure 3.23). In coal ash reactors, U concentration decreased from its initial peak until nearly 50 h. Uranium concentration then increased until the transition stage, after which the concentration decreased until 350 h. Uranium concentration increased slightly before reaching an apparent plateau after 500 h. Thorium release characteristics in coal ash reactors were not easily discernible due to large standard error between replicate coal ash reactor samples. However, Th concentration appeared to decrease as reducing conditions persisted, eventually reaching a plateau after 650 h.

In the control reactor, U concentration increased under oxidizing conditions and during the transition stage. During the reducing stage of the control, U concentration decreased and reached a plateau after 500 h. Thorium release in the control reactor was unidentifiable; many samples were below detection limit.

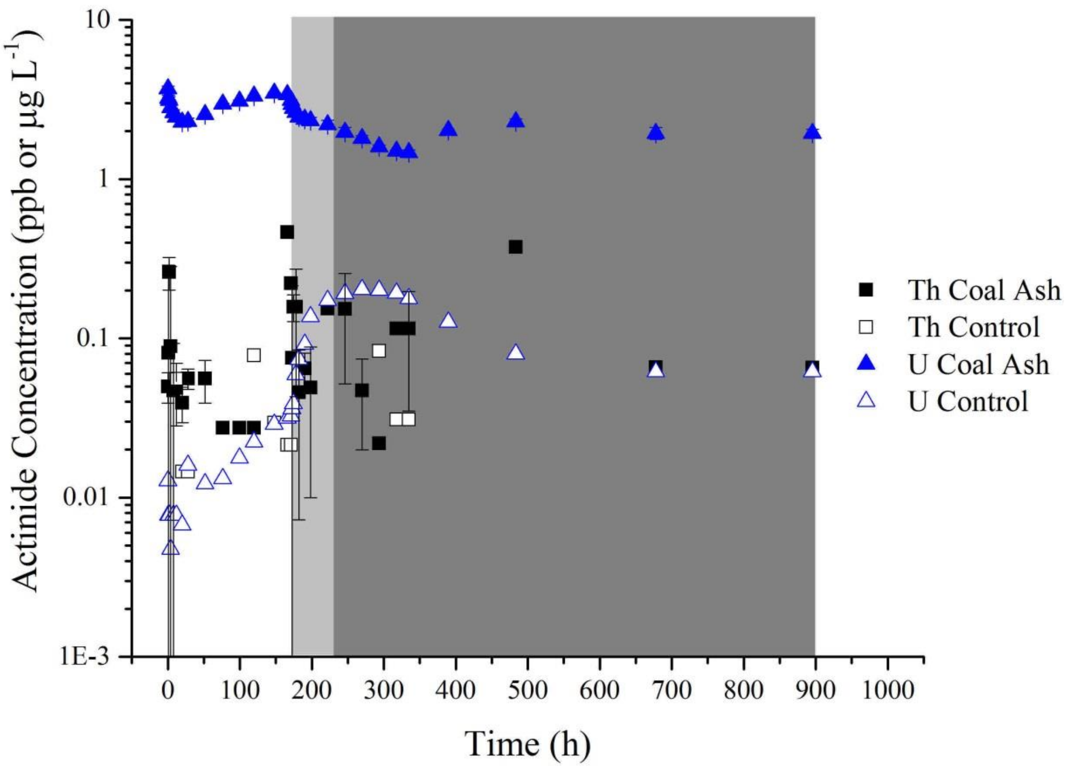

Figure 3.23. Concentration of the Actinides Th, and U as a function of time. Closed symbols correspond to samples taken in coal ash reactors. Open symbols represent samples taken from the control reactor. The oxidizing, transition, and reducing stages are shown in white, light grey and dark grey, respectively. Error bars in coal ash reactor samples represent the standard error between triplicate sample measurements.

Release of lanthanides 57-61**:** Elements within lanthanides 57 through 61 (Ce, La, Nd, Pr) exhibited varying degree of release, but the trend was similar between coal ash and control reactors (Figure 3.24). In coal ash reactors, Ce was below detection limit under oxidizing conditions and experienced over a two order of magnitude increase in concentration after the transition stage. Cerium concentration decreased slightly over the remainder of the experiment, reaching an apparent plateau after 650 h. Lanthanum concentration under oxidizing conditions was either below detection limit or at a concentration with large standard error that prevented identification of release behavior. The transition stage in the coal ash reactor caused increased La concentration, which decreased during the reducing stage and was below detection limit after

350 h. Neodymium in coal ash reactors varied above and below the detection limit; however, several trends were identifiable. In the oxidizing stage of the experiment, Nd concentration decreased, followed by a large increase during the transition stage. Neodymium release in the reducing stage was erratic, and was below detection limit after 350 h. In coal ash reactors, Pr was below detection limit over the entire experiment.

In the control reactor, Ce was below detection limit initially. Cerium concentration increased during the transition stage, and decreased to a plateau after 650 h. Ce release was analogous between the control and coal ash reactors. In the control, La concentration decreased under oxidizing conditions, increased during the transition and reducing stages, and was subsequently below detection limit after 350 h. In the control reactor, Nd concentration decreased under oxidizing conditions, and increased over the remainder of the experiment, reaching an apparent plateau after 650 h. Praseodymium concentration showed an increase under reducing conditions; however, Pr was below detection limit prior to 200 h and after 350 h.

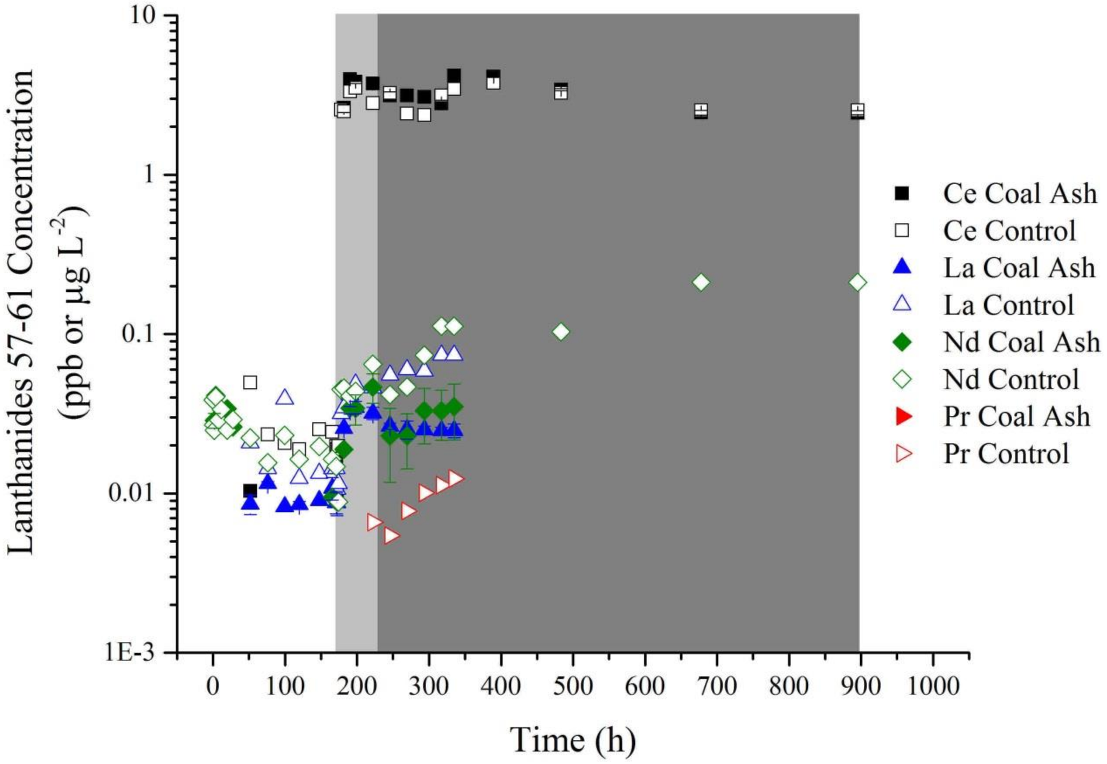

Figure 3.24. Concentration of Lanthanides 57 through 61 (Ce, La, Nd, and Pr) as a function of time. Closed symbols correspond to samples taken in coal ash reactors. Open symbols represent samples taken from the control reactor. The oxidizing, transition, and reducing stages are shown in white, light grey and dark grey, respectively. Error bars in coal ash reactor samples represent the standard error between triplicate sample measurements.

***Release of lanthanides 62-66*:** The release of Lanthanides 62 through 66 (Dy, Eu, Gd, Sm, Tb) was analogous among elements and between control and coal ash reactors (Figure 3.25). In coal ash reactors, Sm and Eu both increased initially before reaching a steady concentration under oxidizing conditions. Gadolinium was present initially, but fell below detection limit until nearly 200 h. Samarium, Eu, and Gd all increased during the transition stage, remaining around the same concentrations until nearly 350 h, at which point Sm, Eu, and Gd concentrations all increased before reaching a plateau after 450 h. Terbium was below detection limit in coal ash reactors over the entire experiment.

The concentration trend of Sm matched in the control reactor and coal ash reactor, the Sm concentration was lower in the control reactor than the coal ash reactor. Europium behavior in the control also matched its coal ash counterpart; however, after 350 h Eu concentration was below detection limit in the control. Gadolinium release was similar between coal ash and control reactors, the exception being that Gd concentration was greater in the control. In the control, Tb was below detection limit prior to the establishment of reducing conditions, at which point Tb increased.

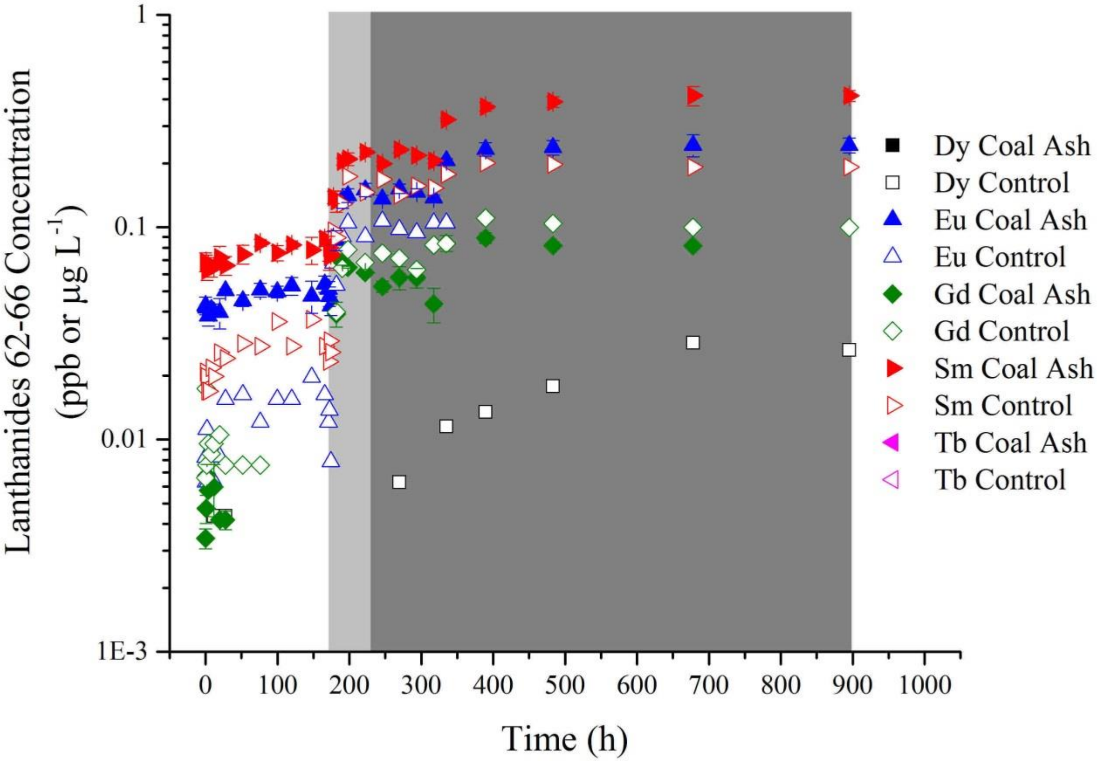

Figure 3.25. Concentration of Lanthanides 62 through 66 (Dy, Eu, Gd, Sm, and Tb) as a function of time. Closed symbols correspond to samples taken in coal ash reactors. Open symbols represent samples taken from the control reactor. The oxidizing, transition, and reducing stages are shown in white, light grey and dark grey, respectively. Error bars in coal ash reactor samples represent the standard error between triplicate sample measurements.

Release of lanthanides 67-71**:** The release of Lanthanides 67 through 71 (Er, Ho, Lu, Tm, Yb) did not occur in coal ash reactors (Figure 3.26). Erbium, Ho, Lu, Tm, and Yb were not released from coal ash reactors during the entire experiment, and their concentrations were all below detection limit. Holmium, Lu, and Tm were not released from the control reactor, and were below detection limit over the experiment. Only Er and Yb were present in measurable concentration in the control reactor. However, both Er and Yb were below the detection limit under oxidizing conditions and during the transition stage. Erbium and Yb began increasing in concentration over the reducing stage of the experiment. In the control, it appeared that Er and Yb concentrations increased during reducing conditions toward the end of the experiment.

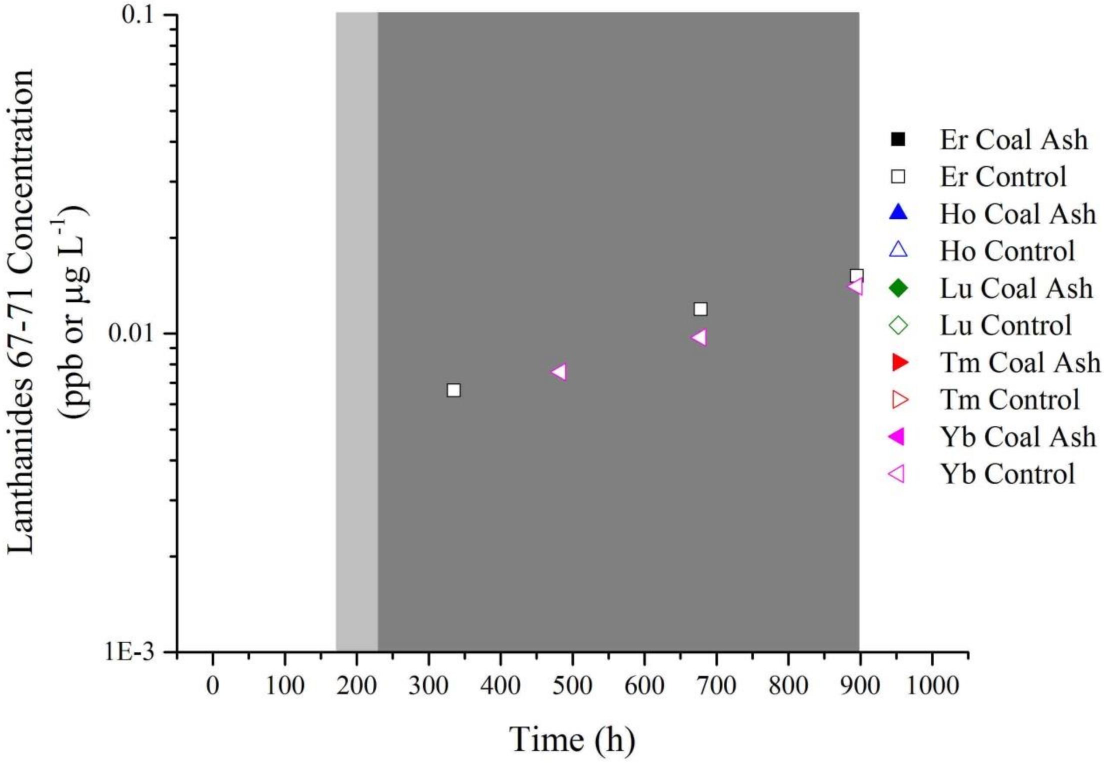

Figure 3.26. Concentration of Lanthanides 67 through 71 (Er, Ho, Lu, Tm, and Yb) as a function of time. Closed symbols correspond to samples taken in coal ash reactors. Open symbols represent samples taken from the control reactor. The oxidizing, transition, and reducing stages are shown in white, light grey and dark grey, respectively. Error bars in coal ash reactor samples represent the standard error between triplicate sample measurements.

Release of environmental anions: The release behavior of environmental anions (NO_2^-, NO_3^-, PO_4^{3-}, and SO_4^{2-}) was generally similar in coal ash reactors, but varied in the control reactor (Figure 3.27). In the coal ash reactor, sulfate was present in the greatest concentration initially, and decreased slightly under oxidizing conditions. Sulfate also decreased during the transition and reducing stages until roughly 350 h, at which point sulfate concentration increased. Nitrate concentration in coal ash reactors decreased over the entire experiment, eventually reaching a plateau after 650 h. Similar to Zn and Cu, large standard errors between replicates made it difficult to identify any release behavior; however, several trends could be identified. Nitrate concentration decreased under oxidizing conditions and the transition stage, and then increased during the reducing stage. Nitrite increased in concentration over oxidizing conditions, decreased during the transition stage, and rebounded slightly during the reducing stage before decreasing to a plateau after 450 h. In the control reactor, sulfate increased slightly in the oxidizing portion of the experiment before decreasing during the transition stage. Phosphate was subject to large standard error, similar to Zn and Cu, and therefore release could not be described over the entire experiment. In coal ash reactors, phosphate appeared to decrease during the reducing stage.

Sulfate concentration in the control reactor decreased before reaching a plateau after 650 h. Nitrate concentration in the control reactor decreased under oxidizing conditions and the transition stage. The concentration of nitrate appeared to increase during the reducing stage; however, this could not be verified because nitrate was below detection limit after 400 h. In the control, nitrite release was opposite to nitrate. Nitrite concentration increased under oxidizing conditions, before decreasing rapidly during the transition stage. During the reducing stage, nitrite was below detection limit. Phosphate was below detection limit in the control reactor prior to 300 h. From 300 to 450 h, control reactor phosphate appeared to increase to a plateau.

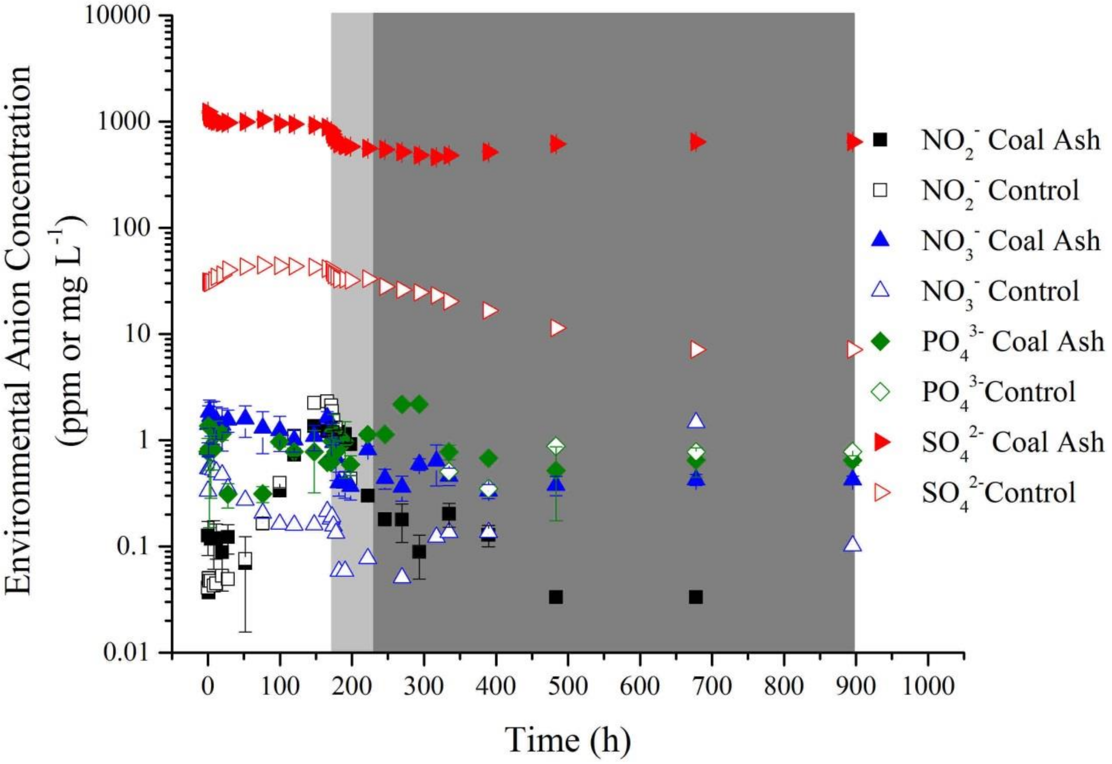

Figure 3.27. Concentration of the Environmental Anions NO_2^-, NO_3^-, PO_4^{3-}, and SO_4^{2-} as a function of time. Closed symbols correspond to samples taken in coal ash reactors. Open symbols represent samples taken from the control reactor. The oxidizing, transition, and reducing stages are shown in white, light grey and dark grey, respectively. Error bars in coal ash reactor samples represent the standard error between triplicate sample measurements.

***Release of halides*:** Halides (F^-, Cl^-, Br^-) had dissimilar release behavior (Figure 3.28). In coal ash reactors, Cl^- concentration increased under oxidizing conditions, decreased during the transition stage, and remained steady until 350 h. At 350 h, Cl^- concentration spiked before decreasing and plateauing over the remainder of the experiment. Fluoride concentration in coal ash reactors increased under oxidizing conditions before it decreased during the transition stage. During the reducing stage, trends in the concentration of F^- were indeterminate due to large standard errors; however, after 350 h the concentration increased to a plateau. Bromide behavior in coal ash reactors is also indeterminate because of large standard errors between sequential samples.

The release of Cl^- showed similar trends in control and the coal ash reactor, but the concentration of Cl^- was lower in the control reactor. Fluoride concentration in the control reactor increased under oxidizing conditions. During the transition stage F^- concentration decreased; however, after roughly 300 h, the concentration increased to a plateau. Bromide was detected in several control samples; however, Br^- release in the control was uncertain because many sample concentrations were below detection limit.

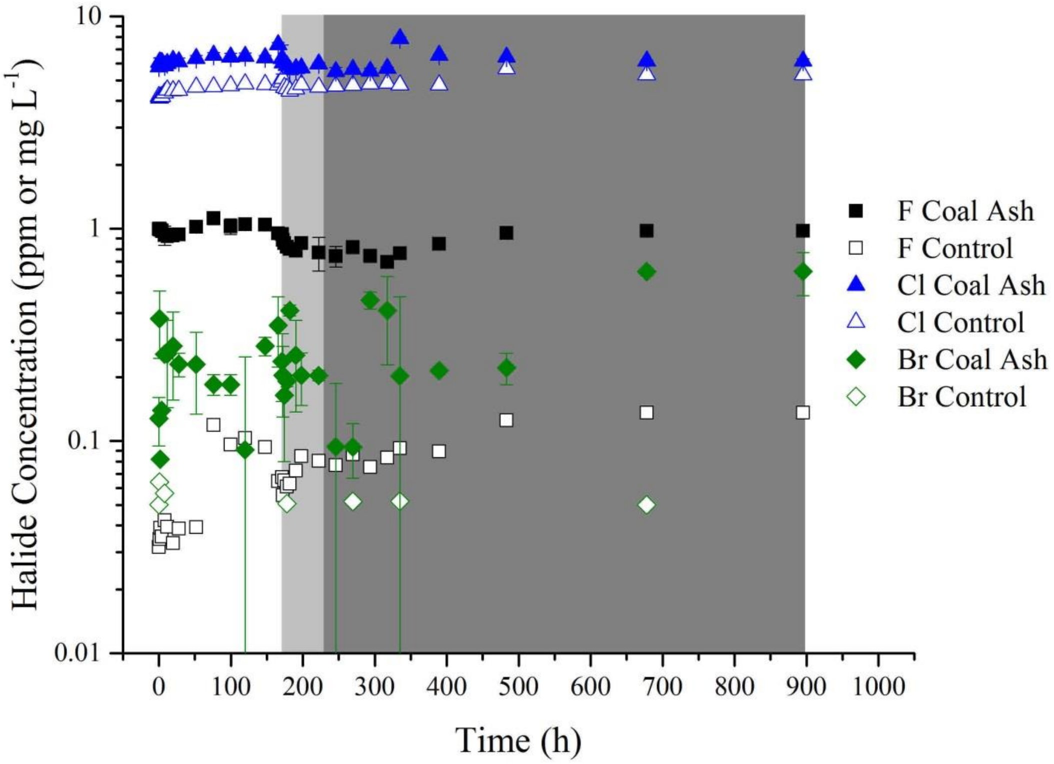

Figure 3.28. Concentration of the halides Cl^-, Br^-, and F^- as a function of time. Closed symbols correspond to samples taken in coal ash reactors. Open symbols represent samples taken from the control reactor. The oxidizing, transition, and reducing stages are shown in white, light grey and dark grey, respectively. Error bars in coal ash reactor samples represent the standard error between triplicate sample measurements.

Characterization of organic matter in batch reactor system**:** In coal ash reactors, DOC and $SUVA_{254}$ were inversely related, while in the control reactor, their behavior was similar

(Figure 3.29). The DOC concentration in coal ash reactors decreased under oxidizing conditions and the transition stage. During the transition stage, DOC in the coal reactor continued to increase until after 500 h, at which point the DOC reached a plateau. The $SUVA_{254}$ in coal ash reactors showed nearly opposite trend to the DOC. Under oxidizing conditions, $SUVA_{254}$ increased rapidly before decreasing through the transition stage. The $SUVA_{254}$ increased during the reducing stage, reaching an apparent plateau after 500 h. However, the trend of $SUVA_{254}$ between 250 and roughly 350 h is difficult to determine exactly because large standard errors between samples suggested that sequential samples may not be statistically different from each other.

In the control reactor, DOC concentration increased over the duration of the experiment, reaching a plateau after 500 h. However, two shoulders exist in the DOC concentration profile at around 100 and 350 h. The $SUVA_{254}$ in the control also increased over the duration of the experiment, reaching a plateau after 500 h. Similar to the DOC in the control, two shoulders were present in the $SUVA_{254}$ profile at 50 and around 165 h.

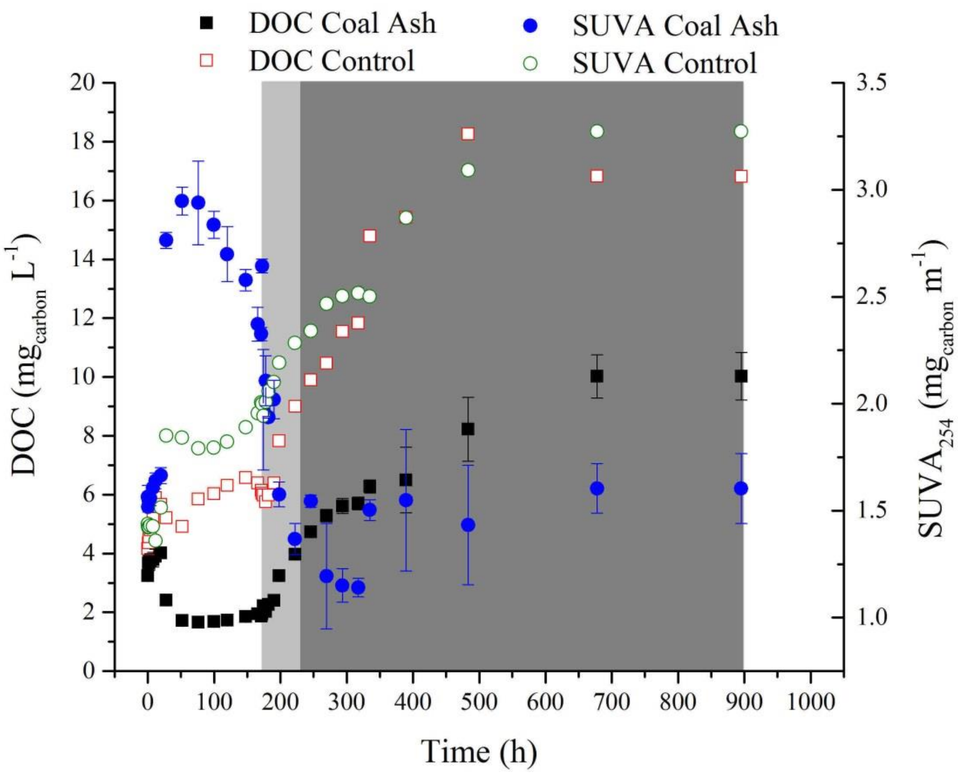

Figure 3.29. DOC concentration and $SUVA_{254}$ as a function of time. Closed symbols correspond to samples taken in coal ash reactors. Open symbols represent samples taken from the control reactor. The oxidizing, transition, and reducing stages are shown in white, light grey and dark grey, respectively. Error bars in coal ash reactor samples represent the standard error between triplicate sample measurements.

Statistical analysis**:** The results of the Spearman's correlation coefficient matrix revealed many correlations between the water quality parameters (i.e., pH, redox potential, DOC, $SUVA_{254}$) and element concentrations. Overall, 37 variables were used in the correlation matrix, including ORP, pH, DOC, $SUVA_{254}$, Ca, Mg, K, Na, Mn, Fe, Si, Al, Ba, Rb, Sr, Se, As, Cr, Mo, V, Cd, Co, Cu, Hg, Ni, Rh, Ru, Zn, Sb, Ge, U, Eu, Sm, NO_2^-, NO_3^-, PO_4^{3-}, and SO_4^{2-}. Only elements that were found to be released from coal ash were included in the correlation matrix. Significant correlations were flagged by OriginPRO using an asterisk, making visual identification of significant correlations simple to identify. The Spearman's correlation coefficient matrix can be found in Appendix 3.A. The significant correlations between variables will be discussed individually in the discussion.

Discussion

***Emory River sediment mineralogy and elemental composition*:** The results of the XRD and chemical characterization (ICP-MS, ICP-DRC-MS, ICP-OES, and solid Hg) did not agree on the content of the Emory River sediment. However, techniques used here relied on few assumptions that may not be valid for all elements or minerals. For instance, all major elements were assumed to be present as oxides in the sediment. Additionally, iron and manganese were presumed to be Fe(III) and Mn(II). A method detection limit of 0.5% for XRD analysis preclude estimation of any minerals that constitute less than 0.5% of the coal ash by weight (Smith, 1999). This limitation caused several disagreements between results obtained from XRD analysis and chemical analysis.

Result of chemical analysis showed that the sediment consisted of appreciable amounts of iron, potassium, and titanium, which were not in complete agreement with the XRD results. The lack of agreement may indicate that these elements were present in an amorphous form, undetectable by XRD. Additionally, XRD did not identify the small amounts of calcium, magnesium, phosphorus, sodium, and manganese-oxides detected by chemical characterization, possibly due to their low concentration or amorphous nature. These elements, however, could have been incorporated into clay minerals that were identified in the XRD analysis. XRD analysis indicates that 10.5% of the bulk sediment was composed of clay minerals including smectite (6.1%), illite (2.4%), and kaolinite (2.1%). Smectite and illite may contain magnesium and aluminum, respectively, which were accounted as their oxide form. Qualitative analysis of the fine clay fraction indicates the presence of chlorite, biotite, and kaolinite that are known to contain iron, manganese, and calcium. All these artifacts could have contributed to the detection of these elements in chemical techniques, but not in the XRD analysis.

***Coal ash mineralogy and elemental composition*:** The results of the XRD and chemical characterization (ICP-MS, ICP-DRC-MS, ICP-OES, and solid Hg) of the coal ash agreed on the content of the coal ash. Analyses of the coal ash revealed that silicon- and aluminum-oxides were the principal components, with smaller fractions of calcium, iron, magnesium, and potassium. However, limitations of both techniques as discussed before could prevent an accurate assessment of the constituents.

Chemical analysis showed appreciable amounts of titanium, calcium, and magnesium and small amounts of sodium, phosphorus, and manganese. Minerals containing these elements were not identified by XRD. However, XRD results indicates that these elements may originate from tephra, a glassy material originating from eruptions of volcanic ash often found alongside or in mixed layers of coal seams (Lowe, 1986; Triplehorn et al., 1986). Glass (i.e., aluminosilicate glass) has been identified as the principal component in many coal ashes (Fernandez-Turiel et al., 1994; Brownfield et al., 1999; Brownfield et al., 2005; Affolter et al., 2011). While tephra was not specifically identified in those studies, a study on the mineral assemblages of tephra in Alaska determined that glass was the primary component in tephra (Reinink-Smith, 1990). Thus, the presence of tephra could explain the detection of titanium, calcium, magnesium, sodium, phosphorus, and manganese by chemical characterization. The specific elements within the tephra were not identified by XRD because tephra is present in RockJock as a mineral standard, and therefore only its presence was identified.

Sillimanite, an aluminosilicate mineral, was also detected by XRD and comprised 9.1% of the coal ash mass. The structure of sillimanite (Al_2SiO_5) is similar to the structure of mullite ($Al_6Si_2O_{13}$) (Cameron, 1976; Cameron, 1977; Tripathi et al., 1998), an aluminosilicate mineral that has been identified by XRD in several other coal ashes (Fernandez-Turiel et al., 1994;

Brownfield et al., 1999; Gomes et al., 2000; Brownfield et al., 2005; Sultana et al., 2011). Sillimanite can decompose to form silica (SiO_2) and mullite (Tripathi et al., 1998), and the peak intensities of mullite and sillimanite in XRD are similar (Brown et al., 1980). However, mullite was not detected by XRD because no mullite standard existed in RockJock.

***Organic matter in batch reactor system*:** The behavior of DOC and $SUVA_{254}$ in coal ash reactors was starkly different from the control, which indicated that organic matter released in the coal ash reactors was chemically different from that released by the control. DOC and $SUVA_{254}$ in coal ash reactors were inversely related – as DOC decreased, the $SUVA_{254}$ increased, and vice versa (Figure 3.29). The increase in $SUVA_{254}$ under oxidizing conditions indicated that the organic matter released by the coal ash was rich in aromatic organic carbon (Weishaar et al., 2003). Organic matter with higher $SUVA_{254}$ has been shown to adsorb on Kingston coal ash more strongly than organic matter with lower $SUVA_{254}$ (Craven, 2012). As $SUVA_{254}$ decreased during the transition stage, DOM would be adsorbed to a lesser degree on the coal ash surface. Aromatic organic carbon can adsorb to oxide minerals (McKnight et al., 1992) or adsorb to the coal ash surface (Craven, 2012), which is important for trace metal release (Waples et al., 2005). Similar to simple organic ligands, DOM can leach elements from and promote dissolution of minerals in coal ash, soils, and sediment (Harris et al., 1983; Janos et al., 2002; Janos et al., 2004). However, the degree of dissolution of minerals depends on the strength of functional group or ligands on DOM to bind the elements. For instance, the affinity of elements is weak towards carboxyl groups, but strong towards phenolic, nitrogen, and sulfur groups or binding sites (Croue et al., 2002).

***Halide release*:** Lack of difference in concentration of halides between control and coal ash reactors suggested that coal ash did not contribute to their release.

Environmental anion release**:** The release behavior of environmental anionic species (i.e., NO_2^-, NO_3^-, SO_4^{2-}, PO_4^{3-}) from Kingston coal ash varied greatly as the experiment progressed from oxic conditions, through the transition stage, and ultimately to reducing conditions. The differences in release of environmental anions throughout the experiment can be attributed to changes in chemical properties of the batch reactors (e.g., pH, redox potential), the presence and aromaticity of DOC, dissolution of mineral phases, competition or interaction with other elements and/or anions, precipitation of immobile phases, or release of mobile phases. The release of each environmental anion is discussed in detail here.

Release of phosphate**:** Phosphate concentration was measurable in the coal ash reactors but was below the detection limit in the control reactor, indicating phosphate was released from the coal ash (Figure 3.27). During the first 250 h of the experiment, standard error between sequential coal ash reactor samples prevented characterization of phosphate release prior to 250 h. A peak in phosphate concentration was observed at 269.6 h, suggesting that it was only sparingly soluble and was released due to the simulated weathering in this experiment. Phosphorus is known to be extremely insoluble in coal ash (Izquierdo et al., 2012), and may occur within the less-soluble aluminosilicate matrix of the ash (Dudas, 1981) or as a highly insoluble calcium-phosphate mineral (Jones, 1995; Dubikova et al., 2006). Therefore, the release of phosphate may have occurred due to the dissolution of the aluminosilicate coal ash matrix, which has been shown to occur due to weathering processes (Gitari et al., 2009). The subsequent decrease in phosphate release after its maximum concentration at 269.6 h could also be caused by precipitation with calcium (i.e., calcium-phosphates) at high pH (Dubikova et al., 2006).

The presence of phosphate in the system is important because it is known to compete with other anions for adsorption sites. Phosphate in coal ash-amended soils (Jackson et al., 2000) and sludge-treated soils (McBride et al., 1999) have been shown to displace molybdate and arsenate due to competitive effects, and it was thought to be responsible for elevated concentrations of other elements, such as antimony, which can be present as hexahydroxoantimonate ($Sb(OH)_6^-$) under oxidizing conditions. The decreased phosphate concentration after 250 h may be due to phosphate out-competing other oxyanion-forming elements for sorption sites.

Nitrate and nitrite release**:** Nitrate was released from the coal ash and nitrite likely formed from nitrate reduction (Figure 3.27). Relative concentrations of both anions were used as an indicator of redox changes in this experiment because nitrite (NO_2^-) is a more reduced form of nitrogen than nitrate (NO_3^-). Under oxidizing conditions, nitrate predominated and nitrate concentrations were low. As the experiment proceeded into the transition stage, the concentration of nitrate decreased as the concentration of nitrite increased, which indicated that nitrate-reducing conditions were created. Nitrate concentration continued to decrease throughout the experiment and had a moderate positive correlation with redox potential (Spearman's ρ=0.52), which indicates that the reducing condition persisted. However, nitrite concentration decreased after the transition stage, indicating that nitrite may also have been reduced, possibly to nitrogen gas or ammonium. Overall, it was apparent from the relationship between nitrate and nitrite that reducing conditions were established after the completion of the oxidizing portion of the experiment.

Release of sulfate**:** Sulfate release decreased overall in the experiment; however, an increase occurred after 350 h (Figure 3.27). The difference in sulfate concentration between the coal ash and control reactors indicated that its release was caused by the coal ash, which agreed with the findings of several other studies on coal ash (Gitari et al., 2009; Akinyemi et al., 2012; Izquierdo et al., 2012). The high initial concentration of sulfate was likely due to the association of the easily-soluble sulfate with the surface of the ash particles (Izquierdo et al., 2012). The initial release was found to be rapid, which agrees with results reported by Akinyemi et al. (2012). After its high initial concentration, sulfate release decreased slowly until the transition stage because of the exhaustion of easily soluble sulfate species, leaving only sparingly soluble sulfate or sulfate locked in the aluminosilicate matrix of the ash to be released (Gitari et al., 2009).

The decrease in sulfate concentration during the transition stage was likely caused by the reduction of sulfate to sulfide. A moderate positive correlation between sulfate and redox potential (Spearman's ρ=0.54) suggested that sulfate decreased in part due to its reduction to sulfide. The increase in pH during the transition stage may also have contributed to decreased sulfate concentration, which has been observed in other studies (Dijkstra et al., 2006; Gitari et al., 2009). This explains a strong negative correlation (Spearman's ρ= -0.77) of sulfate with pH in our study.

The slight increase in sulfate concentration and release after 350 h could have been caused by competition with oxyanion forming elements. This was supported by the positive correlations between sulfate and selenium (Spearman's ρ=0.95), chromium (Spearman's ρ=0.90), and molybdenum (Spearman's ρ=0.42), which showed that their concentrations increased alongside sulfate. On the other hand, arsenic (Spearman's ρ= -0.54) and antimony (Spearman's ρ= -0.39) were found to be negatively correlated with sulfate, which suggested that these elements in their anionic form may have out-competed sulfate and caused its increased release after 350 h.

***Release of Elements from Coal Ash*:** Elements with concentrations below detection limit include Ag, Dy, Er, Ho, Lu, Nb, Pr, Pt, Sn, Ta, Tb, Te, Tl, Tm, and Yb. Additionally, several elements had the same concentration and release behavior in control and coal ash reactors, including Ce, Cs, Gd, Hf, La, Nd, Pb, Pd, Sc, Th, Ti, Y, and Zr. The release of the elements whose concentration differed between control and coal ash reactor were attributed to presence of coal ash. Release was interpreted for groups of elements expected to exhibit similar release behavior:

- major cations (Ca, K, Mg, Na)
- major elements (Al, Fe, Mn, Si)
- alkali and alkaline earth metals (Ba, Rb, Sr)
- oxyanion-forming elements (As, Cr, Mo, Se, V)
- transition metals (Cd, Co, Cu, Hg, Ni, Rh, Ru, Zn)
- metalloids (Ge, Sb), and
- actinides (U) and lanthanides (Eu).

***Release of major cations*:** The release of all major cations (Ca, K, Mg, Na) from coal ash were caused by the dissolution of the ash as the experiment entered the transition stage, and the pH increased. The behavior of major cations indicated that their soluble fractions were released from the coal ash surface when contacted with water, while the less soluble fraction of major cations was released slowly.

***Release of calcium*:** Calcium concentration decreased overall in the experiment; however, an increase in concentration occurred after 350 h (Figure 3.11). Calcium concentration in coal ash reactors was over an order of magnitude greater than in the control, which indicated that calcium was released from the coal ash. Calcium comprised a much greater fraction of the mass of Kingston coal ash (7.5%) compared to Emory River sediment (0.3%), which suggested that a greater amount of calcium was present in the ash to be released. Calcium has been observed to be released from the Kingston coal ash previously (Ruhl et al., 2009). Several studies have attributed a high initial concentration and subsequent decrease in calcium concentration to the dissolution of surface bound calcium from coal ash (Gitari et al., 2009; Izquierdo et al., 2012; Neupane et al., 2013). The soluble calcium-bearing species were found to be released quickly, whereas the insoluble forms of calcium were released slowly, which matches the decreasing calcium concentration observed in this experiment.

The decrease in calcium concentration from the start of the transition stage through nearly 350 h was likely due to the increase in pH during that time, whereas the increased calcium concentration after 350 h may have been facilitated by DOC. Calcium release has been shown to be inversely related to pH in several leaching studies on coal ash (Akinyemi et al., 2011; Akinyemi et al., 2012; Izquierdo et al., 2012; Neupane et al., 2013). Calcium release was also shown to decrease as pH increased from 6.5 to 8.1 in a redox-controlled trace element mobilization study due to the precipitation of carbonate minerals (Ye et al., 2013), which agrees with the behavior of calcium as a function of pH in this experiment. Additionally, a strong negative correlation between pH and calcium was found (Spearman's ρ= -0.72). Therefore, the decrease in calcium release from the start of the transition stage through almost 350 h was likely caused by the increase in pH. Pedrot et al. (2009) also observed decreasing calcium concentrations as pH increased in a study investigating trace element mobility; however, increased DOC concentration (i.e., solubility) was shown to cause an increase in calcium release.

This may elucidate the increase in calcium concentration observed in this experiment after 350 h. A strong positive correlation was found between calcium and sulfate (Spearman's ρ= 0.98), which suggested that sulfate mobilization may have caused increased calcium concentration, possibly due to the dissolution of calcium-sulfate mineral phases.

***Potassium, magnesium, and sodium release*:** The release of potassium, magnesium, and sodium were similar – their concentrations decreased over the duration of the experiment (Figure 3.11). Potassium, magnesium, and sodium were all released from the coal ash to a much greater extent than they were released from the Emory River sediment, which confirmed that they were released from the coal ash.

As the experiment progressed, the difference in potassium, magnesium, and sodium concentrations between the coal ash and control reactors decreased. This suggested that potassium, magnesium, and sodium underwent rapid dissolution before reaching steady concentrations after 350 h. Potassium, magnesium and sodium displayed high initial concentrations followed by decreased concentrations in several other coal ash leaching studies due to the dissolution of easily-soluble surface particles (Neupane et al., 2013) or surface salts (Warren et al., 1989; Izquierdo et al., 2012), whereas additional release was caused by the dissolution of the less soluble coal ash matrix (Dudas, 1981). Magnesium in some cases has been shown to be poorly leachable in water due to its enrichment in the less soluble glass fraction of the ash (Kim, 2002; Ward et al., 2003). Therefore, the decreased concentrations of potassium, magnesium and sodium from Kingston coal ash was likely due to the rapid dissolution of easily soluble particles or salts containing these elements on the surface of the ash.

As the transition stage began, the concentrations of potassium, magnesium, and sodium may have decreased due to the increase in pH from around 7 to nearly 9. A recent study investigating the weathering of coal ash found that potassium, magnesium, and sodium concentrations decreased with increases in pH (Akinyemi et al., 2012), which is consistent with what was observed in this experiment. A similar study on the pH-dependent leaching of elements from municipal solid waste incineration (MSWI) bottom ash also showed that elements in soluble salts (e.g., sodium, potassium) dissolved rapidly until exhaustion, while less soluble elements (e.g., magnesium) underwent rapid dissolution of soluble phase followed by a slower dissolution of a less soluble phase (Dijkstra et al., 2006; Hyks et al., 2009). Therefore, the near-neutral pH present under oxidizing conditions may have facilitated the dissolution of easily soluble fractions of potassium, magnesium, and sodium on or near the surface of the coal ash, resulting in high initial concentrations followed by a rapid decrease in release. The transition stage and the concomitant increase in pH may also have contributed to the decrease in potassium, magnesium, and sodium concentrations due to increased electrostatic attraction between negatively charged coal ash and sediment surfaces and positively charged potassium, magnesium, and sodium cations. This hypothesis was supported by a strong negative correlations between pH and magnesium (Spearman's ρ= -0.86), potassium (Spearman's ρ= -0.84), and sodium (Spearman's ρ= -0.82).

The steady release of potassium, magnesium, and sodium in the batch reactors during the reducing stage suggested a slow dissolution of the less-soluble aluminosilicate glass matrix of the coal ash. Their steady concentration in coal ash reactors may be due to the slow dissolution of the glassy coal ash particles, or the diffusion of these elements from the interior of the ash into solution (Izquierdo et al., 2012; Neupane et al., 2013). During the reducing stage, slow dissolution of the less-soluble glass component of the ash may have caused the nearly steady concentrations of potassium, magnesium, and sodium. The moderate positive correlation between redox potential and magnesium (Spearman’s ρ=0.63), potassium (Spearman’s ρ=0.63), and sodium (Spearman’s ρ=0.61) suggested that reducing conditions contributed to the decrease in their release, in addition to the pH controls.

***Release of major elements*:** The major elements (Al, Fe, Mn, Si) all exhibited different release behavior in the batch reactor system. The major elements were all released either from Kingston coal ash (i.e., aluminum), Emory River sediment (i.e., manganese), or both (i.e., iron, silicon) as the chemical conditions (i.e., redox potential, pH) changed. The release behavior of major elements is important because their oxides have the capacity to sorb many other species, while the dissolution of those oxides can release the attached species back into solution.

***Aluminum release*:** The aluminum release observed in this experiment was also due to coal ash dissolution (Figure 3.12). Chemical characterization showed that aluminum-oxides composed a far greater percentage of the mass of Kingston coal ash (25.1%) than the Emory River sediment (4.4%), which suggested that more aluminum was available to be released from the ash. A recent review of 90 coal ash release studies concluded that aluminum was released due to the dissolution of the amorphous aluminosilicate glass component, not the mineral component (i.e., mullite) of the coal ash (Izquierdo et al., 2012).

Aluminum concentration increased during the first 350 h of this study, and was attributed to its solubility as a function of pH and redox conditions. The initial release of aluminum from the coal ash was likely due to the easily-soluble aluminum fraction being released in short periods of ash contact with water (Gitari et al., 2009; Akinyemi et al., 2011; Akinyemi et al., 2012; Neupane et al., 2013). During the transition stage, the large increase in aluminum concentration was likely due to a higher amount of aluminum locked in the aluminosilicate matrix of the ash particles. A similar study on coal ash found that aluminum was only released through weathering processes (Gitari et al., 2009). Aluminum was present in both amorphous and crystalline forms, and while amorphous aluminum was solubilized at alkaline pH, crystalline aluminum was not as easily soluble. In this experiment, the increase in pH during the transition stage may have caused the dissolution of amorphous aluminum, thereby releasing soluble aluminum into solution. Aluminum is known to be sparingly soluble from pH 5 to 7, and markedly more soluble from pH 9 to 11 (Izquierdo et al., 2012), which matched the observed aluminum behavior as a function of pH in this experiment. The decrease in redox potential may have also contributed to aluminum release during the transition stage. A similar study investigating leachability of major elements during coal ash weathering determined that aluminum solubility is strongly correlated to the age of the ash (Akinyemi et al., 2011). Therefore, the aluminum release in this study is likely due to weathering processes simulated in the experiment (i.e., decreased redox potential). This was corroborated by a strong positive correlation between aluminum and pH (Spearman's ρ=0.89) and a moderate negative correlation between aluminum and redox potential (Spearman's ρ= -0.64).

The steady concentration of aluminum during the reducing stage may have several causes, including precipitation reactions or exhaustion of leachable aluminum. Aluminum concentration may have reached a plateau after 350 h due to the slow release of aluminum from the coal ash owing to weathering processes, and the subsequent formation and precipitation of solid aluminum complexes. Long-term mobilization of aluminum from coal ash has been shown to be inhibited by precipitation or co-precipitation of secondary minerals (Hyks et al., 2009; Neupane et al., 2013). Another possibility is that aluminum concentration reached a plateau because the easily soluble fraction of aluminum had been exhausted. Neupane et al. (2013) demonstrated that aluminum release remained constant after several leaching cycles due to the slow dissolution of the less soluble glass ash particles or the diffusion of elements from the interior of the ash into solution.

Iron release**:** The source of iron release was difficult to determine due to the lack of measurable iron throughout the experiment in coal ash reactors (Figure 3.12). Several other coal ash leaching studies have also shown that iron was below the detection limit in solution, or was released only in small quantities in alkaline conditions (Kim, 2002; Ward et al., 2003; Moreno et al., 2005). Iron has also been shown to form spinel structures in coal ash that are highly resistant to weathering (Izquierdo et al., 2012). Characterization of Kingston coal ash indicated that iron-oxides comprised 5.2% of the coal ash mass. The presence of iron-oxides was confirmed by XRD, which found that hematite and goethite minerals were present.

The spike in iron concentration between 222 and around 350 h in coal ash reactors was likely due to the dissolution of iron minerals as iron was reduced from Fe(III) to Fe(II). Iron-oxides have been shown to be reduced to soluble Fe(II) at low redox potential (Postma et al., 1996; Smith, 2007; Frohne et al., 2011), which is consistent with what occurred in this experiment. During the transition stage the solution pH increased to over 9, which may have contributed to iron release from the coal ash. A similar study on metal leachability from coal ash demonstrated that iron was less likely to be released below pH 9 due to its distribution among the less soluble residual silicate matrix (Jegadeesan et al., 2008). A moderate positive correlation between iron and pH (Spearman's ρ=0.47) and a moderate negative correlation between iron and redox potential (Spearman's ρ= -0.54) suggested that the simulated weathering processes did affect the release of iron. The sudden decrease in dissolved iron concentration may have occurred due to precipitation of solid iron compounds, or sorption of Fe(II) to DOM. The decrease in iron concentration was likely caused by the precipitation of iron compounds under the alkaline pH of the system after the transition stage. Smith et al. found that iron precipitated as hydroxides, carbonates, and sulfides under alkaline conditions (Smith, 2007), which was in agreement with iron behavior in this experiment. Soluble iron has also been shown to form complexes with carboxyl and phenolic compounds in the fulvic acid component of DOM (Carrillo-Gonzalez et al., 2006). The decrease in $SUVA_{254}$ between 222 and 350 h indicated that higher concentrations of fulvic acids were present (Leenheer et al., 2003; Weishaar et al., 2003). Iron was correlated negatively with $SUVA_{254}$ (Spearman's ρ= -0.62) and positively with DOC (Spearman's ρ=0.55), which agreed with the supposition that sorption to less aromatic DOC contributed to the sudden decrease in iron concentration.

Iron concentration in the control reactor was greater than the coal ash reactor over the majority of the experiment. Greater iron concentrations were likely measured in the control because any soluble or mobile iron in the coal ash system would have been scavenged by or complexed with other species or DOM. XRD of the fine clay fraction indicated that two iron containing minerals, biotite and chlorite, were present in the sediment. The release of iron from the control reactor was likely due to the dissolution of chlorite and biotite minerals in the Emory River sediment. Biotite and chlorite are sources of iron, specifically Fe(II) (Banwart et al., 1994). Biotite and chlorite have been shown to release Fe(II) upon their dissolution (Malmstrom et al., 1996; Qafoku et al., 2003), which agreed with what occurred in this study.

***Manganese release*:** Manganese concentration decreased overall in the experiment, and the differences in release between control and coal ash reactors indicated that manganese behavior was affected by coal ash addition (Figure 3.12). Manganese can be associated with the glass fraction of the coal ash (Izquierdo et al., 2012), and has been shown to be leached at extremely low rates (Querol et al., 2001). It is possible that some manganese was released from the coal ash due to rapid dissolution of soluble ash fractions, which would subsequently precipitate on or adsorb to secondary phases (Neupane et al., 2013). This could explain the higher initial manganese concentration (< 24 h) in the coal ash reactors compared to the control.

The differences in manganese behavior between coal ash and control reactors suggested that the addition of coal ash did affect the behavior of manganese, possibly due to the sorption of elements released from the coal ash to manganese-oxides formed under oxidizing conditions or ambiently present in the Emory River sediment. Manganese-oxides have been shown to form and precipitate in solution under oxidizing conditions (Lorite-Herrera et al., 2008), at neutral to alkaline pH (Gitari et al., 2009), and with increasing redox potential (Frohne et al., 2011); (Ye et al., 2013), which agreed with manganese behavior in this experiment. The manganese released into solution from the coal ash likely precipitated as manganese-oxides under oxidizing conditions, resulting in the decreased manganese concentration during the oxidizing stage of the experiment. The decrease in manganese concentration during the transition stage was likely caused by the increase in pH during that time. A similar study on coal ash weathering also found that manganese was controlled by pH (Akinyemi et al., 2011). The strong negative correlation between manganese and pH (Spearman's ρ= -0.78) in coal ash reactors suggested that pH did suppress manganese release.

Manganese concentration increased after 350 h, likely due to the dissolution of manganese-oxides in reducing conditions. Several studies have shown that manganese-oxides dissolve at low redox potential, releasing dissolved manganese into solution (Carrillo-Gonzalez et al., 2006; Smith, 2007; Izquierdo et al., 2012; Ye et al., 2013). Reduced manganese has also been found to be more mobile than oxidized manganese in a mobilization study using varied redox conditions (Frohne et al., 2011).

***Silicon release*:** The release of silicon was difficult to characterize, similar to iron. Silicon release from coal ash reactors was higher initially, but the silicon concentrations in the control reactor approached and exceeded those in the coal ash reactors during the transition stage (Figure 3.12). Overall, silicon concentration decreased in the coal ash reactors, while in the control reactor silicon increased. Thus, silicon was released from coal ash; however, the larger amount of quartz and silica in the sediment may have caused greater silicon release from the control overall.

The release of silicon from coal ash likely occurred due to the dissolution of soluble silicon compounds and the increase in pH during the transition stage. Silicon can be rapidly leached from coal ash because the surface associated silicon fractions can dissolve in short periods of contact with water (Akinyemi et al., 2012). The increase in pH during the transition stage may also have contributed to the increase in silicon concentration. Silica dissolves in solutions of pH greater than 9 (Zevenbergen et al., 1999; Akinyemi et al., 2011), which may explain the increase in silicon concentration during the transition stage. However, after the jump in pH, the concentration of silicon decreased, possibly due to the exhaustion of easily soluble silicon, and the slow dissolution of the remaining glass component of the coal ash, or precipitation of secondary silicate minerals (Akinyemi et al., 2012; Izquierdo et al., 2012; Neupane et al., 2013).

Silicon release in the control reactor was nearly opposite to its behavior in coal ash reactors. Silicon concentration increased slightly during the oxidizing stage of the experiment, which suggested that the easily soluble silica compounds were released from the soil when contacted with water. Silicon concentration in the control reactor may have experienced an increase during the transition stage due to the concomitant increase in pH. Increasing the pH above 8 and 9 has been shown to cause dissolution of quartz and silica, respectively, due to their increasing solubility (White, 1984; Brady et al., 1989; House et al., 1992; Zevenbergen et al., 1999). From the start of the reducing stage through 350 h the concentration of dissolved silicon decreased, which may be due to the exhaustion of soluble silica from the sediment or the slow dissolution of less soluble silica compounds.

***Alkali and alkaline earth metal release*:** The elements in the alkali and alkaline earth metals group that were released from the coal ash are strontium, rubidium and barium (Figure 3.13).

***Strontium release*:** Strontium concentration decreased only slightly over the entire experiment (Figure 3.13). The release of strontium was due to the presence of coal ash, as indicated by the nearly two order of magnitude difference in concentration between the coal ash and control reactors.

Strontium concentration increased under oxidizing conditions, which could be due to the redox potential, release from precipitates, or competition with calcium. The initial increase in redox potential (< 50 h) could have contributed to strontium release because increases in dissolved strontium concentration have been attributed to increases in redox potential previously (Ye et al., 2013). Additionally, dissolved $Sr^{2+}_{(aq)}$ was predicted to be the principal species based on the pH and redox potential measurements in oxidizing conditions (Schweitzer et al., 2010). A moderate positive correlation between strontium and redox potential (Spearman’s ρ=0.51) indicated the increase in redox potential during the first 50 h contributed to strontium release during that time. Additionally, increased strontium concentration and solubility has been attributed to high levels of calcium in a leaching study using sludge amended soils (McBride et al., 1999). This could explain the strontium release from coal ash reactors based on the simultaneously high calcium concentration, as there was strong positive correlation between strontium and calcium (Spearman's ρ=0.77).

Similar to previous studies (Gitari et al., 2009; Ye et al., 2013), strontium concentration decreased as pH increased and redox potential decreased. The increase in pH would increase surface electronegativity that attracts cations (Pedrot et al., 2009), which could have contributed to decreased strontium release. The moderate negative correlation between strontium and pH (Spearman's ρ= -0.54) agreed with this supposition. In addition to pH controls, the simultaneous decrease in sulfate may have decreased strontium concentration due to the reduction of sulfate to sulfide, and subsequent precipitation of strontium-sulfide minerals (Nakayama et al., 2003; Lorite-Herrera et al., 2008). The strong correlation between strontium and sulfate (Spearman's ρ=0.72) suggested that decreased sulfate was related to decreased strontium. The precipitation of strontium-sulfide has been shown to occur at low redox potential (Ye et al., 2013), which suggested that decreased strontium concentration in this experiment was caused by the decrease in redox potential during the transition stage. This was verified by strontium's moderate positive correlation with redox potential (Spearman's ρ=0.51), strong positive correlation with sulfate (Spearman's ρ=0.72).

***Rubidium release*:** Rubidium concentration decreased overall in the experiment (Figure 3.13). Rubidium was released from the coal ash, similar to strontium. Rubidium release was similar to potassium, sodium and magnesium; therefore, its behavior was likely governed by similar mechanisms, such as redox processes and pH facilitated dissolution.

The slight increase in rubidium concentration in the oxidizing stage was likely due to redox conditions and pH. The redox potential in this experiment increased under oxidizing conditions, and this likely caused the slight increase in rubidium before concentrations began to decrease. Rubidium release has been shown to peak at intermediate redox potentials (i.e., 100 to 500 mV) in a mobilization study using controlled redox conditions (Ye et al., 2013), which agreed with rubidium behavior in this experiment. This was supported by a moderate positive correlation between rubidium and redox potential (Spearman's ρ=0.66). In oxidizing conditions, rubidium may have been released because of the decrease in pH in the first 24 h of the experiment. Rubidium concentration may increase with decreasing pH due to the influence of pH sensitive DOC fractionation on trace element mobility (Pedrot et al., 2009). Additionally, a strong negative correlation between rubidium and pH existed (Spearman's ρ= -0.78), which implied that the pH decrease in the first 24 h contributed to rubidium release.

The transition stage caused a decrease in rubidium concentration, which may be due to increased pH, decreased redox potential, and interaction with clays. Rubidium concentration has been shown to decrease with decreasing redox potential (Ye et al., 2013), and increasing pH (Pedrot et al., 2009), which agreed with the rubidium behavior as a function of pH (Spearman's ρ= -0.78) and redox potential (Spearman's ρ=0.66) in this study. Additionally, rubidium has been shown to be geochemically coupled with potassium, an element associated with illite and smectite clays, due to close correspondence of cation radii (Payne et al., 1997). Therefore, the decrease in rubidium concentration may be due to the concomitant decrease in potassium. The presence of smectite and illite clays in the Emory River sediment supported this idea, as well as a very strong positive correlation between rubidium and potassium (Spearman's ρ=0.90).

***Barium release*:** Barium release increased over the course of the experiment, opposite to strontium and rubidium (Figure 3.13). During the oxidizing stage, barium release in coal ash reactors was identical to the control; however, the increased barium release in coal ash reactors during the reducing stage indicated that barium was released from the coal ash.

The steady concentration of barium under oxidizing conditions may be due to its solubility and exchange reactions with other cations. Constant barium concentrations have been attributed to its solubility controlled release in a leaching study on simulated radioactive waste (Nakayama et al., 2003). The amount of dissolved Ba^{2+} was limited by the solubility of $BaSO_{4(s)}$ and was also related to dissolved Sr^{2+}. In this experiment, it is possible that barium was present as barium-sulfate under oxidizing conditions, and the release of mobile Ba^{2+} ions was limited by the solubility of $BaSO_{4(s)}$. Another possibility is that barium and strontium, both present in the +2 oxidation state, would compete for sorption sites, resulting in nearly constant concentrations. A low negative correlation between barium and strontium (Spearman's ρ= -0.45) suggested competition between the two elements was a possibility.

Barium concentration increased during the transition stage, possibly due to competition with other cations, or solubilization with DOC. Barium has been shown to be highly mobile and soluble in bio-solids due to its occurrence as an exchangeable cation (Lasley, 2008; Lasley et al., 2010). The strong negative correlation between barium and magnesium (Spearman's ρ= -0.70), copper (Spearman's ρ= -0.70), and the moderate negative correlation between barium and potassium (Spearman's ρ= -0.67), sodium (Spearman's ρ= -0.66), rubidium (Spearman's ρ= -0.63), manganese (Spearman's ρ= -0.62), cobalt (Spearman's ρ= -0.58), and calcium (Spearman's ρ= -0.50) suggested that these cationic elements may have out-competed barium for sorption sites on the coal ash or sediment. The increase in barium concentration may also be related to the concurrent increase in DOC concentration. Pedrot et al. (2009) proposed that barium may be solubilized and released from soil with DOC, which agreed with the observed increase in DOC concentration in this experiment. Additionally, a strong positive correlation between barium and DOC (Spearman's ρ=0.72) was found, which supported this supposition.

***Oxyanion-forming element release*:** The release of oxyanion-forming elements – arsenic, chromium, molybdenum, selenium, and vanadium – was similar in coal ash reactors (Figure 3.14). Increased concentrations of the oxyanion-forming elements in coal ash reactors compared to the control indicated that they were released from coal ash. These elements combine with oxygen to form a negatively charged anionic species in aquatic systems. Oxyanions of elements with high ionic potential, the ratio of oxidation number to ionic radius, are generally mobile (Smith, 2007), and their mobility increases under alkaline conditions. The mobility of oxyanions is also sensitive to redox conditions.

***Arsenic and selenium release*:** The concentrations of arsenic and selenium under oxidizing conditions were likely dependent on pH, and decreased due to sorption processes. Arsenic and selenium exist primarily as arsenate and selenite in coal ash (Huggins et al., 2007) and are released as oxyanions (Ruhl et al., 2009; Wang et al., 2009; Bednar et al., 2010). Oxyanions leached from coal ash are increasingly sorbed on surfaces at lower pH due to the presence of positively charged surfaces (Jones et al., 2012). Additionally, the release of arsenic and selenium from coal ash has been shown to peak at neutral pH (Gitari et al., 2009), which may explain the decrease in arsenic and selenium concentration alongside a pH decrease in the first 50 h of this study (Figures 3.10 and 3.14). The strong positive correlation between arsenic and pH (Spearman's ρ= 0.71) agreed with this supposition; however, selenium did not. Instead, selenium had a very strong correlations with manganese (Spearman's ρ=0.97), cobalt (Spearman's ρ=0.97), calcium (Spearman's ρ=0.96), germanium (Spearman's ρ=0.94), sodium (Spearman's ρ=0.90) and rubidium (Spearman's ρ=0.90), and strong correlations with potassium (Spearman's ρ=0.89) and magnesium (Spearman's ρ=0.86), which suggested selenite may have complexed with these cationic elements and precipitated out of solution.

As the experiment proceeded into the transition stage, arsenic and selenium behavior differed. Arsenic concentration increased during the transition stage, which is likely due to the changes in pH and redox potential, or the increase in DOC concentration. In oxidizing conditions arsenic exists in +5 oxidation state, As(V), whereas in reducing conditions arsenic exists predominantly in +3 oxidation state, As(III) (Tamaki et al., 1992; Sadiq, 1997). The decrease in redox potential during the transition stage indicated that As(V) may have been reduced to As(III), the most mobile form of arsenic (Wang et al., 2006), thereby contributing to its increased concentration. The moderate negative correlation between arsenic and redox potential supported this idea (Spearman's ρ= -0.69). The increase in pH from roughly 7 to over 9 during the transition stage may also have caused desorption of arsenic from the coal ash. In a similar study, arsenic release increased drastically at pH 9 (Jegadeesan et al., 2008), which agreed with the behavior of arsenic as a function of pH in this study (Spearman's ρ=0.71). Competition with DOM for sorption sites on the sediment or coal ash surfaces may have also increased arsenic concentration (Wang et al., 2006). The DOC concentration increased during the transition stage and had a moderate positive correlation with arsenic (Spearman's ρ=0.65), which supported this idea.

Oppositely, selenium concentration decreased during the transition stage, likely due to increased pH and a high calcium concentration. Wang et al. (2009) found that selenium in coal ash was less soluble under alkaline conditions and high calcium concentrations due to selenite (SeO_3^{2-}) species forming precipitates with calcium ($CaSeO_3$). The pH and redox potential of the system indicated that the major selenium species present during the transition stage was selenite (Schweitzer et al., 2010). Selenite may have complexed with calcium, resulting in the decreased selenium concentration observed. The very strong positive correlation between selenium and calcium (Spearman's ρ=0.96), and the strong negative correlation between selenium and pH (Spearman's ρ= -0.75) supported increased pH and precipitation with calcium as causes of the decrease in selenium concentration during the transition stage.

During the reducing stage arsenic concentration was nearly constant. The high pH, low redox potential, and competition with phosphate and/or sulfate may have contributed to arsenic release. At the alkaline pH of the coal ash reactors, sorption of the negatively charged arsenic oxyanion would be limited due to an increased negative charge on coal ash and sediment surfaces (Jones et al., 2012). Under reducing conditions arsenic would likely be reduced from As(V) to As(III), thus increasing its mobility. Frohne et al. (2011) also found that arsenic mobility increased under reducing conditions due to the reduction of arsenate to arsenite. Additionally, the competitive anion effect may have contributed to arsenic release. In a leaching study by Gitari et al. (2009) sulfate was found to substitute for the arsenic oxyanion in sulfate containing minerals within the coal ash. Phosphate has also been shown to compete and displace oxyanions in a long-term metal leaching study using sludge amended soils (McBride et al., 1999).

Selenium concentration during the reducing stage was steady until around 350 h, at which point a small increase occurred. In a previous study, calcium was found to affect selenium release to a lesser extent than arsenic (Wang et al., 2009), which may explain the increase in selenium concentration after 350 h. One possibility is that phosphate out-competed selenium for sorption sites, which was supported by the concomitant decrease in phosphate concentration alongside selenium. Phosphate has been shown to out-compete both oxidized and reduced selenium in soils during a study on the effects of competitive anions on arsenic and selenium adsorption (Goh et al., 2004), which supported anion competition as a cause for increased selenium release.

Molybdenum release**:** Molybdenum release from coal ash appeared to be controlled by pH, and precipitation and sorption processes (Figure 3.14). The slightly alkaline pH in coal ash reactors in the first 50 h of the experiment may have contributed to the increased molybdenum concentration during the oxidizing stage (Figure 2.10). Previous studies have shown that molybdenum release and mobility are highly dependent on pH (Jackson et al., 2000; Carrillo-Gonzalez et al., 2006; Gitari et al., 2009). Molybdenum is highly soluble and mobile under slightly alkaline pH (Gitari et al., 2009), and the decrease in pH towards neutrality in the first 50 h may explain why molybdenum concentration increased initially before plateauing. Over the remainder of the oxidizing stage, the pH remained steady around 7.3 and molybdenum concentration was also uniform.

The transition stage triggered a decrease in molybdenum concentration, likely caused by sorption processes and precipitation of insoluble molybdenum compounds. Molybdenum can sorb to iron in solution (Gitari et al., 2009), sorb to manganese-oxides (Audry et al., 2006), or form insoluble calcium complexes (Ye et al., 2013), thereby decreasing its concentration. The pH and redox potential during the transition stage suggested that molybdate (MoO_4^{2-}) was the principal form of molybdenum (Schweitzer et al., 2010). During the same time, a simultaneous increase in iron and aluminum concentration occurred, which may have sorbed molybdate (Gitari et al., 2009). The moderate negative correlation between molybdenum and iron (Spearman's ρ= -0.50) implied that complexation with iron may have occurred. Molybdate has also been shown to sorb to manganese-oxides previously (Audry et al., 2006), which agreed with the low positive correlation between molybdenum and manganese found this this experiment (Spearman's ρ=0.39). Another possible explanation for the decrease in molybdenum concentration may be that calcium complexed with MoO_4^{2-} to form $CaMoO_4$. Previous research has shown that molybdenum concentration was controlled by the solubility of $CaMoO_4$, and was independent of redox potential (Niki, 1985; Ye et al., 2013). The moderate positive correlation between molybdenum and calcium (Spearman's ρ=0.51) agreed with this supposition.

Molybdenum concentration may have increased during the reducing stage due to the dissolution of DOM and/or manganese-oxides to which molybdenum was sorbed, as well as anionic competition with phosphate. Molybdenum may have been mobilized by humic substances in the DOM (McBride et al., 1999), which was supported by the moderate positive correlation between molybdenum and $SUVA_{254}$ (Spearman's ρ=0.63). Additionally, molybdenum has a strong association with manganese-oxides, and during the reducing stage, the redox conditions in the system could have dissolved manganese-oxides, thereby releasing molybdenum (Audry et al., 2006). Molybdenum did have a low positive correlation with manganese (Spearman's ρ=0.39), which indicated that dissolution of manganese-oxides contributed to molybdenum release. Another explanation for increased molybdenum concentration during the reducing stage could be competitive anion effects with phosphate. High phosphate concentrations have been shown to out-compete oxyanions and increase molybdenum release in sludge and fly ash amended soils (McBride et al., 1999; Jackson et al., 2000). The low negative correlation was found between molybdenum and phosphate (Spearman's ρ= -0.43) supported this idea.

Chromium release**:** Chromium concentration decreased overall in the experiment (Figure 3.14), primarily due to changes in redox potential, and to a lesser extent by its solubility. The initially high chromium concentration and subsequent decrease under oxidizing conditions may have been caused by the easily soluble chromium fraction associated with the surface of the coal ash particles. Oxyanion-forming elements are highly leachable (Jones et al., 2012), and the easily soluble chromium fraction in the coal ash may have been released quickly when contacted with water, as shown previously (Gitari et al., 2009).

The rapid decline in the concentration of chromium during the transition stage was likely due to the reduction of Cr(VI) to Cr(III), which would have decreased chromium mobility. Under oxidizing conditions, it was predicted that chromium was present as the chromate anion (Cr(VI); $CrO_4^{2-}{}_{(aq)}$), the more mobile chromium species (Schweitzer et al., 2010). It was likely that the chromate was reduced to chromium oxide (Cr(III); Cr_2O_3) as redox potential decreased during the transition stage. A strong positive correlation between chromium and redox potential (Spearman's ρ=0.71) suggested that chromium release did decrease due to its reduction. However, chromate is also a strong oxidizing agent and could have been immediately reduced by OM (Jackson et al., 2000; Egiarte et al., 2006; Du Laing et al., 2007; Zhang et al., 2012). A moderate negative correlation between chromium and DOC (Spearman's ρ= -0.62) indicated that chromate could have been reduced in this way.

***Vanadium release*:** The behavior of vanadium was relatively stable until the reducing stage (350 h), at which point vanadium concentration decreased, which could be due to the low mobility of vanadium under oxidizing conditions (Astrom, 1998). Vanadium is often associated with oxides, due to the tendency of vanadium species to form complexes with hydrous oxides (Astrom, 1998). Vanadium has a strong association with manganese-oxides (Carrillo-Gonzalez et al., 2006), and vanadium may have sorbed to manganese-oxides, thereby decreasing its concentration. A strong positive correlation between vanadium and manganese (Spearman's ρ=0.74) supported this idea. Vanadium is highly sensitive to changes in redox, and the large decrease in its concentration during the reducing stage may be due to the redox conditions present in the system after that time. The reduction of V(V) to V(III) decreases vanadium mobility (Fox et al., 2002, 2003; Carrillo-Gonzalez et al., 2006); therefore, the reducing conditions in the system may have caused its decreased concentration.

Transition metal release**:** Transition metals – cadmium, cobalt, copper, mercury, nickel, rhodium, ruthenium, and zinc – exhibited varied release among elements (Figures 3.15 – 3.20). Transition metals have properties that affect their environmental behavior; most importantly they tend to have multiple oxidation states. Additionally, transition metals can form numerous complexes, and some are redox sensitive, forming either soluble or insoluble compounds with other aqueous chemical species (Smith, 2007).

Cadmium release**:** Cadmium concentration in the coal ash increased overall during the experiment (Figure 3.15). The disparity in cadmium concentration between the coal ash and control reactors implied that it was released from the ash. The release of cadmium appeared to be controlled by sorption and desorption processes related to the DOC concentration, redox potential and pH of the system.

Under oxidizing conditions cadmium concentration increased, which may be attributed to its solubility, or the change in $SUVA_{254}$ and redox conditions. In a previous study on metal mobility, cadmium solubility was significantly correlated with $SUVA_{254}$ (Hernandez-Soriano et al., 2012), which agreed with the correlation between cadmium and $SUVA_{254}$ found in this study (Spearman's ρ=0.58). Cadmium concentration may also have increased oxically due to the increase in redox potential over the same time. Solubility of cadmium has been shown to increase with increasing redox potential (Frohne et al., 2011).

Cadmium concentration decreased from the start of the transition stage until nearly 350 h, which could be due to the simultaneous changes in $SUVA_{254}$, redox potential and pH. Cadmium concentration may have decreased because of the concurrent decrease in $SUVA_{254}$ between the transition stage and 350 h. Cadmium solubilization has been significantly correlated with $SUVA_{254}$ previously (Hernandez-Soriano et al., 2012), which agreed with the moderate positive correlation between cadmium and $SUVA_{254}$ found in this experiment (Spearman's $\rho=0.58$). Therefore, it is likely that the aromaticity of the DOM (i.e., $SUVA_{254}$) in this study affected cadmium release to a greater extent than did pH and redox potential. The increased negative charge with increased pH may have caused cadmium to be more electrostatically attracted to surfaces (Gitari et al., 2009; Jones et al., 2012). This was complimented by the predicted speciation of cadmium as the mobile cation, Cd^{2+}, during the transition stage (Schweitzer et al., 2010). As the redox potential decreased, cadmium solubility would also decline (Frohne et al., 2011).

The increased cadmium concentration during the reducing stage could be explained by the dissolution of OM to which cadmium was sorbed. The dissolution of OM was thought to cause the release of cadmium that had been complexed with OM in previous studies (McBride et al., 1999; Hernandez-Soriano et al., 2012). The increase in DOC and $SUVA_{254}$ after 350 h suggested that cadmium was released due to OM dissolution. Additionally, the correlation between cadmium and $SUVA_{254}$ in this experiment (Spearman's $\rho=0.58$) suggested that cadmium was released during the reducing stage due to the increased solubility of the OM.

Cobalt release**:** Cobalt concentration decreased over the course of the experiment, and after the transition stage, coal ash reactor cobalt concentrations were equivalent to ambient cobalt levels in the control reactor (Figure 3.18). However, the initial disparity in cobalt concentration between the coal ash and control reactors implied that it was released from the ash. The release of cobalt appeared to be controlled by sorption and desorption processes related to the redox potential and pH of the system.

Cobalt concentration was high initially and decreased under oxidizing conditions. Decreased cobalt concentration under oxidizing conditions was likely caused by sorption to manganese-oxides, or because the easily soluble fraction of cobalt was associated with the surface of the ash. A previous study found that manganese-oxides have a greater capacity to sorb cobalt than other transition metals like nickel and zinc due to the oxidation of Co^{2+} to Co^{3+} at the oxide surface (Murray, 1975; Murray et al., 1979; McKenzie, 1980; Astrom, 1998). The very strong positive correlation between cobalt and manganese (Spearman's ρ=0.99) supported sorption to manganese-oxides as the cause of decreased cobalt concentration under oxidizing conditions. Another possibility is that cobalt was associated with the surface of the ash. Gitari et al. (2009) found that the easily soluble fraction of cobalt was released within short periods of ash contact with water.

The transition stage also caused decreased cobalt concentration, possibly due to increased pH and decreased redox potential. The decrease in cobalt concentration could be due to an increase in negative surface sites on the coal ash and sediment with increased pH, which would cause increased electrostatic attraction of positively charged cobalt species (Jones et al., 2012). The strong negative correlation between cobalt and pH (Spearman's ρ= -0.75) agreed with this idea. Previous research has also shown that cobalt precipitates as hydroxides under alkaline conditions (Smith, 2007), which agreed with the strong negative correlation between cobalt and pH found in this study (Spearman's ρ= -0.75).

The increase in cobalt concentration during the reducing stage may be due to the redox conditions present after that time. It is likely that the strong reducing conditions caused the dissolution of manganese-oxides to which cobalt was sorbed, thereby releasing cobalt into solution. The very strong correlation between cobalt and manganese (Spearman's ρ=0.99) implied that cobalt was released from manganese-oxides as they underwent dissolution. However, despite the small increase in cobalt concentration, cobalt in the coal ash reactors was nearly equivalent to the control.

***Copper release*:** Copper concentration decreased throughout the experiment, eventually reaching a level equivalent to ambient copper release in the control reactor (Figure 3.17). The elevated copper concentrations in the coal ash reactors indicated that copper originated from the coal ash. However, the limited copper release from coal ash reactors compared to the control indicated that copper was not easily released from the ash-soil-water mixture.

The decrease in copper concentration overall in this study may have been caused by complexation with DOM, competition with other cations (i.e., calcium), or by precipitation. The high concentration of calcium in the coal ash reactor could compete with copper for bonding sites in the DOM, thereby reducing copper release (Craven, 2012). This observation was confirmed in this study, which showed a moderate positive correlation between copper and calcium (Spearman's ρ=0.65), and a low negative correlation between copper and DOC (Spearman's ρ= -0.46). Additionally, copper can form strong bonds with sulfate, causing precipitation and immobilization of copper under oxidizing conditions, and forming strong sulfide bonds under reducing conditions (Smith, 2007), which is also consistent with the results of this study. The strong positive correlation between copper and sulfate (Spearman's ρ=0.73) implied that copper concentration declined partially due to co-precipitation with sulfate.

The pH and redox potential in the coal ash system throughout the experiment also may elucidate decreased copper concentrations. Copper was likely present initially as the mobile cation Cu^{2+} (Schweitzer et al., 2010), but as redox potential decreased copper may have been reduced to Cu^{+}, reducing its solubility (Frohne et al., 2011). Copper is also reported to be more mobile at low pH (Kumpiene et al., 2009), and the alkaline pH of the batch reactors after the oxidizing stage may contribute to decreased copper concentration. The moderate positive correlation between copper and redox potential (Spearman's ρ=0.65) and the strong negative correlation between copper and pH (Spearman's ρ= -0.74) agreed with this supposition. Additionally, a strong positive correlation between copper and sulfate (Spearman's ρ=0.73) suggested that copper concentration could have decreased because of complexation with sulfate under oxidizing conditions, followed by precipitation of reduced copper-sulfides under reducing conditions. As pH increased and redox potential decreased after the start of the transition stage, copper may have complexed with sulfate before sulfate was reduced to sulfide, which will preferentially precipitate with copper (e.g., $CuS_{(s)}$) (Du Laing et al., 2007; Frohne et al., 2011). Previous studies have shown that only a very small amount of sulfides are required to precipitate all copper (Du Laing et al., 2007; Du Laing et al., 2008).

***Mercury release*:** Mercury behavior in the batch reactor system was unexpected, in that the concentration of mercury was greater in the control, and less in the coal ash reactors (Figure 3.16). The differences in the chemical characteristics of the DOC (i.e., aromaticity) in the control reactor likely caused the decreased mercury release compared to coal ash reactors.

Overall, mercury concentration increased in coal ash reactors, and eventually reached a steady level during the reducing stage. The initial spike in mercury concentration under oxidizing conditions was possibly due to the increased $SUVA_{254}$. The $SUVA_{254}$ has been positively correlated with the release of mercury from Kingston coal ash previously (Craven, 2012), which would explain why increasing $SUVA_{254}$ caused increased mercury concentration in this experiment initially (Figures 3.16 and 3.29). Previous studies have also demonstrated the amount of mercury released was correlated with the aromatic carbon content of solution DOM (Ravichandran et al., 1998; Waples et al., 2005), which is consistent with what was observed in this study.

The decrease in mercury concentration between 2 and 50 h was possibly due to the suppressive effects of calcium. Calcium has been shown to inhibit mercury release from coal ash in the presence of DOM (Suess, 2006; Craven, 2012) by both promoting precipitation of mercury solids (Ravichandran et al., 1999), and decreasing the $SUVA_{254}$ (Langner, 2009). The presence of calcium may have caused the decrease in mercury concentration between 2 and 50 h due to a reduction in the interaction between DOM and the coal ash surface (Suess, 2006; Langner, 2009).

The increased mercury concentration after 50 h may be due related to DOC concentration. Previous work with Kingston coal ash has positively correlated mercury release to DOC concentration (Craven, 2012). The analogous behavior of mercury and DOC concentration in this experiment suggested that DOC concentration may be controlling mercury release. Mercury behavior during the transition stage was indiscernible due to high standard errors between sequential samples. However, during the reducing stage mercury concentration increased, possibly due to calcium inhibiting DOM binding by occupying surface binding sites on the coal ash (Ravichandran et al., 1998; Ravichandran, 2004).

Mercury concentration in the control reactor was unexpectedly higher than the coal ash reactor over the majority of the experiment (Figure 3.16) and was likely caused by increased

DOC concentration and $SUVA_{254}$, and a much lower calcium concentration relative to coal ash reactors. Calcium concentration in the control reactor was over an order of magnitude less than the coal ash reactors; therefore, the effects of calcium on mercury release may have been negligible. Both DOC concentration and $SUVA_{254}$ increased over the duration of the experimental control and may also have contributed to the increase in mercury concentration relative to the coal ash reactors. Both DOC and $SUVA_{254}$ have been positively correlated with mercury release from Kingston coal ash (Craven, 2012).

***Nickel release*:** Nickel concentration exhibited a decreasing trend until 350 h, at which point nickel release increased (Figure 3.17). The release of nickel in this experiment may have been dependent on the pH, redox potential, and DOC and sulfate concentration. Nickel is soluble at acidic pH, but as pH increases toward neutrality the solubility of nickel has been shown to decrease (Gitari et al., 2009; Frohne et al., 2011). Low nickel solubility in the neutral to alkaline pH of the system may have caused the decrease in nickel concentration under oxidizing conditions. Additionally, the solubility and release of nickel has been shown to decrease with pH increases and redox potential decreases (Ye et al., 2013), which is consistent with what was observed in this experiment during the transition stage. Nickel can also be mobilized by DOC (McBride et al., 1999; Koretsky et al., 2007; Frohne et al., 2011), and the release of nickel matched DOC behavior in this experiment: low nickel concentration at low DOC concentration, and increased nickel concentration upon increased DOC concentration. Sulfide precipitation may have also contributed to the initial decrease in nickel release under reducing conditions (Du Laing et al., 2007; Koretsky et al., 2007; Smith, 2007; Du Laing et al., 2008; Frohne et al., 2011). Sulfate concentration decreased initially during the transition stage, which suggested it may have been reduced to sulfide that precipitated with nickel and decrease its release (Frohne et al., 2011). However, after 350 h the concentration of nickel increased alongside sulfate, which could indicate the total sulfate concentration doesn’t reflect sulfate reduction due to rapid internal cycling of sulfur (Koretsky et al., 2007).

***Zinc release*:** Zinc concentration also decreased over the duration of the experiment; however, large standard errors between sequential samples made discerning its release behavior difficult (Figure 3.15). The overall decrease in concentration may be due to complexation and precipitation reactions that are dependent on redox conditions and pH. Zinc may have bonded with sulfate under oxidizing conditions, precipitating in an immobile form and decreasing concentration initially (Smith, 2007). The decrease in DOC concentration may have also contributed to the reduction in zinc concentration under oxidizing conditions (Gungor et al., 2010). Increased zinc solubility has been strongly correlated with solubility of OM in a heavy metal mobility study investigating OM addition (Hernandez-Soriano et al., 2012). Therefore, the decrease in DOC concentration may have decreased the solubility and mobility of zinc under oxidizing conditions.

In the transition stage, the large standard error between sequential samples prevented the characterization of zinc release. The increase in pH during the transition stage may have caused decreased zinc concentration due to increased electrostatic attraction as coal ash surfaces became more negatively charged (Gitari et al., 2009; Jones et al., 2012). Cation adsorption generally increases with pH (Smith, 2007), which is consistent with the results from this experiment. Zinc release may have also decreased due to precipitation with sulfide at low redox potential. Sulfide precipitation under reducing conditions has been found to cause low zinc concentrations (Frohne et al., 2011). The correlation between sulfate concentration and redox potential (Spearman’s ρ=0.54) in this experiment suggested that sulfate was being reduced. Additionally, only a very small amount of sulfide is needed to precipitate all of the zinc (Du Laing et al., 2007; Du Laing et al., 2008), which agreed with this supposition.

***Rhodium and ruthenium release*:** Rhodium and ruthenium release behavior were identical throughout the experiment, and their concentrations increased overall (Figure 3.18). The only difference being that ruthenium concentrations were proportionally higher than rhodium over the entire experiment. The difference in their concentrations between coal ash and control reactors indicated that they were released from the coal ash. In aqueous systems, ruthenium can be present in the 0, II, III, IV, or VII oxidation states, although Ru(III) is the most prevalent. Similarly, Rh(III) is also predominant (Schweitzer et al., 2010). The transport of rhodium and ruthenium in aqueous systems is not understood; however, the results of this study may elucidate both their release from coal ash and their behavior in aquatic environments.

Under oxidizing conditions, the concentrations of rhodium and ruthenium were initially low and increased to a steady level until the start of the transition stage. This may be because ruthenium was oxidized from the solid metal, Ru(0), to Ru(III) or Ru(IV), afterwards forming $Ru(OH)_3$ or RuO_2, respectively. These species may have been more mobile before they were hydrated to their solid $Ru(OH)_3{\cdot}H_2O_{(s)}$ and $RuO_2{\cdot}(H_2O)_{2(s)}$ forms (Schweitzer et al., 2010). Rhodium may have been similar to ruthenium, in that it could have been oxidized from the solid metal, Rh(0), to Rh(III), afterwards forming rhodium-oxide, $Rh_2O_{3(s)}$. Oxidizing conditions may have temporarily allowed for mobile ruthenium and rhodium species before they were fully oxidized and precipitated. This may elucidate the initial increase in their concentration before plateauing during the oxidizing stage; however, oxidation processes could not be confirmed as the cause of their release in oxidizing conditions. Additional study on the redox reactions of ruthenium and rhodium are required to fully understand their release as a function of redox potential.

The increased concentration of rhodium and ruthenium during the transition stage was likely caused by the changes in pH and redox conditions during that time. Both ruthenium (Spearman's ρ=0.77) and rhodium (Spearman's ρ=0.75) had a strong positive correlation with pH, which indicated that the alkaline pH in the system during the transition stage may have facilitated their release from the ash. Additionally, rhodium (Spearman's ρ= -0.53) and ruthenium (Spearman's ρ= -0.52) had a moderate negative correlation with redox potential, which suggested decreased redox potential may have also contributed to their release from the coal ash. However, the hypotheses concerning rhodium and ruthenium during the transition stage could not be confirmed because no literature exists pertaining to their release from coal ash or behavior in aquatic environments.

The increase in rhodium and ruthenium concentration during the reducing stage may be due to the redox conditions present after that time. The moderate negative correlation between rhodium (Spearman's ρ= -0.53), ruthenium (Spearman's ρ= -0.52) and redox potential suggested that decreased redox potential facilitated their release under after 350 h; however, this could not be verified.

Due to ruthenium's location under iron on the periodic table, it could be suggested that ruthenium behaves similar to iron. While ruthenium did have a low positive correlation with iron (Spearman's ρ=0.48), this hypothesis difficult to verify because of iron concentration below detection limits during most of the experiment. Similarly, one might expect rhodium to behave similar to cobalt; however, cobalt release was opposite to rhodium (Spearman's ρ= -0.71).

Overall, the lack of study on both ruthenium and rhodium transport in aqueous environments and their release from coal ash made discerning their release in this experiment difficult.

Release of metalloids**:** The release of metalloids – antimony and germanium – in this experiment differed between elements (Figure 3.22). The disparity in metalloid concentrations and release between coal ash and control reactors indicated that they were released from the ash. Antimony has oxidation states of 0, III, or V, and can be mobile as a cation or present as an insoluble oxide (Schweitzer et al., 2010). Oppositely, germanium has oxidation states of 0, II, or IV and is not present as a cation, but rather exists as germanic acid, the germanium anion, or as a mobile ion. The differences between antimony and germanium likely cause their differences in release.

Antimony release**:** Antimony concentration increased overall; however, a decrease occurred at the start of the transition stage, which subsequently rebounded over the remainder of the experiment (Figure 3.22). The transport of antimony in aqueous systems has become an area of increased interest recently, and the results of this study may elucidate its release from coal ash.

The increase in antimony concentration under oxidizing conditions may be due to its solubility, competition with other anions, or the redox conditions in the system. Antimony is easily extractable in water (Fernandez-Turiel et al., 1994). Furthermore, a large proportion of antimony is retained in the coal ash after combustion, and it has a weak affinity with the aluminosilicate matrix (Qi et al., 2008), which may explain the large increase in its concentration under oxidizing conditions. In a similar study, antimony was also found to be highly leachable from coal ash due to its ability to form oxyanions (Jones et al., 2012). Antimony concentration may also have increased due to competitive anion effects with phosphate, which has been shown to displace oxyanions due to competitive anion effects (McBride et al., 1999). This agreed with the moderate negative correlation between antimony and phosphate found in this study (Spearman's ρ= -0.42). Additionally, antimony would be present as Sb(V) in the oxidizing stage of the experiment (Schweitzer et al., 2010), which has been shown to form oxides that are more soluble than oxides of Sb(III) oxidation state (Resongles et al., 2013).

The anomalous decrease in antimony during the transition stage could be due to precipitation reactions and decreased redox potential. The decreased redox potential likely caused the reduction of Sb(V) to Sb(III), which has been shown to be less mobile.

However, antimony concentration began to increase as the transition stage continued (Figure 2.22), possibly due to the dissolution of iron or aluminum oxides, mobilization with DOC, or decreased anion sorption at alkaline pH. The high pH and strong reducing conditions may have caused dissolution of iron and aluminum oxides (Gitari et al., 2009; Frohne et al., 2011), which could then release sorbed antimony. A simultaneous increase in dissolved iron and aluminum concentrations during the transition stage suggested that antimony may have been released in this way. Increased DOC concentration may have also mobilized antimony. A previous study investigating long term leaching from sludge amended soils postulated that DOM could mobilize antimony (McBride et al., 1999). Another possibility is that the increased pH would decrease sorption of anions (Smith, 2007), thereby increasing the release of antimony.

***Germanium release*:** Germanium concentration decreased overall in this study, opposite to antimony (Figure 3.22). However, the elevated concentration of germanium in coal ash reactors compared to the control confirmed that germanium was released from the coal ash.

The decrease in germanium concentration during the first 350 h of the experiment may be due to changes in pH, or sorption reactions. Germanium concentration was highest initially, and the reason for its decreased concentration under oxidizing conditions was difficult to determine.

It is possible that germanium was associated with the easily soluble fraction of the coal ash, similar to several of the transition, alkali and alkaline earth metals, which were released in short periods of ash contact with water. This idea was supported by the very strong positive correlations between germanium and sodium (Spearman's ρ=0.98), potassium (Spearman's ρ=0.97), cobalt (Spearman's ρ=0.96), magnesium (Spearman's ρ=0.95), calcium (Spearman's ρ=0.93), chromium (Spearman's ρ=0.93), and rubidium (Spearman's ρ=0.92); however, this was not able to be determined with certainty.

The decrease in germanium concentration during the transition stage was possibly related to the increase in pH. A recent coal ash leaching study found that germanium, similar to the transition metals, was sorbed at high pH due to the increase in negatively charged surface sites (Jones et al., 2012). The strong negative correlation between germanium and pH supported this idea (Spearman's ρ= -0.80).

The increase in germanium concentration after 350 h may have also been caused by the dissolution of manganese-oxides to which it was sorbed. This supposition was strengthened by the very strong positive correlation between germanium and manganese (Spearman's ρ=0.98).

Release of Actinides: Uranium was the only actinide released from the coal ash (Figure 3.23). Uranium can exist in several oxidation states (0, III, IV, V, VI), and may be present as an oxyanion (Schweitzer et al., 2010); however U(IV) and U(VI) are the only stable oxidation states in aqueous solutions (Kersting et al., 2003; Johnson et al., 2012; Simmons et al., 2012). The behavior of uranium varied throughout the experiment, although release decreased overall.

Uranium release: A decrease in uranium concentration occurred from the start of the oxidizing stage until 350 h, possibly due to changing redox conditions and pH. The decrease in redox potential may have caused the reduction of U(VI) to U(IV). Uranium(IV) has low solubility, can form insoluble phases, and is relatively immobile (Langmuir et al., 1997; Kersting et al., 2003). The moderate positive correlation between uranium and redox potential (Spearman's ρ=0.63) supported the idea that reduction of uranium contributed to its decreased release. The increase in pH during the transition stage may have caused a decrease in uranium concentration, which was supported by the moderate negative correlation between uranium and pH (Spearman's ρ= -0.61). Additionally, a recent study investigating actinide sorption from natural waters reported the insolubility of U(IV) under basic pH levels (Johnson et al., 2012). The formation of manganese-oxides under oxidizing conditions may have substantially retarded uranium release (Johnson et al., 2012; Simmons et al., 2012) during the transition stage. The strong positive correlation between uranium and manganese (Spearman's ρ=0.74) implied that uranium was sorbed to manganese-oxides as they were formed.

The increase in uranium concentration during the reducing stage was likely due to the dissolution of manganese-oxides in addition to increased DOC concentration. Under reducing conditions, manganese-oxides dissolve, which could release attached uranium (Carrillo-Gonzalez et al., 2006; Gitari et al., 2009; Frohne et al., 2011; Ye et al., 2013). The strong positive correlation between uranium and manganese supported this idea (Spearman's ρ=0.74). Another explanation for increased uranium concentration during the reducing stage was a concurrent increase in DOC. Uranium has been shown to strongly interact with DOC, and aromatic organic molecules (Pedrot et al., 2009), which agreed with the results from this study. The moderate positive correlation between uranium and $SUVA_{254}$ supported this idea (Spearman's ρ=0.57).

***Release of lanthanides*:** Europium and samarium were the only lanthanides released from the coal ash. Europium and samarium exhibited identical release behavior throughout the experiment, the only difference being europium concentrations were slightly higher than samarium (Figure 3.25). Overall, their concentrations increased in the experiment.

Europium and samarium release**:** Europium and samarium concentrations were nearly steady under oxidizing conditions, increasing only slightly until the start of the transition stage (Figure 3.25). Their steady concentrations under oxidizing conditions was likely due to the low solubility of the glass phase of the coal ash, which could have prevented europium and samarium from being released until the glass underwent dissolution. A previous study found that REEs, including europium and samarium, were contained mostly in the glass phase and bound strongly to the coal ash, resulting in poor release (Warren et al., 1989).

The large increase in europium and samarium concentration during the transition stage was likely due to the increase in pH. Pedrot et al. (2009) found that REE concentrations, including europium and samarium, increased significantly with increased pH, which agreed with the strong positive correlations between europium and pH (Spearman's ρ=0.85), and samarium and pH (Spearman's ρ=0.83). Another possibility is that DOM or iron could have mobilized europium and samarium. Several studies have shown that REEs can be bound to DOM or iron-rich nanocolloids that facilitate their release and transport (Pedrot et al., 2009; Stolpe et al., 2013), which agreed with the moderate positive correlation between europium and iron (Spearman's ρ=0.53), and the low positive correlation between europium and DOC (Spearman's ρ=0.49). Similar correlations between samarium and iron (Spearman's ρ=0.52), and between samarium and DOC (Spearman's ρ=0.49) implied that samarium was similar to europium.

Europium and samarium concentrations increased during the reducing stage, possibly caused by the decreasing redox potential in the system and the concomitant dissolution of manganese-oxides containing both europium and samarium. A recent study found that manganese-oxides were effective in sorbing europium, regardless of the organic content or salinity of the water (Johnson et al., 2012). The strong negative correlation between europium and manganese (Spearman's ρ= -0.85), and the moderate negative correlation between europium and redox potential (Spearman's ρ= -0.64) supported this supposition. Although Johnson et al. (2012) did not investigate samarium sorption to manganese-oxides, the similarities between europium and samarium (Spearman's ρ=0.97) and the similarly strong negative correlation between samarium and manganese (Spearman's ρ= -0.86), and redox potential (Spearman's ρ= -0.61) suggested that samarium concentrations increased similar to europium.

Redox couples**:** In order to more accurately approximate the chemical speciation of elements and anions in this study, the measured redox potential in the batch reactor system was compared to various known redox couples (Table 3.6). It was important that the measured redox potentials matched the redox potential at which point a change in chemical speciation would be expected to occur, which would then indicate that the predicted behavior was accurate. Table 3.6 shows several important redox couples in this study, as well as the expected redox potential at which point a change in oxidation state or speciation is known to occur, the time at which the predicted change occurred in this experiment, and the measured redox potential in the batch reactors. For the majority of redox couples considered, the measured redox potential in the batch reactors matched the expected value of redox potential, which indicated that the predicted changes in speciation discussed previously were likely accurate. Nitrate was expected to be reduced to nitrite between 400 and 500 mV (Schweitzer et al., 2010), which agreed with the prediction that nitrate was reduced to nitrite during the oxidizing stage of this experiment. Similarly, manganese reduction from Mn(IV) to mobile Mn(II) was predicted to occur between 200 and 400 mV (Schweitzer et al., 2010) and was observed to occur as the measured redox potential dropped below 200 mV at 350 h. However, arsenic did not agree. It was predicted that arsenate, As(V) or AsO_4^{3-}, was reduced to arsenite, As(III) or AsO_3^{3-}. Arsenate can be present in various forms (i.e., protonated or de-protonated) based on the redox potential and pH of the system; however, it was likely that arsenate was present initially as $HAsO_4^{2-}{}_{(aq)}$. Arsenate may have first been reduced to arsenous acid, $As(OH)_3$ or H_3AsO_3, which is a mobile As(III) species (Wilson et al., 2010), instead of being reduced to arsenite in some form. Arsenous acid is a less-reduced form of arsenic than arsenite, and the reduction of arsenate to arsenous acid would have occurred at a higher redox potential than the reduction of arsenate to arsenite. This may account for the disparity between the expected and measured redox potential of the arsenic redox couple and the behavior of arsenic concentration during the transition stage.

Table 3.6. Important redox couples, the redox potential at which a change in oxidation state or chemical speciation is predicted, the time of the suspected change, and the redox potential measured in the batch reactors. All predicted speciation and oxidation states are based on E-pH diagrams and the conditions of the batch reactor system (Schweitzer et al., 2010) in addition to other specified sources.

Redox Couple		Expected Redox Potential (mV)	Time of Change (h)	Measured Redox Potential (mV)	Expected Match Measured?
Oxidized	Reduced				
NO_3^-	NO_2^-	[a]400 to 500	0 to 166	400 to 550	Yes
Mn(IV)	Mn(II)	[b]200 to 400	350	200	Yes
Fe(III)	Fe(II)	[c]200 to 400	222 to 350	200 to 300	Yes
$HAsO_4^{2-}$	H_3AsO_3	-200 to 0	166	400	No
SO_4^{2-}	S^{2-}	[b]-100 to -200	166 to 895	-200 to 400	Yes
SeO_4^{2-}	SeO_3^{2-}	[c]400 to 500	166 to 222	400 to 500	Yes
U(VI)	U(IV)	100 to 300	166 to 350	200 to 400	Yes

[a] (Borch et al., 2009)
[b] (DeLaune et al., 2005)
[c] (Grundl et al., 2011)

Comparison of laboratory and field investigations: In order to assess if the release of elements and anions from the batch reactor system was similar to the release in the Emory River, the order of release was compared between the results of this study and from Ruhl et al. (2009). Ruhl et al. (2009) measured the concentration of several elements and anions in the Emory River and The Cove, an inlet area on the Emory River, over three months following the spill in December, 2008. A direct comparison between the concentrations measured in this experiment and concentrations measured in the Emory River would not be meaningful because the concentrations measured in the batch reactors were a function of the ash to water ratio. Therefore, a relative comparison was made between the order of the amount of elements and anions released in this study to those found in the Emory River. This order was determined from the average concentration of specified elements and sulfate found in the Emory River and The Cove during each sampling time from Ruhl et al. (2009), and the average concentration of the same elements and sulfate found over the course this study (Table 3.7). The order of release between the Emory River and The Cove was different, as calcium had the highest concentration in the river and sulfate was greatest in The Cove. The order of release in the coal ash reactors was most similar to that found in The Cove by Ruhl et al. (2009), as can be seen in Table 3.7. The similarities between The Cove and the batch reactors used in this experiment may be related to the stagnant nature of both systems. In the Emory River the flow and movement of surface water could have diluted certain elements or anions that were released from the coal ash or simply carried them downstream, whereas the batch reactors had only circulating water and no flow-through. The Cove may have acted similar to the batch reactors because its location could have limited the amount of flow through that area, resulting in circulating effects similar to the batch reactors. The similarities between the coal ash reactors and The Cove, and their shared differences with the Emory River may have caused the differences in their orders of release; however, it is worth noting that strontium was the trace species released to the greatest extent in all three systems. Therefore, strontium release from Kingston coal ash may be of particular concern for the water quality of the Emory River.

Table 3.7. Amount of elements and sulfate released in order of highest to lowest concentration measured. All information regarding the Emory River or The Cove is based on results from Ruhl et al. (2009) and all information regarding the coal ash reactors is from this study.

Order of Release (Highest to Lowest Concentration)

Location	Major Species						Trace Species									
Emory River	Ca	Na	Mg	SO_4^{2-}	Al	Mn	Sr	Cu	Zn	Co	Rb	Se	As	Ni	Cr	U
The Cove	SO_4^{2-}	Ca	Mg	Mn	Na	Al	Sr	As	Zn	Rb	Ni	Cr	Co	Cu	Se	U
Coal Ash Reactors	SO_4^{2-}	Ca	Mg	Na	Al	Mn	Sr	Cr	As	Rb	Se	Ni	Zn	U	Co	Cu

Conclusion

***Implications*:** This study demonstrated that several chemical species were released from Kingston coal ash as the result of a shift from oxidizing to reducing conditions. Species associated with the easily-soluble surface of the coal ash were found to be released quickly when contacted with water in the batch reactors. Conversely, species associated with the less-soluble aluminosilicate core of the coal ash were released as the ash matrix underwent dissolution as a result of changing chemical conditions. The results indicated that changes in chemical speciation and oxidation state as a result of decreasing redox potential contributed to an increase in the dissolved concentrations of some species and a decrease in other species as they underwent reduction.

The differences in release of each chemical species from the coal ash were attributed to several mechanisms involving changes in the chemical properties of the batch reactors, dissolution of mineral phases, precipitation of immobile phases, release of mobile phases, the presence and aromaticity of DOC, or competition or interaction with other elements and/or anions. The decrease in redox potential likely contributed to the alteration of chemical speciation and oxidation state, which in turn could have affected mobility. Uranium concentration in this study was thought to decrease as a result of U(VI) being reduced to U(IV). The increase in pH during the transition stage may have caused an increase in negatively charged surfaces, which could have caused increased electrostatic attraction of cationic species and repulsion of anionic species. The high concentrations of calcium in the coal ash reactors may have affected the release of other species from the ash or their concentration in solution. Selenium concentration was thought to decrease in this study due to its complexation with calcium and subsequent precipitation. The DOC may have also affected the release of species from the coal ash, as chromium in this study was thought to be reduced from Cr(VI) to Cr(III) by OM. Certain anionic species or oxyanion-forming elements may have also been affected by competitive anion effects. Antimony concentration was thought to increase as a result of competition with phosphate in this study.

Several elements had a trend of increasing concentration or release under reducing conditions, including aluminum, arsenic, barium, cadmium, europium, molybdenum, nickel, rhodium, ruthenium, antimony, selenium, samarium, strontium, and uranium, which indicated that these elements may cause water quality issues over time. However, the water quality issues related to the aforementioned elements would not likely affect the surface Emory River water, as these elements were only released under reducing conditions and the surface water would be well-oxidized. Therefore, the potential risk would be in regards to groundwater aquifers that may be connected to the Emory River through its hyporheic zone. Groundwater aquifers are known to have sub-oxidizing to reducing conditions and the reduced forms of the aforementioned elements may still be soluble and mobile as they move through the aquifer. This may pose concerns for those who rely on that groundwater for drinking water and general use.

***Future considerations*:** One of the challenges in interpreting the results of this experiment was that the speciation and oxidation state of the elements in this study were approximated based on E-pH diagrams and previous research. E-pH diagrams are useful in approximating speciation; however, they do not generally include agents that produce complexes or insoluble compounds aside from H_2O and OH^-. While the chemical conditions of the system were known (i.e., redox potential and pH), the overall complexity of the system prevented the exact speciation from being determined with certainty. Therefore, numerous other species, complexes, or phases could have formed that would not be able to be predicted from E-pH diagrams alone. The exact speciation of individual elements should be considered in future studies in order to fully understand the effect of decreasing redox potential on the release of elements from coal ash in aqueous environments. Using techniques such as x-ray adsorption near-edge structure (XANES) and x-ray adsorption fine structure (XAFS) analysis, the exact oxidation state and speciation of a given element could be determined. Future studies that focus on a smaller number of elements may be able to use the aforementioned techniques to more accurately determine speciation, and therefore may be able to better assess the effects of altering redox conditions on the release of elements from coal ash.

The amount of a given element released from the coal ash in terms of mass may also be an important consideration for future studies. The amount of individual elements released from the ash, in terms of the mass released into solution as a ratio of the total mass contained in the ash, was not considered in this study. However, this idea is important in understanding the long-term risks associated with coal ash spills. One idea would be to calculate the mass of each element of concern released into solution over a change in redox conditions from oxidizing to reducing, as a ratio of the total mass of each element contained in the coal ash total. This would allow for the quantification of release, and in turn, might provide an estimation of how long coal ash could persist in the environment.

References

Affolter, R. H., et al. (2011), *Geochemical database of feed coal and coal combustion products (CCPs) from five power plants in the United States*, US Department of the Interior, US Geological Survey.

Akinyemi, S. A., et al. (2011), The Leachability of Major Elements at Different Stages of Weathering in Dry Disposed Coal Fly Ash, *Coal Combustion and Gasification Products*, *3*, 28-40.

Akinyemi, S. A., et al. (2012), Natural weathering in dry disposed ash dump: Insight from chemical, mineralogical and geochemical analysis of fresh and unsaturated drilled cores, *Journal of Environmental Management*, *102*(0), 96-107.

Astrom, M. (1998), Partitioning of transition metals in oxidised and reduced zones of sulphide-bearing fine-grained sediments, *Applied Geochemistry*, *13*(5), 607-617.

Audry, S., et al. (2006), Early diagenesis of trace metals (Cd, Cu, Co, Ni, U, Mo, and V) in the freshwater reaches of a macrotidal estuary, *Geochimica et Cosmochimica Acta*, *70*(9), 2264-2282.

Banwart, S., et al. (1994), Large-scale Intrusion of shallow water into a vertical fracture zone in crystalline bedrock: Initial hydrochemical perturbation during tunnel construction at the Äspö Hard Rock Laboratory, southeastern Sweden, *Water Resources Research*, *30*(6), 1747-1763.

Bednar, A. J., et al. (2010), Geochemical investigations of metals release from submerged coal fly ash using extended elutriate tests, *Chemosphere*, *81*(11), 1393-1400.

Bednar, A. J., et al. (2013), Characterization of metals released from coal fly ash during dredging at the Kingston ash recovery project, *Chemosphere*, *92*(11), 1563-1570.

Bencala, K. E. (2005), Hyporheic exchange flows, *Encyclopedia of hydrological sciences*.

Borch, T., et al. (2009), Biogeochemical redox processes and their impact on contaminant dynamics, *Environmental science & technology*, *44*(1), 15-23.

Boulton, A. J., et al. (1998), The Functional Significance of the Hyporheic Zone in Streams and Rivers, *Annual Review of Ecology and Systematics*, *29*, 59-81.

Brady, P. V., and J. V. Walther (1989), Controls on silicate dissolution rates in neutral and basic pH solutions at 25°C, *Geochimica et Cosmochimica Acta*, *53*(11), 2823-2830.

Brown, G., and G. W. Brindley (1980), Crystal structures of clay minerals and their X-ray identification, *Mineralogical Society, London*, 361-410.

Brownfield, M. E., et al. (1999), Characterization of feed coal and coal combustion products from power plants in Indiana and Kentucky: Proceedings of the 24th International Technical Conference on Coal Utilization and Fuel Systems, *Clearwater, FL*, 989-1000.

Brownfield, M. E., et al. (2005), *Characterization and modes of occurrence of elements in feed coal and coal combustion products from a power plant utilizing low-sulfur coal from the Powder River Basin, Wyoming*, US Department of the Interior, US Geological Survey.

Buschmann, J., et al. (2006), Arsenite and Arsenate Binding to Dissolved Humic Acids: Influence of pH, Type of Humic Acid, and Aluminum, *Environmental Science & Technology, 40*(19), 6015-6020.

Cameron, W. E. (1976), A mineral phase intermediate in composition between sillimanite and mullite, *American Mineralogist, 61*(9-10), 1025-1026.

Cameron, W. E. (1977), Nonstoichiometry in sillimanite: mullite compositions with sillimanite-type superstructures, *Physics and Chemistry of Minerals*, *1*(3), 265-272.

Carrillo-Gonzalez, R., et al. (2006), Mechanisms and Pathways of Trace Element Mobility in Soils, in *Advances in Agronomy*, edited, pp. 111-178, Academic Press.

Craven, A. M. (2012), The importance of dissolved organic matter to the binding of copper and the release of trace elements from coal ash, edited.

Croue, J. P., et al. (2002), Characterization and Copper Binding of Humic and Nonhumic Organic Matter Isolated from the South Platte River: Evidence for the Presence of Nitrogenous Binding Site, *Environmental Science & Technology, 37*(2), 328-336.

de Groot, G. J., et al. (1989), Leaching characteristics of selected elements from coal fly ash as a function of the acidity of the contact solution and the liquid/solid ratio, *Environmental aspects of stabilization and solidification of hazardous and radioactive wastes*, *1033*, 170.

DeLaune, R. D., and K. R. Reddy (2005), Redox potential, *Encyclopedia of Soils in the Environment, 3*.

Dijkstra, J. J., et al. (2006), The leaching of major and trace elements from MSWI bottom ash as a function of pH and time, *Applied Geochemistry*, *21*(2), 335-351.

Du Laing, G., et al. (2007), Influence of hydrological regime on pore water metal concentrations in a contaminated sediment-derived soil, *Environmental Pollution*, *147*(3), 615-625.

Du Laing, G., et al. (2008), Metal accumulation in intertidal marshes: Role of sulphide precipitation, *Wetlands*, *28*(3), 735-746.

Dubikova, M., et al. (2006), *Modelling Element Mobility in Water-flyash Interactions*, QCAT Technology Transfer Centre.

Dudas, M. J. (1981), Long-term leachability of selected elements from fly ash, *Environmental Science & Technology, 15*(7), 840-843.

Dytham, C. (2011), *Choosing and using statistics: a biologist's guide*, John Wiley & Sons.

Eberl, D. D. (2003), *User Guide to Rockjock: A Program for Determining Quantitative Mineralogy from X-Ray Diffraction Data*, BiblioBazaar.

Egiarte, G., et al. (2006), Study of the chemistry of an acid soil column and of the corresponding leachates after the addition of an anaerobic municipal sludge, *Chemosphere*, *65*(11), 2456-2467.

Fernandez-Turiel, J. L., et al. (1994), Mobility of heavy metals from coal fly ash, *Environmental Geology*, *23*(4), 264-270.

Fox, P. M., and H. E. Doner (2002), Trace Element Retention and Release on Minerals and Soil in a Constructed Wetland, *J. Environ. Qual.*, *31*(1), 331-338.

Fox, P. M., and H. E. Doner (2003), Accumulation, Release, and Solubility of Arsenic, Molybdenum, and Vanadium in Wetland Sediments, *J. Environ. Qual.*, *32*(6), 2428-2435.

Franken, R. M., et al. (2001), Biological, chemical and physical characteristics of downwelling and upwelling zones in the hyporheic zone of a north-temperate stream, *Hydrobiologia*, *444*(1-3), 183-195.

Frohne, T., et al. (2011), Controlled variation of redox conditions in a floodplain soil: Impact on metal mobilization and biomethylation of arsenic and antimony, *Geoderma*, *160*, 414-424.

Fuller, C. C., and J. W. Harvey (2000), Reactive Uptake of Trace Metals in the Hyporheic Zone of a Mining-Contaminated Stream, Pinal Creek, Arizona, *Environmental Science & Technology*, *34*(7), 1150-1155.

Gandy, C. J., et al. (2007), Attenuation of mining-derived pollutants in the hyporheic zone: A review, *Science of The Total Environment*, *373*, 435-446.

Geelhoed, J. S., et al. (1997), Phosphate and sulfate adsorption on goethite: Single anion and competitive adsorption, *Geochimica et Cosmochimica Acta*, *61*(12), 2389-2396.

Gitari, W. M., et al. (2009), Leaching characteristics of selected South African fly ashes: Effect of pH on the release of major and trace species, *Journal of Environmental Science and Health, Part A*, *44*(2), 206-220.

Goh, K.-H., and T.-T. Lim (2004), Geochemistry of inorganic arsenic and selenium in a tropical soil: effect of reaction time, pH, and competitive anions on arsenic and selenium adsorption, *Chemosphere*, *55*(6), 849-859.

Goldberg, S., et al. (1996), Molybdenum adsorption on oxides, clay minerals, and soils, *Soil Science Society of America Journal*, *60*(2), 425-432.

Gomes, S., and M. Fransois (2000), Characterization of mullite in silicoaluminous fly ash by XRD, TEM, and 29Si MAS NMR, *Cement and Concrete Research*, *30*(2), 175-181.

Grundl, T. J., et al. (2011), Introduction to Aquatic Redox Chemistry, in *Aquatic Redox Chemistry*, edited, pp. 1-14, American Chemical Society.

Gungor, E., and M. Bekbolet (2010), Zinc release by humic and fulvic acid as influenced by pH, complexation and DOC sorption, in *Geoderma*, edited, pp. 131-138.

Hancock, P. J. (2002), Human Impacts on the Stream-Groundwater Exchange Zone, *Environmental Management*, *29*(6), 763-781.

Harris, W. R., and D. Silberman (1983), Time-dependent leaching of coal fly ash by chelating agents, *Environmental Science & Technology*, *17*(3), 139-145.

Hernandez-Soriano, M. C., and J. C. Jimenez-Lopez (2012), Effects of soil water content and organic matter addition on the speciation and bioavailability of heavy metals, *Science of The Total Environment*, *423*(0), 55-61.

House, W. A., and D. R. Orr (1992), Investigation of the pH dependence of the kinetics of quartz dissolution at 25 C, *Journal of the Chemical Society, Faraday Transactions*, *88*(2), 233-241.

Hower, J. C., et al. (2005), Characteristics of coal combustion products (CCP's) from Kentucky power plants, with emphasis on mercury content, *Fuel*, *84*(11), 1338-1350.

Huggins, F. E., et al. (2007), Selenium and Arsenic Speciation in Fly Ash from Full-Scale Coal-Burning Utility Plants, *Environmental Science & Technology*, *41*(9), 3284-3289.

Hyks, J., et al. (2009), Leaching from MSWI bottom ash: Evaluation of non-equilibrium in column percolation experiments, *Waste Management*, *29*(2), 522-529.

Izquierdo, M., and X. Querol (2012), Leaching behaviour of elements from coal combustion fly ash: An overview, *International Journal of Coal Geology*, *94*(0), 54-66.

Jackson, B. P., and W. P. Miller (2000), Soil solution chemistry of a fly ash-, poultry litter-, and sewage sludge-amended soil, *Journal of Environmental Quality*, *29*(2), 430-436.

Janos, P., et al. (2002), Leaching of metals from fly ashes in the presence of complexing agents, *Waste Management*, *22*(7), 783-789.

Janos, P., et al. (2004), Assessment of heavy metals leachability from metallo-organic sorbent "iron humate" with the aid of sequential extraction test, *Talanta*, *62*(3), 497-501.

Jegadeesan, G., et al. (2008), Influence of trace metal distribution on its leachability from coal fly ash, *Fuel*, *87*, 1887-1893.

Johnson, B. E., et al. (2012), Collection of Lanthanides and Actinides from Natural Waters with Conventional and Nanoporous Sorbents, *Environmental Science & Technology*, *46*(20), 11251-11258.

Jones, D. R. (1995), The leaching of major and trace elements from coal ash, in *Environmental aspects of trace elements in coal*, edited, pp. 221-262, Springer.

Jones, K. B., et al. (2012), Leaching of elements from bottom ash, economizer fly ash, and fly ash from two coal-fired power plants, *International Journal of Coal Geology*, *94*(0), 337-348.

Kersting, A. B., et al. (2003), Colloid-facilitated transport of low-solubility radionuclides: A field, experimental, and modeling investigation, Lawrence Livermore National Laboratory (LLNL), Livermore, CA.

Kim, A. G. (2002), CCB leaching summary: Survey of methods and results, paper presented at Proceedings: Coal combustion by-products and western coal mines: A technical interactive forum.

Kim, A. G., and P. Hesbach (2009), Comparison of fly ash leaching methods, *Fuel*, *88*(5), 926-937.

Koretsky, C., et al. (2007), Spatial variation of redox and trace metal geochemistry in a minerotrophic fen, *Biogeochemistry*, *86*(1), 33-62.

Kukier, U., et al. (2003), Composition and element solubility of magnetic and non-magnetic fly ash fractions, *Environmental Pollution*, *123*(2), 255-266.

Kumpiene, J., et al. (2009), Impact of water saturation level on arsenic and metal mobility in the Fe-amended soil, *Chemosphere*, *74*(2), 206-215.

Langmuir, D., et al. (1997), *Environmental Geochemistry*, Prentice Hall, New Jersey.

Langner, P. (2009), Investigations of factors controlling mercury release from marine influenced sediments (Grizzly Bay and Liberty Island, CA, USA), University of Freiberg, Germany.

Lasley, K. K. (2008), Chemistry and Transport of Metals from Entrenched Biosolids at a Reclaimed Mineral Sands Mining Site in Dinwiddie County, Virginia, Virginia Polytechnic Institute and State University.

Lasley, K. K., et al. (2010), Chemistry and Transport of Metals from Entrenched Biosolids at a Reclaimed Mineral Sands Mining Site, *Journal of Environmental Quality*, *39*(4), 1467-1477.

Leenheer, J. A., and J.-P. Croue (2003), Peer Reviewed: Characterizing Aquatic Dissolved Organic Matter, *Environmental Science & Technology*, *37*(1), 18A-26A.

Lin, H.-T., et al. (2004), Complexation of arsenate with humic substance in water extract of compost, *Chemosphere*, *56*(11), 1105-1112.

Lorite-Herrera, M., and R. Jimanez-Espinosa (2008), Impact of agricultural activity and geologic controls on groundwater quality of the alluvial aquifer of the Guadalquivir River (province of Jaen, Spain): a case study, *Environmental Geology*, *54*(7), 1391-1402.

Lowe, D. J. (1986), Revision of the age and stratigraphic relationships of Hinemaiaia Tephra and Whakatane Ash, North Island, New Zealand, using distal occurrences in organic deposits, *New Zealand Journal of Geology and Geophysics*, *29*(1), 61-73.

Malmstrom, M., et al. (1996), The dissolution of biotite and chlorite at 25°C in the near-neutral pH region, *Journal of Contaminant Hydrology*, *21*, 201-213.

Manning, B. A., and S. Goldberg (1996), Modeling competitive adsorption of arsenate with phosphate and molybdate on oxide minerals, *Soil Science Society of America Journal*, *60*(1), 121-131.

McBride, M. B., et al. (1999), Long-Term Leaching of Trace Elements in A Heavily Sludge-Amended Silty Clay Loam Soil, *Soil Science*, *164*(9), 613-623.

McKenzie, R. M. (1980), The adsorption of lead and other heavy metals on oxides of manganese and iron, *Soil Research*, *18*(1), 61-73.

McKnight, D. M., et al. (1992), Sorption of dissolved organic carbon by hydrous aluminum and iron oxides occurring at the confluence of Deer Creek with the Snake River, Summit County, Colorado, *Environmental science & technology*, *26*(7), 1388-1396.

Mizutani, S., et al. (1996), Acid neutralizing capacity (ANC) and leaching test scheme for short and long term behaviour of granular waste, *Environment Preservation Center, Kyoto University, Kyoto (submitted).* .

Moreno, N., et al. (2005), Physico-chemical characteristics of European pulverized coal combustion fly ashes, *Fuel*, *84*(11), 1351-1363.

Murray, J. W. (1975), The interaction of cobalt with hydrous manganese dioxide, *Geochimica et Cosmochimica Acta*, *39*(5), 635-647.

Murray, J. W., and J. G. Dillard (1979), The oxidation of cobalt(II) adsorbed on manganese dioxide, *Geochimica et Cosmochimica Acta*, *43*(5), 781-787.

Nagorski, S. A., and J. N. Moore (1999), Arsenic mobilization in the hyporheic zone of a contaminated stream, *Water Resources Research*, *35*(11), 3441-3450.

Nakayama, S., et al. (2003), Leaching Behavior of a Simulated Bituminized Radioactive Waste Form under Deep Geological Conditions, *Journal of Nuclear Science and Technology*, *40*(4), 227-237.

Neupane, G., and R. J. Donahoe (2013), Leachability of elements in alkaline and acidic coal fly ash samples during batch and column leaching tests, *Fuel*, *104*(0), 758-770.

Niki, K. (1985), Chromium, Molybdenum, and Tungsten, *Bard, AJ, Parsons, R., Jordan, J., Standard Potentials in Aqueous solution. New York, Marcel Dekker*, 453-483.

Otero-Rey, J. R., et al. (2005), Influence of several experimental parameters on As and Se leaching from coal fly ash samples, *Analytica chimica acta*, *531*(2), 299-305.

Payne, M., et al. (1997), Spatial Variation of Sediment-Bound Zinc, Lead, Copper and Rubidium in Lake Illawarra, a Coastal Lagoon in Eastern Australia, *Journal of Coastal Research*, *13*(4), 1181-1191.

Pedrot, M., et al. (2009), Double pH control on humic substance-borne trace elements distribution in soil waters as inferred from ultrafiltration, *Journal of Colloid and Interface Science*, *339*(2), 390-403.

Postma, D., and R. Jakobsen (1996), Redox zonation: Equilibrium constraints on the Fe(III)/SO4-reduction interface, *Geochimica et Cosmochimica Acta*, *60*(17), 3169-3175.

Qafoku, N. P., et al. (2003), Effect of coupled dissolution and redox reactions on Cr (VI) aq attenuation during transport in the sediments under hyperalkaline conditions, *Environmental science & technology*, *37*(16), 3640-3646.

Qi, C., et al. (2008), Environmental geochemistry of antimony in Chinese coals, *Science of The Total Environment*, *389*, 225-234.

Querol, X., et al. (2001), Extraction of soluble major and trace elements from fly ash in open and closed leaching systems, *Fuel*, *80*(6), 801-813.

Ravichandran, M., et al. (1998), Enhanced Dissolution of Cinnabar (Mercuric Sulfide) by Dissolved Organic Matter Isolated from the Florida Everglades, *Environmental Science & Technology*, *32*(21), 3305-3311.

Ravichandran, M., et al. (1999), Inhibition of Precipitation and Aggregation of Metacinnabar (Mercuric Sulfide) by Dissolved Organic Matter Isolated from the Florida Everglades, *Environmental Science & Technology*, *33*(9), 1418-1423.

Ravichandran, M. (2004), Interactions between mercury and dissolved organic matter - a review, *Chemosphere*, *55*(3), 319-331.

Redman, A. D., et al. (2002), Natural organic matter affects arsenic speciation and sorption onto hematite, *Environmental Science & Technology*, *36*(13), 2889-2896.

Reinink-Smith, L. M. (1990), Mineral assemblages of volcanic and detrital partings in Tertiary coal beds, Kenai Peninsula, Alaska, *Clays and Clay Minerals*, *38*(1), 97-108.

Resongles, E., et al. (2013), Fate of Sb (V) and Sb (III) species along a gradient of pH and oxygen concentration in the Carnoules mine waters (Southern France), *Environ. Sci.: Processes Impacts*.

Ruhl, L., et al. (2009), Survey of the Potential Environmental and Health Impacts in the Immediate Aftermath of the Coal Ash Spill in Kingston, Tennessee, *Environmental Science & Technology*, *43*(16), 6326-6333.

Ryan, J. N., and S. Mohanty (2011), Release of Major and Trace Elements from Smelter Slag separated from the Upper Columbia River in Batch and Fluidized Bed Reactors, 20.

Ryden, J. C., et al. (1987), Inorganic anion sorption and interactions with phosphate sorption by hydrous ferric oxide gel, *Journal of Soil Science*, *38*(2), 211-217.

Sadiq, M. (1997), Arsenic chemistry in soils: an overview of thermodynamic predictions and field observations, *Water, Air, and Soil Pollution*, *93*(1-4), 117-136.

Schweitzer, G. K., and L. L. Pesterfield (2010), *The aqueous chemistry of the elements*, Oxford University Press New York.

Seferinoglu, M., et al. (2003), Acid leaching of coal and coal-ashes, *Fuel*, *82*(14), 1721-1734.

Simmons, A. M., and L. A. Neymark (2012), Conditions and processes affecting radionuclide transport, *Geological Society of America Memoirs*, *209*, 277-362.

Smith, F. (1999), *Industrial applications of X-ray diffraction*, CRC Press.

Smith, J. W. N., and G. Britain (2005), *Groundwater-surface water interactions in the hyporheic zone*, Environment Agency.

Smith, K. S. (2007), Strategies to predict metal mobility in surficial mining environments, *Reviews in engineering geology*, *17*, 25-45.

Stolpe, B. r., et al. (2013), Binding and transport of rare earth elements by organic and iron-rich nanocolloids in Alaskan rivers, as revealed by field-flow fractionation and ICP-MS, *Geochimica et Cosmochimica Acta*, *106*(0), 446-462.

Suess, E. (2006), Mercury distributions between particulate and dissolved states in wetlands in California, USA, University of Freiberg, Germany.

Sultana, P., et al. (2011), Mullite Formation in Coal Fly Ash is Facilitated by the Incorporation of Magnesium Oxide, *Rev. Adv. Mater. Sci*, *27*, 69-74.

Tamaki, S., and W. T. Frankenberger Jr (1992), *Environmental biochemistry of arsenic*, Springer.

Tripathi, H. S., and G. Banerjee (1998), Synthesis and mechanical properties of mullite from beach sand sillimanite: effect of TiO2, *Journal of the European Ceramic Society*, *18*(14), 2081-2087.

Triplehorn, D., and B. Bohor (1986), Volcanic Ash Layers in Coal: Origin, Distribution, Composition, and Significance, in *Mineral Matter and Ash in Coal*, edited, pp. 90-98, American Chemical Society.

TVA (2009), Action Memorandum: Request for Removal Action at the TVA Kingston Fossil Fuel Plant Release Site, Roane County, Tennessee, Tennesse Valley Authority.

USEPA (2009), EPA to oversee cleanup of TVA Kingston Fossil Fuel Plant release.

Van der Bruggen, B., et al. (1998), Simulation of acid washing of municipal solid waste incineration fly ashes in order to remove heavy metals, *Journal of Hazardous Materials*, *57*, 127-144.

Wadge, A., et al. (1986), The concentrations and particle size relationships of selected trace elements in fly ashes from U.K. coal-fired power plants and a refuse incinerator, *Science of The Total Environment*, *54*(0), 13-27.

Wang, S., and C. Mulligan (2006), Effect of natural organic matter on arsenic release from soils and sediments into groundwater, *Environmental Geochemistry and Health*, *28*(3), 197-214.

Wang, T., et al. (2009), Leaching Characteristics of Arsenic and Selenium from Coal Fly Ash: Role of Calcium, *Energy & Fuels*, *23*(6), 2959-2966.

Waples, J. S., et al. (2005), Dissolution of cinnabar (HgS) in the presence of natural organic matter, *Geochimica et Cosmochimica Acta*, *69*(6), 1575-1588.

Ward, C. R., et al. (2003), Comparative evaluation of leachability test methods and element mobility for selected Australian fly ash samples, paper presented at Twenty-First Annual International Pittsburgh Coal Conference: Coal-Energy and the Environment: CD-ROM Proceedings.

Warren, C. J., and M. J. Dudas (1985), Formation of secondary minerals in artificially weathered fly ash, *Journal of environmental quality*, *14*(3), 405-410.

Warren, C. J., and M. J. Dudas (1989), Leachability and partitioning of elements in ferromagnetic fly ash particles, *Science of the total environment*, *84*, 223-236.

Weishaar, J. L., et al. (2003), Evaluation of Specific Ultraviolet Absorbance as an Indicator of the Chemical Composition and Reactivity of Dissolved Organic Carbon, *Environmental Science & Technology*, *37*(20), 4702-4708.

White, A. F. (1984), Weathering characteristics of natural glass and influences on associated water chemistry, *Journal of Non-Crystalline Solids*, *67*, 225-244.

Wielinga, B., et al. (1999), Microbiological and geochemical characterization of fluvially deposited sulfidic mine tailings, *Applied and environmental microbiology*, *65*(4), 1548-1555.

Wilson, S. C., et al. (2010), The chemistry and behaviour of antimony in the soil environment with comparisons to arsenic: a critical review, *Environmental Pollution*, *158*(5), 1169-1181.

Winde, F., and I. Jacobus van der Walt (2004), The significance of groundwater-stream interactions and fluctuating stream chemistry on waterborne uranium contamination of streams - a case study from a gold mining site in South Africa, *Journal of Hydrology*, *287*(1), 178-196.

Wu, C.-H., et al. (2000), Competitive adsorption of molybdate, chromate, sulfate, selenate, and selenite on γ-Al2O3, *Colloids and Surfaces A: Physicochemical and Engineering Aspects*, *166*, 251-259.

Wu, C.-H., et al. (2001), Modeling Competitive Adsorption of Molybdate, Sulfate, and Selenate on γ-Al2O3 by the Triple-Layer Model, *Journal of Colloid and Interface Science*, *233*(2), 259-264.

Xu, N., et al. (2006), Adsorption of molybdate and tetrathiomolybdate onto pyrite and goethite: Effect of pH and competitive anions, *Chemosphere*, *62*(10), 1726-1735.

Yan, J., et al. (1999), Neutralising processes of municipal solid waste incineration bottom ash in a flow-through system, *Science of The Total Environment*, *227*(1), 1-11.

Ye, S., et al. (2013), Trace element remobilization following the resuspension of sediments under controlled redox conditions: City Park Lake, Baton Rouge, LA, *Applied Geochemistry*, *28*(0), 91-99.

Zevenbergen, C., et al. (1994), Morphological and chemical properties of MSWI bottom ash with respect to the glassy constituents, *Hazardous waste and hazardous materials*, *11*(3), 371-383.

Zevenbergen, C., et al. (1996), Mechanism and conditions of clay formation during natural weathering of MSWI bottom ash, *Clays and Clay Minerals*, *44*(4), 546-552.

Zevenbergen, C., et al. (1999), Clay Formation and Metal Fixation during Weathering of Coal Fly Ash, *Environmental Science & Technology*, *33*(19), 3405-3409.

Zhang, H., et al. (2012), Leaching of heavy metals from artificial soils composed of sewage sludge and fly ash, *Bulletin of environmental contamination and toxicology*, *88*(3), 406-412.

Appendix 3.A

Table 3.8. Spearman’s ρ correlation matrix of chemical properties (i.e., redox potential, pH, DOC, and $SUVA_{254}$), elements, and anions. Overall, 37 variables were used, which were selected because they were affected by the coal ash. Significant correlations are flagged with an asterisk. Only significant correlations were considered in the discussion.

Na	**K**	**Mg**	**Ca**	**DOC**	**SUVA**	**pH**	**ORP**	
0.60726*	0.62621*	0.63105*	0.45323*	-0.82218*	0.78105*	-0.72889*	1	**ORP**
-0.82192*	-0.84351*	-0.85683*	-0.7192*	0.60821*	-0.55857*	1		**pH**
0.44798*	0.44839*	0.39597*	0.43387*	-0.82016*	1			**SUVA**
-0.53387*	-0.55363*	-0.54476*	-0.39194*	1				**DOC**
0.91129*	0.89718*	0.83871*	1					**Ca**
0.97258*	0.97298*	1						**Mg**
0.98831*	1							**K**
1								**Na**
								Mn
								Fe
								Si
								Al
								Ba
								Rb
								Sr
								Se
								As
								Cr
								Mo
								V
								Cd
								Co
								Cu
								Hg
								Ni
								Rh
								Ru
								Zn
								Sb
								Ge
								U
								Eu
								Sm
								NO2
								NO3
								PO4
								SO4

Mo	**Cr**	**As**	**Se**	**Sr**	**Rb**	**Ba**	**Al**	**Si**	**Fe**	**Mn**
0.30766	0.71452*	-0.69315*	0.45645*	0.5125*	0.6629*	-0.78508*	-0.64395*	-0.04637	-0.53833*	0.53413*
-0.2204	-0.87519*	0.71093*	-0.74644*	-0.53678*	-0.78378*	0.80537*	0.89214*	-0.2167	0.47157*	-0.78385*
0.63266*	0.53831*	-0.62056*	0.37298*	0.70726*	0.62056*	-0.68105*	-0.42379*	-0.35806*	-0.62286*	0.4446*
-0.3226	-0.62379*	0.65484*	-0.3387	-0.57419*	-0.62823*	0.71815*	0.52581*	0.13831	0.54797*	-0.43815*
0.50847*	0.8371*	-0.49435*	0.96452*	0.76653*	0.93508*	-0.50524*	-0.80968*	0.26613	-0.65205*	0.96421*
0.08347	0.95726*	-0.57097*	0.86371*	0.48468*	0.85282*	-0.70323*	-0.98065*	0.50847*	-0.56421*	0.91925*
0.22823	0.95968*	-0.54919*	0.88831*	0.59556*	0.90323*	-0.66976*	-0.94718*	0.42419*	-0.60386*	0.94868*
0.23145	0.94919*	-0.54194*	0.90282*	0.59677*	0.9*	-0.66048*	-0.9496*	0.44677*	-0.63553*	0.95816*
0.38693*	0.89263*	-0.53009*	0.96865*	0.67527*	0.92449*	-0.62204*	-0.89989*	0.31072	-0.68461*	1
-0.49675*	-0.55127*	0.41304*	-0.64957*	-0.56972*	-0.67546*	0.4962*	0.55512*	0.00881	1	
-0.59153*	0.38548*	0.11976	0.30927	-0.2811	0.13952	0.00121	-0.48427*	1		
-0.0766	-0.93185*	0.59153*	-0.84597*	-0.44597*	-0.80968*	0.73992*	1			
-0.2472	-0.74032*	0.87742*	-0.55363*	-0.45403*	-0.63911*	1				
0.53992*	0.90444*	-0.60282*	0.90403*	0.83992*	1					
0.85766*	0.59798*	-0.55645*	0.66935*	1						
0.4254*	0.82419*	-0.53589*	1							
-0.41129*	-0.59516*	1								
0.20685	1									
1										

Ge	Sb	Zn	Ru	Rh	Ni	Hg	Cu	Co	Cd	V
0.59153*	-0.13669	0.04597	-0.51573*	-0.52984*	-0.22621	-0.2871	0.65242*	0.49516*	0.24556	0.43185*
-0.80194*	0.34608	-0.1861	0.77046*	0.75754*	-0.0692	0.15982	-0.74301*	-0.74846*	-0.2075	-0.77207*
0.45766*	0.20565	-0.1492	-0.2657	-0.2835	-0.123	-0.0524	0.3375	0.44073*	0.57702*	0.12177
-0.50847*	0.03427	-0.0512	0.40806*	0.41492*	0.34556	0.23266	-0.45847*	-0.39113*	-0.3186	-0.3085
0.93185*	-0.2734	0.15202	-0.63306*	-0.61371*	0.60242*	0.24153	0.64597*	0.9746*	0.56895*	0.70887*
0.95927*	-0.6246*	0.27097	-0.87419*	-0.86613*	0.23911	-0.0476	0.83427*	0.88871*	0.13911	0.87218*
0.97137*	-0.53831*	0.23105	-0.81129*	-0.80282*	0.31653	0.0629	0.79194*	0.92742*	0.27903	0.81694*
0.98387*	-0.54274*	0.23952	-0.80484*	-0.79355*	0.35484	0.08669	0.77863*	0.94194*	0.30081	0.80968*
0.98337*	-0.43412*	0.16937	-0.78738*	-0.78072*	0.46597*	0.19034	0.76117*	0.98881*	0.43875*	0.73596*
-0.70079*	0.15035	0.04433	0.48133*	0.50914*	-0.1655	-0.1738	-0.48023*	-0.66114*	-0.48518*	-0.2129
0.4*	-0.74839*	0.23427	-0.36492*	-0.36129*	0.32298	-0.0557	0.325	0.31734	-0.49516*	0.64073*
-0.93871*	0.61774*	-0.2383	0.88508*	0.88468*	-0.1992	0.05202	-0.8125*	-0.86815*	-0.1085	-0.84556*
-0.64798*	0.24194	-0.2355	0.6996*	0.71169*	0.23548	0.14556	-0.70323*	-0.58871*	-0.1794	-0.49073*
0.91774*	-0.2121	0.11452	-0.63347*	-0.61613*	0.4125*	0.09274	0.72016*	0.91855*	0.5875*	0.70524*
0.61935*	0.29556	-0.0686	-0.219	-0.2044	0.41048*	0.25524	0.35	0.70484*	0.88024*	0.35081
0.94234*	-0.3359	0.1629	-0.71694*	-0.70081*	0.55927*	0.22702	0.72903*	0.96976*	0.45726*	0.75161*
-0.52984*	-0.0621	-0.2903	0.48911*	0.49315*	0.15605	0.05	-0.56169*	-0.53065*	-0.3113	-0.45887*
0.92782*	-0.51008*	0.24153	-0.79435*	-0.77742*	0.2371	-0.098	0.79476*	0.87016*	0.24879	0.83226*
0.28992	0.60645*	-0.1968	0.08992	0.08952	0.35524*	0.4*	0.0621	0.43145*	0.93831*	-0.0855
0.77379*	-0.54153*	0.29194	-0.68508*	-0.65*	0.35726*	-0.1403	0.71976*	0.72903*	-0.0137	1
0.34435	0.51411*	-0.1794	0.07097	0.07823	0.44879*	0.41774*	0.0871	0.48145*	1	
0.96573*	-0.37581*	0.15645	-0.72056*	-0.71331*	0.54919*	0.24718	0.72177*	1		
0.78992*	-0.54597*	0.32661	-0.8*	-0.79315*	0.11694	-0.0867	1			
0.12782	0.18992	-0.0073	0.16734	0.15645	0.46613*	1				
0.39435*	-0.0081	-0.071	0.0121	0.03952	1					
-0.80726*	0.73629*	-0.2923	0.98952*	1						
-0.8129*	0.73145*	-0.3165	1							
0.18871	-0.3399	1								
-0.51371*	1									
1										

SO4	PO4	NO3	NO2	Sm	Eu	U
0.54435*	0.04759	0.52379*	0.49945*	-0.61411*	-0.64073*	0.63468*
-0.7751*	-0.0093	-0.86873*	-0.0714	0.82575*	0.85198*	-0.60922*
0.4754*	-0.2734	0.41976*	0.45146*	-0.38226*	-0.38427*	0.57298*
-0.47581*	0.10545	-0.46452*	-0.62305*	0.4875*	0.49435*	-0.77097*
0.9746*	-0.1234	0.73548*	-0.2333	-0.73105*	-0.72177*	0.70484*
0.90806*	0.15667	0.82621*	0.01996	-0.94113*	-0.92702*	0.73065*
0.95524*	0.10485	0.80484*	-0.0131	-0.89355*	-0.88468*	0.76008*
0.95605*	0.08106	0.79597*	-0.0159	-0.89718*	-0.87903*	0.75968*
0.98619*	0.02178	0.79343*	-0.1375	-0.86017*	-0.84646*	0.74181*
-0.6504*	0.20089	-0.41001*	-0.236	0.52153*	0.53172*	-0.68867*
0.29113	0.28692	0.25565	-0.2549	-0.42863*	-0.4*	0.03831
-0.88226*	-0.17	-0.84637*	-0.0222	0.94798*	0.94758*	-0.66855*
-0.60444*	-0.0792	-0.75161*	-0.3307	0.79798*	0.79637*	-0.61089*
0.94556*	-0.1532	0.74677*	-0.0115	-0.75403*	-0.7246*	0.79234*
0.72339*	-0.3541	0.51573*	0.0127	-0.37702*	-0.3484	0.7*
0.95323*	-0.0421	0.76774*	-0.1901	-0.80282*	-0.78548*	0.68024*
-0.53992*	0.05666	-0.69597*	-0.3299	0.63871*	0.65484*	-0.64032*
0.90323*	0.02278	0.82298*	0.00968	-0.89274*	-0.86089*	0.69516*
0.42298*	-0.42706*	0.21532	0.00141	-0.0294	-0.0359	0.42097*
0.74355*	0.13328	0.76532*	-0.1821	-0.78548*	-0.74919*	0.47823*
0.48065*	-0.42988*	0.23226	-0.078	-0.0492	-0.0387	0.46008*
0.98508*	-0.0065	0.78508*	-0.1787	-0.82782*	-0.80887*	0.7121*
0.73145*	0.17381	0.72339*	0.05807	-0.84274*	-0.82903*	0.58226*
0.18468	0.05162	0.06774	-0.2224	0.02097	0.04677	0.12137
0.48387*	-0.2266	0.19718	-0.68555*	-0.1246	-0.0786	0.04073
-0.72944*	-0.292	-0.7375*	-0.0863	0.91532*	0.92419*	-0.58065*
-0.73871*	-0.2706	-0.75323*	-0.0536	0.91815*	0.91935*	-0.57379*
0.19153	-0.1482	0.36935*	-0.0061	-0.2802	-0.2552	0.18266
-0.38911*	-0.4196*	-0.38185*	0.09618	0.64274*	0.62097*	-0.1625
0.96935*	0.0488	0.79597*	-0.0381	-0.89435*	-0.8746*	0.76532*
0.75403*	-0.0075	0.58508*	0.40669*	-0.64476*	-0.64194*	1
-0.81734*	-0.2692	-0.82258*	-0.0613	0.96895*	1	
-0.82984*	-0.218	-0.84315*	-0.0436	1		
-0.1309	0.15497	-0.0797	1			
0.7996*	0.00625	1				
-0.0123	1					
1						